Quarkonium States in an Anisotropic Quark-Gluon Plasma

Dissertation

zur Erlangung des Doktorgrades
der Naturwissenschaften

vorgelegt beim Fachbereich Physik
der Johann Wolfgang Goethe-Universität
in Frankfurt am Main

von
Yun Guo
aus China

Frankfurt am Main 2009
(D30)

vom Fachbereich Physik (13) der Johann Wolfgang Goethe-Universität
als Dissertation angenommen.

Dekan: Prof. Dr. D. H. Rischke

Gutachter: Prof. Dr. C. Greiner, Assoc. Prof. Dr. A. Dumitru

Datum der Disputation: 10 Sep. 2009

Zusammenfassung

Übersicht

In dieser Arbeit untersuchen wir die Eigenschaften gebundener Zustände zweier schwerer Quarks ("Quarkonium") in einem Quark-Gluon Plasma, das aufgrund seiner kollektiven Expansion und nichtverschwindender Viskosität lokal eine Anisotropie im Impulsraum aufweist. Wir bestimmen den resummierten Gluonpropagator in der sogenannten "harte thermische Schleifen" (engl.: "hard thermal loop") Hochtemperaturnäherung in einem solchen anisotropen Plasma. Wir berechnen den Propagator in linearen Eichungen und definieren aus seinem statischen Limes durch Fouriertransformation das Potential zwischen (unendlich) schweren Quarks. Dieses durch Eingluonaustausch bestimmte Potential beschreibt die Wechselwirkung des Quark-Antiquark Paares bei kleinen Abständen. Wir finden, dass die Anisotropie die Debye-Abschirmung der Wechselwirkung reduziert und sich das Potential somit wieder dem Vakuumpotential annähert. Darüber hinaus hängt die Stärke der attraktiven Wechselwirkung nicht nur vom Abstand der Quarks ab sondern ist auch winkelabhängig: ein Quark-Antiquark Paar das entlang der Plasmaanisotropie ausgerichtet ist zieht stärker an als ein dazu transversal ausgerichtetes Quarkpaar.

Bei grossen Abständen dominieren nichtperturbative Beiträge. Wir modellieren hier das Potential als QCD String der auf der gleichen Längenskala wie das perturbative Coulombpotential abgeschirmt wird. Das Potential verschwindet nicht bei asymptotischen Abständen sondern ist vielmehr umgekehrt proportional zur Temperatur. Nach Konstruktion des Potentials bestimmen wir numerische Lösungen der Schrödingergleichung in drei Raumdimensionen. Diese Lösungen bestätigen, dass Quarkoniumzustände in einem expandierenden, viskosen Plasma stärker gebunden sind als in einem idealen Plasma im Gleichgewicht. Die Anisotropie führt zudem zu einer Polarisation der P-Wellen.

Im Anschluss bestimmen wir auch Viskositätskorrekturen zum Imaginärteil des Potentials. Auch hier finden wir, dass die Nichtgleichgewichtseffekte die thermischen Effekte reduzieren, d.h., dass der Imaginärteil des Potentials absolut kleiner ist als im perfekten Gleichgewicht. Dies impliziert eine kleinere Breite der gebundenen Zustände im anisotropen Plasma.

Einleitung

Kollisionen schwerer Ionen bei hohen Energien werden ausgeführt um einen neuen Materiezustand zu untersuchen, d.i. das sogenannte Quark-Gluon Plasma (QGP). Die Existenz dieses Zustands bei hohen Temperaturen wird von der Quantenchromodynamik auf dem Gitter bestätigt. Unserem aktuellen Verständnis solcher Schwerionenkollisionen zufolge wird in der zentralen Rapiditätsregion ein sehr heisser "Feuerball" stark wechselwirkender Materie erzeugt in dem die üblichen "farb"-neutralen Hadronen nicht (in gebundener Form) existieren können. Sie lösen sich stattdessen in ein Gas fast freier Quarks und Gluonen

auf, das das Quark-Gluon Plasma darstellt. Solche Experimente bei sehr hohen Energien werden z.Zt. hauptsächlich am "Relativistic Heavy-Ion Collider" (RHIC) des Brookhaven National Lab in New York und in naher Zukunft am "Large Hadron Collider" (LHC) des European Center for Particle Physics (CERN) in Genf ausgeführt. Am RHIC wurde bereits eine grosse Menge an Daten über $p+p$, $D+Au$, und $Au+Au$ Kollisionen bei einer Schwerpunktsenergie von $\sqrt{s} = 20 - 200$ GeV pro Nukleon gesammelt. Der LHC wird Energien von bis zu $\sqrt{s} = 5.5$ ATeV für $Pb+Pb$ Kollisionen erreichen.

Die in diesem Feld tätigen Physiker haben viele Anstrengungen unternommen die Existenz eines Quark-Gluon Plasma in Schwerionenkollisionen überzeugend nachzuweisen. Eines der vorgeschlagenen experimentellen Signale für die Formation eines QGP ist die Dissoziation von Quarkonium. Matsui und Satz argumentierten, dass die Abschirmung der elektrostatischen Wechselwirkung durch das Medium zur Dissoziation gebundener Quarkoniumzustände führen sollte. Eine unterdrückte Ausbeute von Quarkonium wäre im experimentell gemessenen Dileptonenspektrum zu sehen.

Die Eigenschaften von Quarkoniumzuständen können u.U. mit Hilfe eines einfachen Potentialmodells phänomenologisch untersucht werden. Aufgrund der hohen Masse des "bottom" Quarks (gilt mit Einschränkungen auch für das "charm" Quark) kann der gebundene Zustand quantenmechanisch beschrieben werden, als zwei einzelne Quarks die über ein geeignetes Potential wechselwirken. Es gilt dann, die Schrödinger-Gleichung für das spezifizierte Potential zu lösen woraus die Wellenfunktionen und Bindungsenergien der jeweiligen Eigenzustände folgen.

Es ist wichtig hervorzuheben, dass das in einer Schwerionenkollision erzeugte QGP nicht homogen und lokal isotrop ist. Die vornehmlich entlang der Strahlachse verlaufende Expansion, die zu frühen Zeiten deutlich schneller als die radiale Expansion verläuft, führt zu einer Anisotropie der Teilchenimpulse im lokalen Ruhesystem. Durch die beiden obigen Apekte motiviert unternehmen wir in dieser Arbeit einen ersten Versuch die Effekte der lokalen Anisotropie des Mediums auf das Potential zwischen schweren Quarks zu untersuchen. Wir bestimmen darüber hinaus auch die Verschiebung der Bindungsenergien gebundener Quarkoniumzustände sowie ihrer Zerfallsbreite im Medium.

Theoretischer Hintergrund

Wir beginnen mit der Beschreibung der Hochtemperaturphase der QCD, d.h. des Quark-Gluon Plasma, im Bereich kleiner Eichkopplung g wo störungstheoretische Methoden angewendet werden können. In nullter Ordnung der Entwicklung in der Kopplungskonstanten ist das QGP ein Gas freier, nichtwechselwirkender Partonen. Schwache, als Störung betrachtete Wechselwirkungen ändern dieses Bild etwas. Die Plasmakonstituenten, Quarks und Gluonen mit Impulsen $k \sim T$, nehmen an kollektiven Wechselwirkungen die auf der Impulsskala gT auftreten teil. Es existiert eine Hierarchie von Skalen und Freiheitsgraden die die Konstruktion effektiver Theorien durch Eliminierung von Freiheitsgraden bei höheren Skalen erlaubt. Langwellige Anregungen auf der Skala gT beispielsweise separieren von den Einteilchenanregungen mit typischer Energie und können durch eich-kovariante kinetische Gleichungen vom Typ der Vlasov Gleichung beschrieben werden.

Durch formale Lösung dieser kinetischen Gleichungen für die harten Teilchen können diese harten Freiheitsgrade ausintegriert werden und der induzierte Strom kann allein durch die

weichen Eichfelder ausgedrückt werden. Vernachlässigen wir nichtlineare Effekte so können wir die Gluon Selbstenergie aus dem induzierten Strom ablesen,

$$\Pi^{\mu\nu}_{ab}(P) = g^2\delta_{ab}\int_{\mathbf{k}} V^\mu \frac{\partial f(\mathbf{k})}{\partial K^\beta}\left(g^{\nu\beta} - \frac{V^\nu P^\beta}{P\cdot V + i\epsilon}\right). \tag{0.1}$$

In dieser Gleichung bezeichnet $V_\mu = (1, \hat{\mathbf{k}}) \equiv (1, \mathbf{k}/k)$ die Geschwindigkeit harter, masseloser Partonen deren Verteilungsfunktion $f(\mathbf{k})$ an dieser Stelle beliebig ist. Die Herleitung des Selbstenergietensors ist der Startpunkt für eine Untersuchung der Dispersonsrelationen kollektiver Moden und des Potentials zwischen schweren Quarks.

Um die aus der Transporttheorie gewonnenen Resultate zu überprüfen werden wir auch eine diagrammatische Analyse vorstellen. Quantenfeldtheorien bei endlichen Temperaturen können sowohl im Imaginär- als auch im Realzeitformalismus untersucht werden. Letzterer ist für Anwendungen auf nicht-äquilibrierte Systeme, in unserem Fall also dem anisotropen QCD Plasma, besser geeignet. Wir berechnen die Selbstenergie eines Photons oder Gluons explizit im Rahmen der sogenannten "harte Schleifennäherung" (engl.: "hard-loop approximation") und beweisen damit die Äquivalenz des diagrammatischen und des transporttheoretischen Zugangs.

Mit dem folgenden von Romatschke und Strickland erstmals eingeführten Ansatz für die anisotrope Impulsraumverteilung,

$$f(\mathbf{k}) = f_{\text{iso}}\left(\sqrt{k^2 + \xi(\mathbf{k}\cdot\mathbf{n})^2}\right), \tag{0.2}$$

kann die Gluon Selbstenergie explizit in eine geeignete Tensorbasis zerlegt und berechnet werden. Obige anisotrope Verteilung gewinnt man aus einer isotropen Teilchenverteilung durch entfernen von Teilchen mit hohem Impuls entlang einer gegebenen Anisotropierichtung. Der Parameter ξ bestimmt dabei die Stärke der Anisotropie. Insbesondere folgt, dass für eine thermische Verteilung f_{iso}, die ein ideales Gas beschreibt, und für kleinen Anisotropieparameter ξ dieser wiederum in Beziehung zur Scherviskosität des Plasmas steht.

Zur Berechnung des "hard-loop" resummierten Gluonpropagators im anisotropen Plasma benutzen wir die Dyson-Schwinger Gleichung

$$iD^* = iD + iD\left(-i\Pi\right)iD^*. \tag{0.3}$$

D^* und D bezeichnen jeweils den resummierten und den nackten Propagator. Durch einsetzen des expliziten Ausdrucks für die Selbstenergie bestimmen wir daraus den resummierten Propagator in allgemeinen linearen Eichungen. Dieser ermöglicht uns dann die Definition des Quark-Antiquark Potentials als Fourier Transformation des Propagators im statischen Grenzfall. Dieses aus dem Eingluonaustausch perturbativ bestimmte Potential beschreibt die $Q\bar{Q}$ Wechselwirkung bei kurzen Abständen.

Ergebnisse

Die Wechselwirkung schwerer Quarks im anisotropen QCD Plasma

Im Realzeitformalismus definieren wir das Wechselwirkungspotential statischer Quarks (durch Eingluonaustausch) aus der Fourier-Transformation der physikalischen "11" com-

ponent des statischen Gluon Propagators:

$$V(\mathbf{r},\xi) \;=\; -g^2 C_F \int \frac{\mathrm{d}^3\mathbf{p}}{(2\pi)^3}\,(e^{i\mathbf{p}\cdot\mathbf{r}}-1)\left(D^{*00}(p_0=0,\mathbf{p},\xi)\right)_{11}\,. \tag{0.4}$$

Wir haben in dieser Gleichung auch einen $\mathbf{r}$-unabhängigen Term eingeführt der als die perturbative freie Energie des Quarkpaares bei unendlicher Separation angesehen werden kann; dies entspricht dem Doppelten der freien Energie eines einzelnen schweren Quarks im Plasma. Im statischen Grenzfall gilt $(D^{*00})_{11} \equiv \frac{1}{2}(D^{*00}_R + D^{*00}_A + D^{*00}_F)$, and $\frac{1}{2}(D^{*00}_R + D^{*00}_A) = D^{*00}_R = D^{*00}_A$. Die FOURIER Transformation des retardierten bzw. des avancierten Propagators bestimmt den Realteil des Potentials, aus dem sich wiederum die Bindungsenergien ergeben. Das Potential besitzt ausserdem einen Imaginärteil der von der FOURIER Transformation des symmetrischen Propagators kommt.

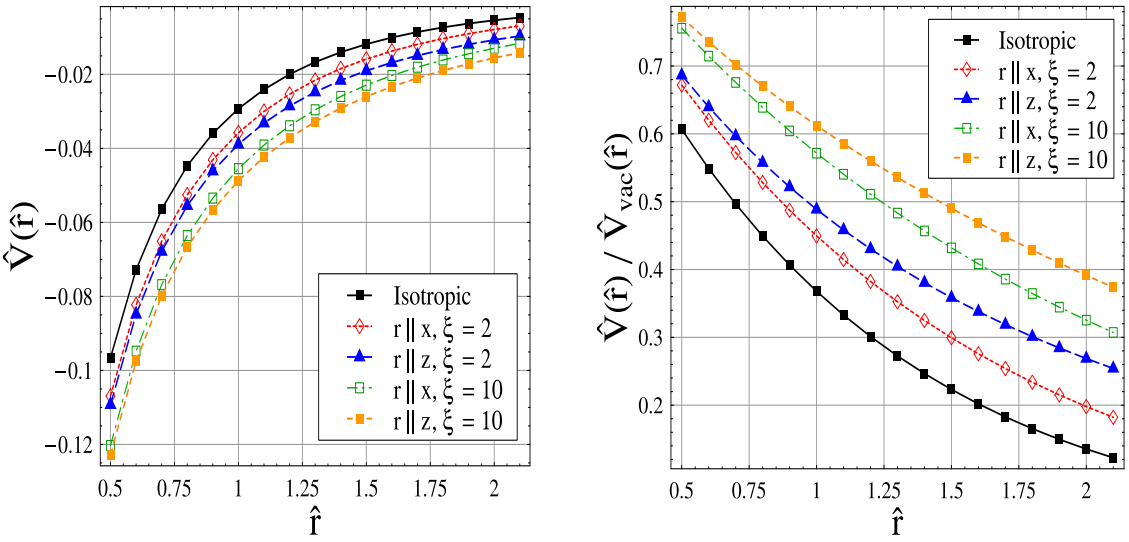

Figure 0.1: Das Potential zwischen schweren Quarks in führender Ordnung als Funktion des Abstands ($\hat{r} \equiv r m_D$) für $\hat{V}(\mathbf{r} \parallel \mathbf{n}, \xi)$ und $\hat{V}(\mathbf{r} \perp \mathbf{n}, \xi)$. Hierbei entspricht $\mathbf{r} \parallel \mathbf{z}$ einer Ausrichtung parallel zur Plasmaanisotropie während $\mathbf{r} \parallel \mathbf{x}$ dazu senkrechter Ausrichtung korrespondiert.
Links: das Potential dividiert durch die DEBYE Masse und Kopplung, $\hat{V} \equiv V/(g^2 C_F m_D)$.
Rechts: Potential relativ zum Vakuum.

Numerisch gewonnene Ergebnisse für den Realteil des Potentials sind in Fig. 0.1 für verschiedene Werte von ξ gezeigt. Wir sehen, dass die Abschirmung durch das Plasma im allgemeinen reduziert ist, d.h. dass das Potential bei $\xi > 0$ tiefer und näher am Vakuumspotential ist. Dieser Effekt ist zum Teil auf die niedrigere Dichte des anisotropen Plasmas zurückzuführen. Allerdings ist der Effekt als Funktion des Polarwinkels nicht uniform: die Winkelabhängigkeit verschwindet bei kurzen Abständen $\hat{r} \equiv r m_D$ (m_D ist die DEBYE Masse) schneller, während wir bei großen Abständen eine stärkere Anziehung in Richtung der Anisotropie beobachten. Man erwartet daher, dass Quarkoniumzustände deren Wellenfunktion auf das Potential bei Längenskalen $\hat{r} \sim 1$ sensitiv sind im anisotropen Plasma stärker gebunden sind, vor allem wenn das Quark-Antiquark Paar entlang $\mathbf{n}$ ausgerichtet ist.

Der Imaginärteil des Potentials kann analytisch in führender Ordnung von ξ bestimmt werden und ist in Fig. 0.2 gezeigt. Wir finden, dass dieser (betragsmässig) mit ξ (bzw. mit der Viskosität) abfällt. Das impliziert, dass die Quarkonium Zerfallsbreite in führender Ordnung der Viskosität ebenfalls kleiner ist. Für Zustände sehr schwerer Quarks, deren BOHR Radien $\sim 1/(g^2 M_Q)$ kleiner als die DEBYE Länge $1/m_D$ ist, liefert eine grobe Abschätzung, dass die Zerfallsbreite bereits für moderate Anisotropie, $\xi \simeq 1$, um ungefähr 50% gegenüber einem idealen, vollständig äquilibrierten Plasma absinkt.

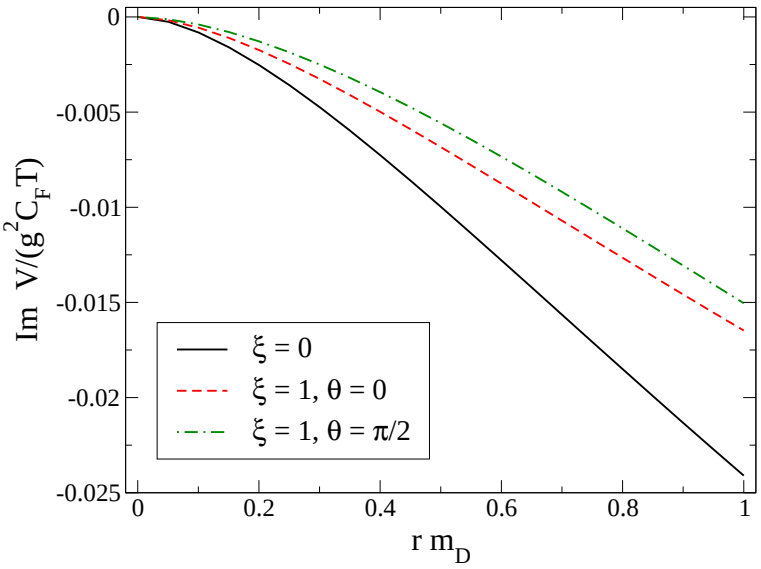

Figure 0.2: Imaginärteil des statischen Potentials als Funktion des Abstands ($\hat{r} \equiv r\, m_D$). Die vertikale Achse zeigt Im $V/(g^2 C_F T)$. Die Kurven korrespondieren, von unten nach oben, zu Anisotropieparametern und Polarwinkeln von $\xi = 0$ und $\xi = 1$, $\theta = 0$, $\theta = \pi/2$.

Quarkoniumzustände im anisotropen QCD Plasma

Das Potential bei kurzen Abständen folgt aus dem "hard-loop" resummierten Gluonpropagator. Dies reicht allerdings nicht aus um die Eigenschaften von Charmonium und Bottomonium im Medium zu bestimmen. Der langreichweitige Teil der Wechselwirkung kann allerdings nicht störungstheoretisch berechnet werden. Wir folgen daher dem Modell von KARSCH-MEHR-SATZ (KMS) demzufolge die gleiche Abschirmskala m_D, die für die Abschirmung des COULOMB Potentials sorgt, auch im nicht-perturbativen, langreichweitigen Beitrag vom QCD "String" auftaucht. Die "String"-Wechselwirkung ist also auf der gleichen Längenskala wie das COULOMB Feld abgeschirmt. Wir übertragen diese Annahme auf das anisotrope Plasma indem wir die DEBYE Masse $m_D(T)$ durch eine anisotrope Abschirmung $\mu(\theta; \xi, T)$ ersetzen die effektiv durch das perturbative DEBYE-COULOMB Potential bestimmt wird, und gewinnen somit eine Verallgemeinerung des KMS Potentialmodells für anisotrope Plasmen. Aus den Lösungen der drei-dimensionalen SCHRÖDINGER Gleichung mit diesem phänomenologischen Potential erhalten wir dann Bindungsenergien für diverse Quarkoniumzustände.

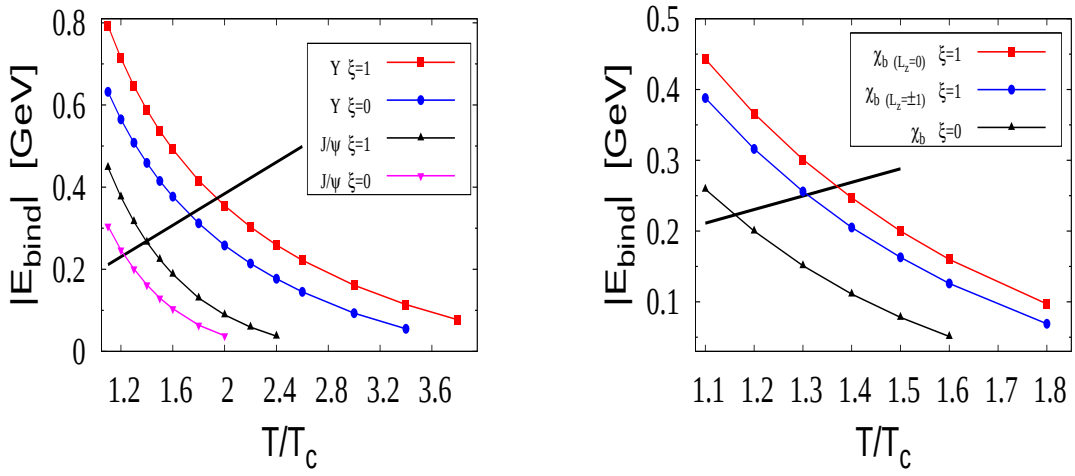

Figure 0.3: Links: Temperaturabhängigkeit der Bindungsenergien $|E_{\rm bind}|$ der Grundzustände von Charmonium (untere Kurven) und Bottomonium (obere Kurven) im Vektorkanal für zwei verschiedenen Werte der Plasmaanisotropie ξ. Die Gerade entspricht der Temperature selbst.
Rechts: Temperaturabhängigkeit der Bindungsenergien der $1P$ Zustände von Bottomonium für zwei verschiedenen Werte von ξ. Die Gerade entspricht der Temperature selbst.

Die zwei Hauptresultate sind in Fig. 0.3 dargestellt. Für festes T wächst die Abschirmmasse mit ansteigendem ξ. Der asymptotische Wert des Potentials ist im KMS Modell intrinsisch mit der Abschirmmasse über $V_\infty(\theta) \sim 1/\mu(\theta;\xi,T)$ verbunden. Schwächere Abschirmung enspricht daher einem höheren Potential bei unendlichem Abstand was zu einer höheren Bindungsenergie führt. Dieser Effekt ist selbst für moderate Anisotropien von $\xi \simeq 1$, wie sie hier betrachtet werden, signifikant: wir finden beispielsweise, dass sich die Bindungsenergie des Bottomonium Grundzustands knapp oberhalb von T_c um etwa 30% erhöht, die von $1S$ Charmonium und von $1P$ Bottomonium steigt sogar um bis zu 50%. Solche Zustände könnten daher bis zu höheren Temperaturen als im Gleichgewicht existieren (für $\xi = 0$ dissoziieren das J/ψ und das Υ bei $1.2\,T_c$ bzw. bei $1.8\,T_c$, in Übereinstimmung mit vorangegangenen Studien im Rahmen von Potentialmodellen).

Wir finden darüber hinaus einen weiteren neuen Effekt, nämlich dass die Winkelabhängigkeit des Potentials im anisotropen Medium eine Polarisation von Zuständen mit nichtverschwindendem Drehimpuls induziert. Nach unseren Abschätzungen ist die Aufspaltung des χ_b mit $L_z = 0$ bzw. $L_z = \pm 1$ von der Grössenordnung 50 MeV. Bei $T \simeq 200$ MeV würde daher die Besetzung des Zustands mit $L_z = 0$ um ca. 30% höher als die der Zustände mit Drehimpuls entlang der Anisotropie sein (aufgrund des Boltzmann Faktors). Eine experimentelle Bestätigung solch einer Polarisation am RHIC oder LHC könnte Evidenz für eine nichtverschwindende Viskosität des QCD Plasmas in der Umgebung von T_c liefern.

Die Motivation das KMS Modell zu adoptieren liegt in seiner recht einfachen funktionalen Form die eine Verallgemeinerung auf anisotrope Plasmen ermöglicht. Es wird allerdings weitgehend nur ein qualitatives Verständnis der Eigenschaften von Quarkonium im Medium

ermöglichen. Für präzisere Vorhersagen sind verfeinerte Beschreibungen notwendig. Auch unsere grobe Abschätzung der Dissoziation bei $|E_{\mathrm{bind}}| \sim T$ ist eher qualitativer Natur. Für realistische Quarkonia sind perturbativen Berechnungen des Potentials nicht sehr zuverlässig. Eine präzisere Bestimmung der Breite der Quarkoniumzustände erfordert ebenfalls weitere Untersuchungen und die Berücksichtigung zusätzlicher Beiträge wie z.B. von Kollisionen.

Abstract

In this work we study the properties of quarkonium states in a quark-gluon plasma which, due to expansion and non-zero viscosity, exhibits a local anisotropy in momentum space. We determine the hard-loop resummed gluon propagator in an anisotropic QCD plasma in general linear gauges and define a potential between heavy quarks from the FOURIER transform of its static limit. This potential which arises due to one-gluon exchange describes the force between a quark and anti-quark at short distances. It is closer to the vacuum potential as compared to the isotropic DEBYE screened potential which indicates the reduced screening in an anisotropic QCD plasma. In addition, angular dependence appears in the potential; we find that there is stronger attraction on distance scales on the order of the inverse DEBYE mass for quark pairs aligned along the direction of anisotropy than for transverse alignment. The potential at long distances, however, is non-perturbative and modeled as a QCD string which is screened at the same scale as the COULOMB field. At asymptotic separation the potential energy is non-zero and inversely proportional to the temperature. With a phenomenological potential model which incorporates the different behaviors at short and long distances, we solve the three-dimensional SCHRÖDINGER equation. Our numerical results show that quarkonium binding is stronger at non-vanishing viscosity and expansion rate, and that the anisotropy leads to polarization of the P-wave states. Furthermore, we determine viscosity corrections to the imaginary part of the heavy-quark potential in the weak-coupling hard-loop approximation. The imaginary part is found to be smaller (in magnitude) than at vanishing viscosity. This implies a smaller decay width of quarkonium bound states in an anisotropic plasma.

Contents

1 Introduction

1.1 The quark-gluon plasma

It is believed that the matter in the universe was created during the Big Bang about 14 billion years ago [1, 2]. This cosmological model describes the initial conditions and subsequent development of the universe. After the Big Bang [1], the universe continued to grow in size and fall in temperature. At about 10^{-6} seconds, a quark-hadron phase transition happened when the universe was at a temperature of approximately 150– 200 MeV [3, 4]. In heavy-ion experiments, it is expected to reproduce the conditions which have existed for a brief time shortly after the Big Bang, with temperatures exceeding 200 MeV$\sim 2 \times 10^{12}$ K. The Relativistic Heavy-Ion Collider (RHIC) at Brookhaven National Labs in New York and the Large Hadron Collider (LHC) at European Center for Particle Physics (CERN) in Geneva, Switzerland are used to collide ions travelling at relativistic speeds which enables physicists to study the primordial form of matter that existed in the universe shortly after the Big Bang. Over the past twenty years, one of the most important aims in the heavy-ion experiments is to explore a new form of matter: the *quark-gluon plasma* (QGP), which has been predicted by lattice Quantum Chromodynamics at finite temperature [5].

Our current understanding of the heavy-ion experiments is such that when nuclei are collided at very high energies, it is expected that in the central collision region a very hot dense pocket of nuclear matter will be formed. In this extreme condition, hadrons dissolve into a gas of almost free quarks and gluons which is the so-called quark-gluon plasma [6]. To estimate when the transition to the QGP phase takes place, one can use the bag model which attempts to incorporate the two main features of QCD: asymptotic freedom and confinement. In this model, quarks move freely inside the bag where the interactions with gluons are neglected. Outside the bag, quarks and gluons are no longer free particles. Such a picture can be achieved by the introduction of a constant energy density for the vacuum in order to keep quarks and gluons confined. By calculating the pressure in the plasma and hadron phases, we can determine the critical temperature at which the quark-hadron phase transition happens. At zero chemical potential ($\mu_B = 0$), with certain degrees of freedom for the two different phases [2], the bag model predicts the critical temperature is about 150 MeV. Here, we refer the temperature for which the system undergoes the phase transition as the critical temperature. In fact, the transition between the confined hadronic phase and the deconfined QGP phase is not defined in the strict statistical mechanical sense. The QGP transition may in fact be a "crossover" [7]. The corresponding energy density at the

[1] The hot and dense phase at the very beginning of the universe evolution is itself referred to as the "Big Bang".

[2] The hadronic system mainly consists of pions. The degrees of freedom for a gas of massless pions are 3. In the QGP phase, the bosonic degrees of freedom are $2(N_c^2 - 1)$, where N_c is the number of colors. While for fermions, they are $2N_cN_f$, with N_f being the number of flavors. So the physical degrees of freedom for quarks and gluons are 12 and 16, respectively.

critical point is about $1\,\mathrm{GeV}\cdot\mathrm{fm}^{-3}$, roughly 7.5 times that of normal nuclear matter.

Actually, at zero chemical potential the lattice QCD simulation confirms the above critical temperature [8, 9, 10, 11]. As shown in Fig. 1.1, there is a sharp rise of the energy density in the vicinity of the critical temperature. This can be understood as a signal of the phase transition. Since the sharp rise of the energy density occurs in a narrow range of temperatures, one can expect that the change in the degrees of freedom between the confined and deconfined phases leads to such a rapid rise. Note that the energy density is roughly proportional to the number of degrees of freedom. For $N_f = 2$ [3], the critical temperature is about 150 MeV, approximately the same as that obtained by the rough estimate with the bag model.

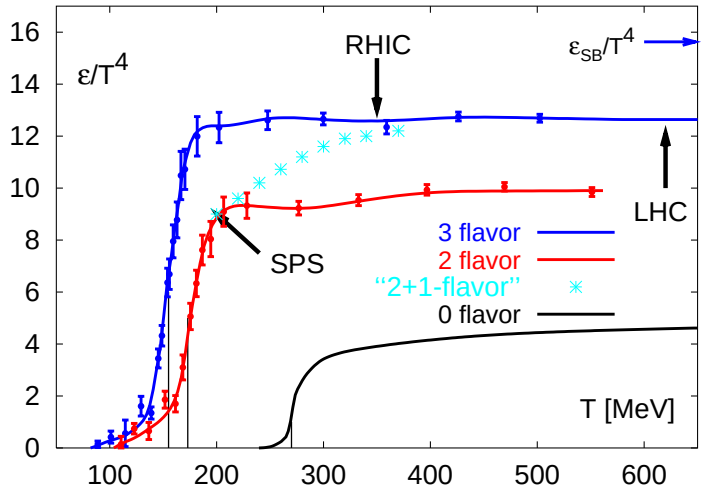

Figure 1.1: The energy density as a function of temperature scaled by T^4 from lattice QCD. Various number of species of quarks are shown in this figure. Figure taken from [12].

In principle the bag model could be used to determine the transition line between hadronic phase and plasma phase in the whole (μ_B, T) plane which generates the *QCD phase diagram*. Due to the crudeness of the model, it is much less convincing for non-zero chemical potential. In fact, the full structure of the phase diagram is complicated and it requires a combination of several models. As shown in Fig. 1.2, at low temperature and baryon density, it is a hadronic confined phase and chiral symmetry is broken in this phase. At high baryon density and low temperature, the color-superconducting phase exists [13]. At high temperature, the quarks and gluons are deconfined and the chiral symmetry is restored in the QGP phase [14]. The early universe descended from high temperature at extremely small baryon chemical potential while neutron star cores have high baryon chemical potential at lower temperature.

[3] Since the critical temperature is on the order of 10^2 MeV, which is much smaller than the masses of charm, bottom and top quarks. These heavy quarks are not relevant for the physics near the deconfinement transition. So the number of quark flavors is restricted to $N_f = 3$. The up and down quarks can be treated as massless particles and the strange quark has a intermediate mass, therefore the number of active quark flavors near the transition point is between 2 and 3, which is denoted as $N_f = 2 + 1$.

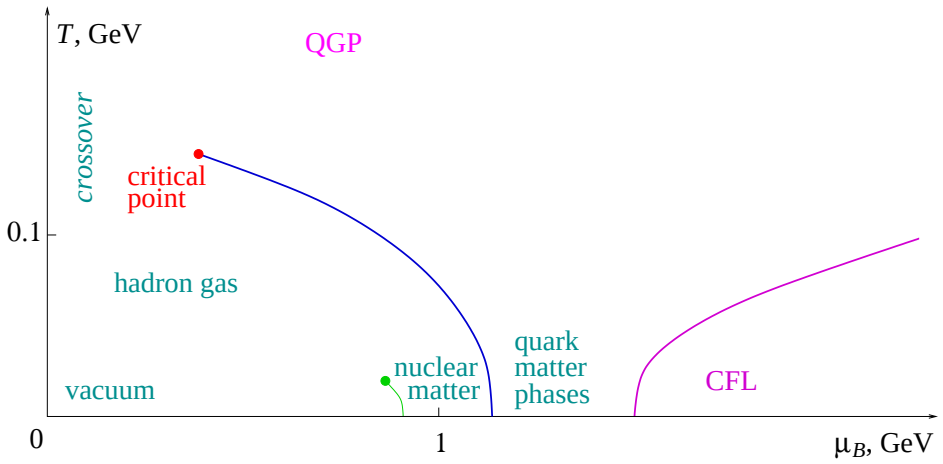

Figure 1.2: Semi-quantitative QCD phase diagram. Figure taken from [15].

1.2 Quantum Chromodynamics

The well-established quantum field theory which is considered to be one of the most successful theories in modern physics is the Quantum Electrodynamics (QED). Such a theory provides an accurate description to the electromagnetic interactions. It is an Abelian gauge theory with gauge group U(1) and the gauge boson associated with the gauge group is photon. The corresponding quantum field theory of the strong interaction, a fundamental force describing the interactions of quarks and gluons is Quantum Chromodynamics (QCD) [16, 17, 18]. Bearing several similarities to QED, QCD is a quantum field theory of a special kind called a non-Abelian gauge theory, having the color group SU(3) as a gauge group. The corresponding gauge bosons associated with the SU(3) color group are gluons. Unlike the single photon in QED, there are eight independent types (or colors) of gluons in QCD which correspond to eight independent color states. Gluons themselves carry color charge and therefore participate in the strong interaction in addition to mediating it. This is different from the electric charge neutral photon in QED. Actually, the gluon-gluon interactions make QCD significantly harder to analyze than QED.

QCD is an important part of the Standard Model of particle physics. In this theory, quarks are introduced as spinor fields in N_f flavors [4] in the fundamental representation of the color gauge group, SU(3). The gluons are vector fields in the adjoint representation of color SU(3). For a general gauge group, the number of force-carriers (like photons or gluons) is always equal to the dimension of the adjoint representation. As mentioned before, QCD enjoys two peculiar properties: *asymptotic freedom* and *confinement*.

In quantum field theory, a beta-function $\beta(g)$ encodes the running of a coupling parameter, g. It is defined by the relation:

$$\beta(g) = \mu \frac{\partial g}{\partial \mu} \equiv \frac{\partial g}{\partial \ln \mu} \,. \tag{1.1}$$

[4] Again, N_f corresponds to the active flavors with masses much smaller than the energy scale under consideration.

In QED, one finds by using perturbation theory that the beta-function is positive. So the corresponding coupling increases with increasing energy. In non-Abelian gauge theories, the beta-function can be negative. In QCD, the renormalized coupling shows renormalization scale μ dependence. The running coupling $\alpha_s(\mu)$ can be written as:

$$\alpha_s(\mu) \equiv \frac{g^2}{4\pi} \approx \frac{4\pi}{\beta_0 \ln \frac{\mu^2}{\Lambda^2_{\mathrm{QCD}}}}\,, \tag{1.2}$$

where the QCD scale $\Lambda_{\mathrm{QCD}} \sim 200\,\mathrm{MeV}$ and β_0 is the coefficient at one-loop order of the beta-function. The coupling becomes smaller at shorter distances or with larger momentum transfers ($\alpha_s \to 0$ as $\mu \to \infty$). Asymptotic freedom means that in very high-energy reactions, quarks and gluons interact very weakly. This prediction of QCD was first discovered in the early 1970s by David Politzer [18] and by Frank Wilczek and David Gross [17]. In high-energy regime, perturbative QCD becomes a powerful tool to study the strong interaction. However, as energy scale gets smaller, the coupling constant becomes larger. As a result, the perturbation theory breaks down in this strong-coupled theory. In contrast to QCD, the coupling constant in Abelian gauge theory increases for larger energy scales. The experimental verification of the running coupling and asymptotic freedom is in excellent agreement with the predictions from QCD [19].

Confinement means that there is no single quark as a color-triplet state observed experimentally. Only color-singlet bound states can propagate over macroscopic distances. Because of this, it would take an infinite amount of energy to separate two quarks; they are forever bound into hadrons such as the proton and the neutron. The constituent quarks in a hadron cannot be separated from their parent hadron, and this is why quarks can never be studied or observed in any more direct way than at a hadron level. Although analytically unproven, confinement is widely believed to be true because it explains the consistent failure of free quark searches, and it is easy to demonstrate in lattice QCD.

The analysis of such a non-Abelian theory is very complicated. Several theoretical methods have been proposed. As we already mentioned before, perturbative QCD which is based on asymptotic freedom, can provide predictions accurately to experiments performed at very high energies. The large N_c expansion is a well-known approximation scheme which starts from the premise that the number of colors is infinite, and makes a series of corrections to account for the fact that it is not. Until now it has been the source of qualitative insight rather than a method for quantitative predictions. Modern variants include the anti-de-Sitter space/conformal field theory (AdS/CFT) approach [20, 21, 22]. The Monte-Carlo simulations of QCD on the lattice provides a non-perturbative approach to study the strong interactions [5, 23]. This approach uses a discrete set of space-time points to reduce the analytically intractable path integrals of the continuum theory to a very difficult numerical computation which is then carried out on supercomputers like the QCDOC [5] which was constructed for precisely this purpose. While it is a slow and resource-intensive approach, it has wide applicability, giving insight into parts of the theory inaccessible by other means. So far, this is the only method which can provide quantitative results for the intermediate energy range near the deconfinement transition. For specific problems some theories

[5] The abbreviation for Quantum Chromodynamics On a Chip which is a supercomputer designed and built jointly by University of Edinburgh, Columbia University, the RIKEN Brookhaven Research Center and IBM.

may be written down which seem to give qualitatively correct results. In the best of cases, these may then be obtained as systematic expansions in some parameter of the QCD Lagrangian. Among the best such effective models one should now count chiral perturbation theory (which expands around light-quark masses near zero) [24], heavy-quark effective theory (which expands around heavy-quark mass near infinity) [25], and soft-collinear effective theory (which expands around large ratios of energy scales) [26, 27]. Other less accurate models are the Nambu-Jona-Lasinio model and the chiral model.

1.3 Heavy quarkonia in quark-gluon plasma

The results from the heavy-ion experiments have shown very rich physics which can not be interpreted by simple extrapolation from proton-proton collisions. For example, hadron spectra at high transverse momentum region are suppressed by up to a factor of 5 relative to proton-proton collisions, which is indicative for a strong absorption of high-energy partons traversing the medium [28]. The inclusive production of charm-quark bound states (J/Ψ mesons) is suppressed by a factor of 3– 5 at both Super Proton Synchrotron (SPS) and RHIC, indicative for their dissolution in the medium [29, 30, 31]. Such information may imply that a new form of matter could be generated in the heavy-ion experiments which is the so-called quark-gluon plasma. Physicists have made many efforts to obtain the convincing evidence of the existence of QGP in heavy-ion collisions. Among different experimental observations which may be served as the signals for the QGP formation, heavy quarkonium dissociation has been proposed long time ago as a clear probe of the QGP formation in colliders [32].

Unlike light quarks, due to their smaller size, bound states of heavy quarks could survive inside the plasma to temperatures higher than the deconfinement temperature. However, in a deconfined matter the force between the constituents of a quarkonium state, a heavy quark and its anti-quark, is weakened due to the presence of the color screening produced by the light quarks and gluons. It was suggested by Maisui and Satz that this screening leads to the dissociation of quarkonium bound states [32]. Since higher excited quarkonium states are more weakly bound than lower ones, as the temperature increases, quarkonia will dissociate subsequently from the higher to the lower states which could provide a thermometer of the quark-gluon plasma [33]. A suppressed yield of quarkonium can be visible in the dilepton spectrum, which is measured in experiments.

Theoretically, we can study the quarkonium states by using effective field theories. If we assume that the quark mass M_Q is much larger than any other scales in the system, in particular $\Lambda_{\rm QCD}$, the heavy quark and anti-quark are expected to move slowly about each other at a relative velocity $v_Q \ll 1$. The effective field theory based on these assumptions is non-relativistic QCD (NRQCD) [34, 35, 36]. Since $M_Q \gg \Lambda_{\rm QCD}$, NRQCD can be made equivalent to QCD at any desired order in $1/M_Q$ and $\alpha_s(M_Q) \ll 1$ by enforcing suitable matrix elements to be equal at that order in both theories. However, such an effective theory does not fully exploit the fact that v_Q is small. The typical relative three-momentum of the heavy quarks which is at the order of $M_Q v_Q$, remains explicit degrees of freedom in NRQCD whereas they can never be produced at energies $\sim M_Q v_Q^2$. For lower lying states the scale $M_Q v_Q$ corresponds both to the typical momentum transfer and to the typical relative three-momentum. It is then convenient to introduce a further effective field theory where degrees of freedom of energy $\sim M_Q v_Q$ are integrated out. This effective field theory

is called potential non-relativistic QCD (pNRQCD) [25, 37]. The degrees of freedom of pNRQCD depend on the interplay of the scales $M_Q v_Q$, $M_Q v_Q^2$ and $\Lambda_{\rm QCD}$.

The basic tools of phenomenological approach to study the properties of quarkonium states are *potential models*. Due to the fact that the bottom and, to a lesser extent, the charm masses are large as compared to $\Lambda_{\rm QCD}$, the non-relativistic potential models have been widely used to study quarkonium. In the non-relativistic limit, a quantum mechanical description of the bound states based on two heavy quarks interacting through a suitable potential appears reasonable. One can study the quarkonium bound states by solving the SCHRÖDINGER equation with some specified potential which determines the wave-functions and the corresponding binding energies for different bound states. The potential is usually chosen in such a way that at short distances it coincides with the weak-coupling QCD one-gluon exchange COULOMB potential and in the long range it incorporates confinement, for instance, by including a linearly rising potential. The potential at short distances can be computed by perturbative QCD, whereas its long distance shape can be computed by lattice simulations. Relativistic effects are also taken into account in potential models. Such effects appear to be sizable for some states, mostly in charmonium.

At zero temperature, the CORNELL potential which takes a form of a COULOMB plus a linear part has made great success. It describes well the experimentally observed quarkonium spectroscopy and also agrees with the lattice simulation [38, 39]. Actually, the CORNELL potential can be derived directly from QCD as an effective field theory (pNRQCD) by integrating out modes above the scales M_Q and then $M_Q v_Q$, respectively [25, 37]. At finite temperature, the essence of the potential model in the context of deconfinement is to use a finite temperature extension of the zero temperature CORNELL potential to understand the modifications of the quarkonia properties in the medium. In the pioneering paper, KARSCH, MEHR and SATZ introduced a potential model at finite temperature by using a phenomenological screened CORNELL potential [40]. This is all right for merely qualitative purposes. Quantitative understanding of the bound state properties needs the exact potential at finite temperature which, in principle, should be derived directly from QCD, just as the CORNELL potential at zero temperature. Such derivation, however, is complicated by the existence of temperature-driven scales, T, gT, g^2T and has only been addressed recently [41]. Due to these difficulties, the lattice-based potentials become popular. The lattice simulation provides the information of the singlet free energy or internal energy of a static quark antiquark ($Q\bar{Q}$) pair. However, neither the free energy nor the internal energy can be directly used as the potential. The free energy contains an entropy contribution and can be only considered as a lower limit of the potential; while the internal energy was thought to serve as a sort of upper limit since at very small separation, there is no entropy should be extracted from the free energy. In fact, what kind of screened potential should be used in the SCHRÖDINGER equation, that describes well the bound states at finite temperature is still an open question. The lattice data only provide some constraints on the potential models.

Besides the binding energy which can be obtained by solving the SCHRÖDINGER equation with a specified potential, the decay width is another quantity which is also important to determine the dissociation of the bound states. The calculation based on a real-valued potential model doesn't include the true width of a state. Therefore just seeing the peak structure in these spectral functions [6] is incomplete on its own and can be misleading.

[6] Spectral function is an alternative approach to study the properties of quarkonium states at finite tem-

Actually, the static potential was calculated in the weak-coupling resummed perturbation theory with hard-thermal-loop (HTL) approximation in the regime where the inverse size of the bound state is much larger than the DEBYE mass. By performing an analytical continuation of the Euclidean WILSON loop to Minkowski space, the potential has an imaginary part which clearly broadens the peak [41, 48].

1.4 Anisotropic system

Over the last decades, the problem of in-medium modification of inter-quark forces was extensively studied in terms of finite-temperature heavy-quark potentials. However, all the studies were limited in an isotropic quark-gluon plasma where the parton distributions can be described by the FERMI-DIRAC or BOSE-EINSTEIN distributions. Actually, the parton system generated in the ultra-relativistic heavy-ion collisions can not be homogeneous and isotropic. The utilization of equilibrium field theory requires a fast thermalization of the system so that at least a local scale can be described by the equilibrium field theory.

In a heavy-ion collision the longitudinal expansion (along the beam-line) is the most relevant, because at early times it is much faster than the radial expansion. At weak coupling this longitudinal expansion causes the system to quickly become much colder in the longitudinal than in the transverse (radial) direction. As a result, an anisotropy in momentum space develops. As has been pointed by MRÓWCZYŃSKI [49, 50, 51], due to anisotropic momentum distributions the parton system produced at the early stage of relativistic heavy-ion collisions is unstable with respect to the chromo-magnetic plasma modes. The instabilities work to isotropize the system and thus speed up the process of its equilibration.

Actually, the color kinetic instabilities are fully analogous to the WEIBEL instabilities known in the electromagnetic plasma [52]. In plasma physics, it has been shown that the instabilities generate strong magnetic fields resulting in the filamentation of the electron current by simulations and experiments [53, 54]. It is interesting to investigate the effects that an anisotropic momentum distribution function has on the thermalization, or more precisely the isotropization of the quark-gluon plasma. ARNOLD, LENAGHAN and MOORE investigated the case corresponding to the infinitely large anisotropy [55], and argued that it drastically modifies the scenario of "bottom-up" thermalization advocated by BAIER, MUELLER, SCHIFF and SON [56], which would then have to be replaced by a different scheme. The accelerated equilibration is obviously very important though it is only an indirect signal. It has been suggested that strong chromo-magnetic fields generated by the instabilities can lead to a specific pattern of jet's deflections [57, 58].

MRÓWCZYŃSKI and RANDRUP have performed a phenomenological estimate of the growth rate of the instabilities for scenarios relevant to the quark-gluon plasma by using a specified anisotropic distribution function [59]. They found that the degree of amplification of the instabilities is not expected to dominate the dynamics of the quark-gluon plasma, but instead their effect would be comparable to the contribution from elastic BOLTZMANN collisions. However, they also pointed out that if a large number of unstable modes would be excited then their combined effect on the overall dynamics could well be significant.

Motivated by the above introduction, in this work, we make a first attempt to investigate the effects due to a local anisotropy in momentum space on the heavy-quark potential and

perature. More information can be found in Refs. [42, 43, 44, 45, 46, 47].

the corresponding binding energies. In addition, we also study how the anisotropy will affect the decay width of the quarkonium bound states. Particularly, we will concentrate on a comparison between the behavior of the quarkonium states in an equilibrium plasma and that in an anisotropic plasma with a specified anisotropic distribution function firstly introduced by Strickland and Romatschke [60].

1.5 Outline of this work

This work is organized as follows. In Chapter 2, we introduce the kinetic theory for QCD plasmas. By solving the non-Abelian Vlasov equations which are also known as the collisionless transport equations for quarks and gluons, we get the induced current which occurs due to the deviation from the colorless state. In the weak-coupling limit, the theory becomes effectively Abelian. Neglecting the non-linear effects, the gluon self-energy tensor can be simply obtained from the induced current. We also discuss the dispersion relations for an equilibrium QCD plasma by finding the zeros in the gluon self-energy tensor.

In order to know to what extent the results from the transport theory approach are reliable, a QCD diagrammatic analysis is discussed in Chapter 3. The quantum field theory at finite temperature can be performed in both imaginary time formalism and real time formalism. The latter is more appropriate for dealing with the non-equilibrium situations; one example is the anisotropic QCD plasma we are interested in the work. We perform the explicit calculations of photon or gluon self-energy with the so-called hard-loop [7] (HL) approximation which shows the full equivalence of the two different approaches: transport theory approach and diagrammatic approach.

In Chapter 4, we extend the discussion to a hot QCD plasma which, due to expansion and non-zero viscosity, exhibits a local anisotropy in momentum space. With the specified anisotropic distribution function which is obtained from an isotropic distribution by removing particles with a large momentum component along some direction of anisotropy, we determine the gluon self-energy tensor for such an anisotropic system. The dispersion relations are also discussed. Unlike the isotropic system, unstable modes appear when the distribution of the parton system becomes anisotropic which may cause the system to be unstable with the exponentially growing chromo-magnetic fields. Finally, we give a brief introduction about the qualitative origin of the instabilities.

In Chapter 5, we investigate the static potential between heavy quark and anti-quark pairs. At leading order in the perturbative expansion, the potential arises due to one-gluon exchange which can be defined from the Fourier transform of the gluon propagator in the static limit. The hard-loop resummed gluon propagator in an anisotropic QCD plasma is determined in general linear gauges and a possible gauge independent definition of the static potential is discussed. Our results show that there is stronger attraction on distance scales on the order of the inverse Debye mass for quark pairs aligned along the direction of anisotropy than for transverse alignment. Some analytical estimates of the binding energy for quarkonium bound states are discussed in the limit of extremely large quark mass which

[7] Note that the HTL approach can be applied to any momentum distribution of hard particles which is static and homogeneous [61]. When dealing with a far from equilibrium system, the term "thermal" is rather misleading and one uses "hard-loop" instead. In this work, we assume that the deviation from the equilibrium is moderate.

indicates the heavy quarkonia are bound more strongly in an anisotropic QCD plasma.

The in-medium properties of charmonium and bottomonium are investigated in Chapter 6. At short distances the heavy-quark potential is known at tree level from the hard-loop resummed gluon propagator in anisotropic perturbative QCD. The potential at long distances is modeled as a QCD string which is screened at the same scale as the COULOMB field. At asymptotic separation the potential energy is non-zero and inversely proportional to the temperature. We obtain numerical solutions of the three-dimensional SCHRÖDINGER equation for this potential. Our results show that quarkonium binding is stronger at non-vanishing viscosity and expansion rate, and that the anisotropy leads to polarization of the P-wave states.

The decay width of the bound states in an anisotropic QCD plasma is studied in Chapter 7. As real time formalism is employed, we determine viscosity corrections to the retarded, advanced and symmetric gluon self-energies and to the static propagators in the weak-coupling hard-loop approximation to high-temperature QCD. We apply these results to calculate the imaginary part of the heavy-quark potential which is found to be smaller (in magnitude) than at vanishing viscosity. This implies a smaller decay width of quarkonium bound states in an anisotropic plasma.

We give the conclusions and outlook of this work in Chapter 8.

2 Kinetic theory for hot QCD plasmas

We start with the description of the high temperature phase of QCD, the so-called quark-gluon plasma, in a regime where the effective gauge coupling constant g becomes small enough and the weak-coupling calculations become feasible [62, 63]. The resulting picture of the quark-gluon plasma is very similar in many respects as an ordinary electromagnetic plasma in the ultra-relativistic regime [64] with, however, some specific effects due to the non-Abelian nature of QCD [65, 66, 67].

At zeroth order in an expansion in powers of the coupling at high temperature T, the quark-gluon plasma is a gas of non-interacting partons. The appearance of interactions will slightly change this simple picture. The plasma constituents, i.e. the quarks and gluons, with momenta $k \sim T$ will take part in collective excitations, which typically develop at a momentum scale gT. At weak coupling, there exists a hierarchy of scales and degrees of freedom which enables us to construct effective theories at various scales by eliminating the degrees of freedom at higher scales [65, 66, 68, 69]. For example, the long wavelength excitations with typical momentum scale gT which are well separated from the typical energy of single particle excitations can indeed be described by simple gauge-covariant kinetic equations of the VLASOV type [70, 69].

By formally solving these kinetic equations for the hard particles, we effectively integrate out the hard degrees of freedom and the induced current can be expressed in terms of the soft gauge fields. Furthermore, we can obtain an effective YANG-MILLS equation, which involves the soft fields alone. Neglecting the non-linear effects, the gluon self-energy tensor can be simply obtained from the induced current. The derivation of self-energy tensor is of particular interest for us which is the starting point to study the dispersion relations for the collective modes and the perturbative heavy-quark potential.

In this chapter we will revisit the kinetic equations for both an electromagnetic plasma and the quark-gluon plasma. By solving these kinetic equations, it turns out the corresponding self-energy is formally the same when the non-linear effects have been neglected in QCD. We also study the collective modes for an equilibrium quark-gluon plasma based on the obtained gluon self-energy tensor.

2.1 Scales in weakly coupled relativistic plasmas

It is well understood that there are three distinct length scales on which a hot weakly coupled relativistic plasma exhibits different characteristic behavior [69, 71].

The first scale is the *hard scale*, corresponding to the plasma particles with momenta $k \sim T$. This is the characteristic scale of momentum or energy for the vast majority of the excitations comprising the plasma. Such excitations give a dominant contribution to the bulk thermodynamic properties and the transport properties [72, 73]. The interactions of such excitations can be treated as a small perturbation as compared to their kinetic energies.

The second scale is the *soft scale*, corresponding to the plasma particles with momenta $k \sim gT$. In fact, this scale is that at which collective phenomena develop. For such excitations, plasma effects such as DEBYE screening, plasma oscillations and LANDAU damping become important. The interactions of the gT scale fields with the thermal bath of the hard scale excitations can not be treated as perturbation anymore. Instead, one should resum these interactions into the propagators and vertices [65, 68]. This resummation is commonly referred to as HTL resummation. The interactions amongst the soft scale degrees of freedom are weak and can be ignored. In this sense the soft modes with $k \sim gT$ are still perturbative.

Moving down to lower momenta, one meets the contribution of the unscreened magnetic fluctuations which play a dominant role for $k \sim g^2T$. The mutual interactions among the *ultrasoft scale* degrees of freedom are truly strongly coupled, the perturbative treatments break down [74].

Having identified the main scales and degrees of freedom, one should construct appropriate effective theories at the various scales. In the following, we will focus on the effective theory at the scale gT. The basic starting point of this work is the expression for the soft gauge field self-energy in the presence of a given distribution of hard particles.

2.2 Transport equations for electromagnetic plasmas

In this section, we briefly review the known result of the self-energy $\Pi^{\mu\nu}(P)$ from collisionless kinetic theory. Here, we consider an electromagnetic plasma and assume that we can describe its charged particles in terms of classical distribution functions [69, 63]. In addition, we neglect collisions among the charged particles and the only relevant interactions are those of particles with average electric ($\mathbf{E}$) and magnetic ($\mathbf{B}$) fields. We starts with the VLASOV equations, which are the collisionless BOLTZMANN equations for hard particle distributions $f_{\mathrm{q}}(\mathbf{k}, X)$ with the space-time point $X \equiv (t, \mathbf{x})$ and the charge q carried by the hard particles.

$$\partial_t f_{\mathrm{q}} + \mathbf{v} \cdot \nabla_{\mathbf{x}} f_{\mathrm{q}} + \mathrm{q}(\mathbf{E} + \mathbf{v} \times \mathbf{B}) \cdot \nabla_{\mathbf{k}} f_{\mathrm{q}} = 0\,. \tag{2.1}$$

The collisionless approximation is valid if $T \gg \mathrm{q}^2/\bar{r}$, where $\bar{r}$ is the average distance between neighbouring particles which is proportional to the inverse temperature. In the weak-coupling limit, we can expect the kinetic energy of the hard particles is much larger than the potential energy of two neighbouring particles and the collisionless approximation holds.

The MAXWELL equations for the soft gauge fields read

$$\partial_\nu F^{\mu\nu} = j^\mu_{ind} = \sum_{\mathrm{q}} \mathrm{q} \int_{\mathbf{k}} V^\mu f_{\mathrm{q}}\,. \tag{2.2}$$

Here, $\mathbf{v} = \mathbf{v}(\mathbf{k})$ is the hard particle velocity for a given momentum $\mathbf{k}$ and $V^\mu \equiv (1, \mathbf{v})$. The massless particles satisfy the mass-shell constraint and $k \equiv |\mathbf{k}| = E_{\mathbf{k}}$. LORENTZ force on hard particles of charge q is denoted by $\mathrm{q}(\mathbf{E} + \mathbf{v} \times \mathbf{B})$. The sum on the right-hand side of Eq. (2.2) denotes the sum over particle species. Furthermore, we introduce the shorthand notation

$$\int_{\mathbf{k}} \cdots = \int \frac{\mathrm{d}^3\mathbf{k}}{(2\pi)^3} \cdots\,. \tag{2.3}$$

The plasma is considered to be in equilibrium and the distribution function is isotropic in momentum space [1]; $f_0(\mathbf{k}) \equiv f_0(E_\mathbf{k})$ and does not depend on the space-time coordinates homogeneous. The induced current j^μ_{ind} which is the source term in the MAXWELL equations for the mean fields vanishes with such a distribution;

$$j^\mu_{ind} = \sum_{\mathrm{q}} \mathrm{q} \int_\mathbf{k} V^\mu f_0(E_\mathbf{k}) = 0\,. \tag{2.4}$$

If the plasma is weakly perturbed, the distribution functions deviate slightly from their homogeneous values and we can linearize $f_\mathrm{q}(\mathbf{k}, X) = f_0(\mathbf{k}) + f_1(\mathbf{k}, X)$ in small fluctuations f_1 about the equilibrium distribution $f_0(\mathbf{k})$. In the absence of external fields, one can treat $\mathbf{E}(X)$ and $\mathbf{B}(X)$ as small. Finally, we find in the linear approximation, the fluctuations in the distribution functions obey

$$\partial_t f_1 + \mathbf{v}\cdot\nabla_\mathbf{x} f_1 + \mathrm{q}\,\mathbf{E}\cdot\mathbf{v}\frac{\mathrm{d}f_0}{\mathrm{d}E_\mathbf{k}} = 0\,, \tag{2.5}$$

$$\partial_\nu F^{\mu\nu} = j^\mu_{ind} = \sum_{\mathrm{q}} \mathrm{q} \int_\mathbf{k} V^\mu f_1\,. \tag{2.6}$$

Note that the magnetic field does not contribute because of the isotropy of the equilibrium distribution function.

It is convenient to set

$$f_1 = -\mathrm{q}W(\mathbf{v}, X)\,\frac{\mathrm{d}f_0}{\mathrm{d}E_\mathbf{k}}\,. \tag{2.7}$$

The hard particle distribution function can be written as

$$f_\mathrm{q} = f_0 - \mathrm{q}W(\mathbf{v}, X)\,\frac{\mathrm{d}f_0}{\mathrm{d}E_\mathbf{k}} \approx f_0(E_\mathbf{k} - \mathrm{q}W(\mathbf{v}, X))\,, \tag{2.8}$$

and Eq. (2.5) becomes

$$\partial_t W(\mathbf{v}, X) + \mathbf{v}\cdot\nabla_\mathbf{x} W(\mathbf{v}, X) = \mathbf{E}\cdot\mathbf{v}\,. \tag{2.9}$$

By assuming the perturbation is introduced adiabatically so that the fields and the fluctuations vanish as $e^{\epsilon t_0}(\epsilon \to 0^+)$ when $t_0 \to -\infty$, we obtain the retarded solution

$$W(\mathbf{v}, X) = \int_{-\infty}^{t} \mathrm{d}t' e^{-\epsilon(t-t')}\mathbf{v}\cdot\mathbf{E}(\mathbf{x} - \mathbf{v}(t-t'), t')\,. \tag{2.10}$$

It is now straightforward to derive the corresponding induced current

$$j^\mu_{ind}(X) = -2\mathrm{q}^2 \int_\mathbf{k} V^\mu \frac{\mathrm{d}f_0}{\mathrm{d}E_\mathbf{k}} \int_0^\infty \mathrm{d}\tau e^{-\epsilon\tau}\mathbf{v}\cdot\mathbf{E}(X - V\tau)\,. \tag{2.11}$$

FOURIER transforming from X to P, we obtain

$$j^\mu_{ind}(P) = -2i\,\mathrm{q}^2 \int_\mathbf{k} V^\mu \frac{\mathbf{v}\cdot\mathbf{E}(P)}{V\cdot P + i\epsilon}\,\frac{\mathrm{d}f_0}{\mathrm{d}E_\mathbf{k}}\,, \tag{2.12}$$

[1] As we will see later, this assumption for the distribution functions is not necessary. For simplicity, we consider the equilibrium (isotropic) distribution for the moment being.

where we make use of

$$\int_0^\infty \mathrm{d}\tau e^{-\epsilon\tau} f(X - V\tau) \xrightarrow{\text{Fourier}} i\frac{f(P)}{V\cdot P + i\epsilon}\,. \tag{2.13}$$

In momentum space, electric fields take the following form

$$\mathbf{E}(P) = -iA_0\,\mathbf{p} + ip_0\,\mathbf{A}\,, \tag{2.14}$$

then Eq. (2.12) can be rewritten as

$$j^\mu_{ind}(P) = -2\mathrm{q}^2 \int_{\mathbf{k}} V^\mu \frac{V_\sigma A_\nu(-P\cdot V g^{\sigma 0} g^{\nu 0} + \omega g^{\sigma\nu})}{V\cdot P + i\epsilon}\frac{\mathrm{d}f_0}{\mathrm{d}E_{\mathbf{k}}}\,, \tag{2.15}$$

where we denote $P \equiv (\omega, \mathbf{p})$. It shows the induced current is a linear function of A^ν. Therefore, we can rewrite the induced current as

$$j^\mu_{ind}(P) = \Pi^{\mu\nu} A_\nu\,, \tag{2.16}$$

and extract the result for the retarded self-energy $\Pi^{\mu\nu}$,

$$\Pi^{\mu\nu}(P) = m_D^2\left(-g^{\mu 0}g^{\nu 0} + \omega\int\frac{\mathrm{d}\Omega}{4\pi}\frac{V^\mu V^\nu}{K\cdot P + i\epsilon}\right)\,. \tag{2.17}$$

Note that $\int \mathrm{d}\Omega V^\mu = 4\pi\, g^{\mu 0}$ and the Debye mass is defined as

$$m_D^2 = -\frac{2\mathrm{q}^2}{\pi^2}\int_0^\infty \mathrm{d}k k^2 \frac{\mathrm{d}f_0}{\mathrm{d}E_{\mathbf{k}}}\,. \tag{2.18}$$

In Eq. (2.18), we take the helicity degrees of freedom into account. Therefore, there is an extra factor of 2. Actually, Eq. (2.17) gives the dominant contribution at high temperature to the one-loop photon self-energy in QED. Using the Fermi-Dirac distribution for f_0, we find the QED Debye mass equals to $e^2T^2/3$.

2.3 Transport equations for quark-gluon plasma

The distribution of hard particles in the QCD plasma is described by a Hermitian density matrix in color space. For a SU(N_c) color group, the distribution of hard (anti-)quarks is a $N_c \times N_c$ matrix while for gluons it is a $(N_c^2-1)\times(N_c^2-1)$ matrix. The linearized kinetic equations for the QCD plasma look formally as Vlasov equations [75, 69]

$$\begin{aligned} V\cdot D_X\,\delta n(\mathbf{k}, X) &= -gV_\mu F^{\mu\nu}(X)\partial_\nu n(\mathbf{k})\,,\\ V\cdot D_X\,\delta \bar{n}(\mathbf{k}, X) &= gV_\mu F^{\mu\nu}(X)\partial_\nu \bar{n}(\mathbf{k})\,,\\ V\cdot \mathcal{D}_X\,\delta N(\mathbf{k}, X) &= -gV_\mu \mathcal{F}^{\mu\nu}(X)\partial_\nu N(\mathbf{k})\,. \end{aligned} \tag{2.19}$$

In the above equations, δn, $\delta\bar{n}$ and δN are the fluctuating parts of the density matrices for quarks, anti-quarks and gluons, respectively. We discuss here how the plasma, which is (on

average) colorless, homogeneous and stationary, responds to small color fluctuations. The distribution functions are assumed to be of the form

$$\begin{aligned} Q_{ij}(\mathbf{k},X) &= n(\mathbf{k})\delta_{ij} + \delta n_{ij}(\mathbf{k},X)\,, \\ \bar{Q}_{ij}(\mathbf{k},X) &= \bar{n}(\mathbf{k})\delta_{ij} + \delta \bar{n}_{ij}(\mathbf{k},X)\,, \\ G_{ab}(\mathbf{k},X) &= N(\mathbf{k})\delta_{ab} + \delta N_{ab}(\mathbf{k},X)\,, \end{aligned} \tag{2.20}$$

where the functions describing the deviation from the colorless state are assumed to be much smaller than the respective colorless functions. Note that δn and $\delta\bar{n}$ transform as a color vector in the fundamental representation ($\delta n = \delta n^a t^a$, $\delta\bar{n} = \delta\bar{n}^a t^a$) and δN transforms as a color vector in the adjoint representation ($\delta N = \delta N^a T^a$). Here, t^a and T^a are the SU(N_c) group generators in the fundamental and adjoint representations respectively. The velocity of hard and massless partons is given by $V_\mu = (1, \hat{\mathbf{k}}) \equiv (1, \mathbf{k}/k)$. D_μ and $\mathcal{D}_\mu$ are the covariant derivatives which act as

$$D_\mu = \partial_\mu - ig[A_\mu(X), \dots]\,, \quad \mathcal{D}_\mu = \partial_\mu - ig[\mathcal{A}_\mu(X), \dots]\,, \tag{2.21}$$

with A_μ and $\mathcal{A}_\mu$ being the mean-field or background four-potentials

$$A^\mu(X) = A^\mu_a(X)\tau_a\,, \quad \mathcal{A}^\mu(X) = \mathcal{A}^\mu_a(X)T_a\,. \tag{2.22}$$

$F_{\mu\nu}$ and $\mathcal{F}_{\mu\nu}$ are the mean-field stress tensors with a color index structure analogous to that of the four-potentials.

The presence of covariant derivative on the left-hand side of Eq. (2.19) is a new feature of the non-Abelian theory. These equations are covariant under local gauge transformations [76, 77].

In the weak-coupling limit, we neglect terms of subleading order in g and the theory becomes effectively Abelian as $D_X \to \partial_X$ and $F_{\mu\nu} \to \partial_\mu A_\nu - \partial_\nu A_\mu$. The color channels decouple and Eq. (2.19) can be written for each color channel separately [69, 78]

$$\begin{aligned} V\cdot\partial_X\, \delta n^a(\mathbf{k},X) &= -gV_\mu F^{\mu\nu\,a}(X)\partial_\nu n(\mathbf{k})\,, \\ V\cdot\partial_X\, \delta \bar{n}^a(\mathbf{k},X) &= gV_\mu F^{\mu\nu\,a}(X)\partial_\nu \bar{n}(\mathbf{k})\,, \\ V\cdot\partial_X\, \delta N^a(\mathbf{k},X) &= -gV_\mu \mathcal{F}^{\mu\nu\,a}(X)\partial_\nu N(\mathbf{k})\,, \end{aligned} \tag{2.23}$$

and the induced current in the fundamental representation reads

$$j^{\mu\,a}_{ind} = -g\int_{\mathbf{k}} V^\mu \left\{2N_c\delta N^a(\mathbf{k},X) + N_f[\delta n^a(\mathbf{k},X) - \delta\bar{n}^a(\mathbf{k},X)]\right\}\,. \tag{2.24}$$

As seen, the induced current occurs due to the deviation from the colorless state.

It is more convenient to solve these linearized equations in the momentum space. Taking the quark distribution as an example, we firstly perform the FOURIER transform

$$(-i\,\omega + i\mathbf{p}\cdot\mathbf{v})\delta n^a(\mathbf{k},P) + gV_\mu F^{\mu\nu\,a}(P)\partial_\nu n(\mathbf{k}) = 0\,. \tag{2.25}$$

It is now straightforward to obtain the fluctuating part for quark distribution

$$\begin{aligned}
\delta n^a(\mathbf{k},P) &= -g\frac{V_\mu F^{\mu\nu\,a}(P)\partial_\nu n(\mathbf{k})}{-i\,\omega+i\,\mathbf{p}\cdot\mathbf{v}+\epsilon} = i\,g\frac{i\,V_\mu(P^\mu A^{\nu\,a}-P^\nu A^{\mu\,a})\partial_\nu n(\mathbf{k})}{\omega-\,\mathbf{p}\cdot\mathbf{v}+i\epsilon} \\
&= -g\frac{[(\omega-\mathbf{p}\cdot\mathbf{v})A^{\nu\,a}-V_\mu P^\nu A^{\mu\,a}]\,\partial_\nu n(\mathbf{k})}{\omega-\,\mathbf{p}\cdot\mathbf{v}+i\epsilon} \\
&= -g\,\partial_\nu n(\mathbf{k})\left(A^{\nu\,a}-\frac{V_\mu P^\nu A^{\mu\,a}}{\omega-\,\mathbf{p}\cdot\mathbf{v}+i\epsilon}\right) \\
&= -g\,\partial_\beta n(\mathbf{k})\left(g^{\nu\beta}-\frac{V^\nu P^\beta}{\omega-\,\mathbf{p}\cdot\mathbf{v}+i\epsilon}\right)A^a_\nu\,. \qquad (2.26)
\end{aligned}$$

We introduce a small positive number ϵ in order to get the retarded solution. Similarly, we can solve the linearized kinetic equations for anti-quarks and gluons and the induced current finally reads

$$j^{\mu\,a}_{ind}(P) = g^2\int_{\mathbf{k}} V^\mu\frac{\partial f(\mathbf{k})}{\partial K^\beta}\left(g^{\nu\beta}-\frac{V^\nu P^\beta}{P\cdot V+i\epsilon}\right)A^a_\nu(P)+\mathcal{O}(g^3A^2)\,, \qquad (2.27)$$

where we combined the gluon and quark distributions in

$$f(\mathbf{k}) = 2N_cN(\mathbf{k})+N_f\left[n(\mathbf{k})+\bar{n}(\mathbf{k})\right]\,. \qquad (2.28)$$

We also present the more general solution for the induced current which reads [70, 77]

$$j^\mu_{ind}(X) = g^2\int_{\mathbf{k}} V^\mu K^\lambda\int \mathrm{d}^4Y\,G_K(X-Y)\,U(X,Y)\,F_{\lambda\nu}(Y)\,U(Y,X)\,\frac{\partial f(\mathbf{k})}{\partial K_\nu}\,, \qquad (2.29)$$

where the gauge parallel transporter defined in the fundamental representation is

$$U(X,Y) = \mathcal{P}\exp\Big[-ig\int_X^Y \mathrm{d}Z_\mu\,A^\mu(Z)\Big]\,, \qquad (2.30)$$

and the retarded Green function satisfies

$$K_\mu\partial^\mu G_K(X) = \delta^{(4)}(X)\,, \qquad (2.31)$$

or

$$G_K(X) = E^{-1}_{\mathbf{k}}\Theta(t)\,\delta^{(3)}(\mathbf{x}-\mathbf{v}t)\,. \qquad (2.32)$$

In Eq. (2.30), $\mathcal{P}$ denotes the ordering along the path from X to Y. The Θ function is the usual step-function. There is an analogous formula of the gauge transporter $\mathcal{U}(X,Y)$ in the adjoint representation. Consider the contribution at leading order in g, the Fourier transform of Eq. (2.29) gives the same result as Eq. (2.27). Note that in this approximation, the gauge transporters are approximated by unity. However, with the approximation, the induced current is no longer gauge covariant.

The higher order terms in Eq. (2.27) represent gluon vertex corrections. In fact, beyond the linear approximation, we can express the induced current as a formal series in powers of the gauge potentials [76, 77]

$$j^\mu_{ind\,a} = \Pi^{\mu\nu}_{ab}A^b_\nu+\frac{1}{2}\Gamma^{\mu\nu\rho}_{abc}A^b_\nu A^c_\rho+\ldots\,. \qquad (2.33)$$

These amplitudes are the "hard-thermal-loops" [79, 80, 81] which define the effective theory for the soft gauge fields at the scale gT. The linear approximation in QCD holds as long as the mean-field four-potential is much smaller than the temperature [69]. Actually, for the soft scales we consider here, the mean-field four-potential is at the order of $\sqrt{gT}$ and the linear approximation holds in the weak-coupling limit.

By functional differentiation

$$\Pi^{\mu\nu}_{ab}(P) = \frac{\delta j^{\mu}_{ind\,a}(P)}{\delta A^{b}_{\nu}(P)}\,, \tag{2.34}$$

we obtain the *retarded gluon self-energy*

$$\Pi^{\mu\nu}_{ab}(P) = g^2\delta_{ab}\int_{\mathbf{k}} V^{\mu}\frac{\partial f(\mathbf{k})}{\partial K^{\beta}}\left(g^{\nu\beta} - \frac{V^{\nu}P^{\beta}}{P\cdot V + i\epsilon}\right). \tag{2.35}$$

The distribution function in the above equation is arbitrary at this point. Actually, the kinetic theory of quarks and gluons has been shown to be fully consistent with the QCD dynamics not only for equilibrium systems but also the systems which are far from equilibrium. However, the space-time homogeneity must be invoked. The reliability of the kinetic theory methods is proved in Chapter 3 based on the QCD diagrammatic approach where we calculate the self-energy tensor explicitly for both equilibrium and non-equilibrium systems.

Now we are going to show that this self-energy tensor is symmetric $\Pi^{\mu\nu} = \Pi^{\nu\mu}$ and transverse $P_{\mu}\Pi^{\mu\nu} = 0$. We demonstrate the transversality

$$P_{\mu}\Pi^{\mu 0} = -g^2 p^{j}\int_{\mathbf{k}}\frac{\partial f(\mathbf{k})}{\partial k^{j}}\,. \tag{2.36}$$

Since the energy density carried by partons is expected to be finite, $f(\mathbf{k}\to\infty)$ must vanish. Consequently, the above integral vanishes as well. To prove that $P_{\mu}\Pi^{\mu i} = 0$, we first perform partial integration and assume that $f(\mathbf{k}\to\infty) = 0$,

$$\begin{aligned} P_{\mu}\Pi^{\mu i} &= g^2\int_{\mathbf{k}} P\cdot V\frac{\partial f(\mathbf{k})}{\partial K^{\beta}}\left(g^{i\beta} - \frac{v^{i}P^{\beta}}{P\cdot V + i\epsilon}\right) \\ &= g^2\int_{\mathbf{k}} f(\mathbf{k})p^{j}\left(\frac{\partial v^{i}}{\partial k^{j}} - \frac{\partial v^{j}}{\partial k^{i}}\right). \end{aligned} \tag{2.37}$$

Using $\mathbf{v} = \nabla_{\mathbf{k}}E_{\mathbf{k}}$ and $\partial_{k^j}v^{i} = \partial_{k^j}\partial_{k^i}E_{\mathbf{k}}$, it is clear to see $P_{\mu}\Pi^{\mu i} = 0$. Analogously, we can show the symmetry of the self-energy tensor.

As we discussed above, in linear approximation the current that is induced by the fluctuations can be expressed as

$$j^{\mu}_{ind}(P) = \Pi^{\mu\nu}(P)A_{\nu}(P)\,. \tag{2.38}$$

Insert Eq. (2.38) into Maxwell equation

$$-iP_{\mu}F^{\mu\nu}(P) = j^{\nu}_{ind} + j^{\nu}_{ext}\,, \tag{2.39}$$

we obtain

$$\left[P^2 g^{\mu\nu} - P^{\mu}P^{\nu} + \Pi^{\mu\nu}(P)\right]A_{\mu}(P) = -j^{\nu}_{ext}(P)\,, \tag{2.40}$$

where j^{ν}_{ext} is an external current. Note that the mean-field stress tensor in Eq. (2.39) is effectively Abelian which is consistent with our approximation. The self-energy is gauge invariant in HL approximation therefore we can write Eq. (2.40) in terms of a physical electric field by specifying a certain gauge. In temporal axial gauge defined by $A_0 = 0$, we have

$$\left[-P^2\delta^{ij} - p^i p^j + \Pi^{ij}(P)\right] E^j(P) = [D^{-1}(P)]^{ij} E^j(P) = i\omega j^i_{ext}(P)\,. \tag{2.41}$$

The response of the system to the external source is given by

$$E^i(P) = i\omega D^{ij}(P) j^j_{ext}(P)\,. \tag{2.42}$$

In the next section, we will study the dispersion relations for the collective modes. They can be obtained by finding the poles in the propagator $D^{ij}(P)$ defined in Eq. (2.41).

2.4 Dispersion relations for an equilibrium system

In order to determine the *dispersion relations* for an equilibrium system, we assume the (anti-)quark and gluon distribution functions $n(\mathbf{k})$, $\bar{n}(\mathbf{k})$, $N(\mathbf{k})$ have the Fermi-Dirac or Bose-Einstein forms, i.e.

$$\begin{aligned} n_{\rm eq}(\mathbf{k}) &= \frac{1}{\exp(k/T)+1}\,, \\ \bar{n}_{\rm eq}(\mathbf{k}) &= \frac{1}{\exp(k/T)+1}\,, \\ N_{\rm eq}(\mathbf{k}) &= \frac{1}{\exp(k/T)-1}\,, \end{aligned} \tag{2.43}$$

where the quark chemical potential is set to zero and the distribution function f depends only on the length of $\mathbf{k}$. The spatial components of the self-energy can be rewritten as:

$$\begin{aligned} \Pi^{ij}_{ab}(P) &= -g^2\delta_{ab}\int_{\mathbf{k}} v^i \frac{\partial f_{\rm eq}(\mathbf{k})}{\partial k^l}\left(\delta^{jl} + \frac{v^j p^l}{P\cdot V + i\epsilon}\right) \\ &= -g^2\delta_{ab}\int_{\mathbf{k}} v^i \frac{k^l}{k}\frac{\mathrm{d}f_{\rm eq}(k)}{\mathrm{d}k}\left(\delta^{jl} + \frac{v^j p^l}{P\cdot V + i\epsilon}\right)\,. \end{aligned} \tag{2.44}$$

It is possible to integrate out the k-dependence giving

$$\Pi^{ij}(P) = m_D^2 \int \frac{\mathrm{d}\Omega}{4\pi}\, v^i v^l \left(\delta^{jl} + \frac{v^j p^l}{P\cdot V + i\epsilon}\right)\,, \tag{2.45}$$

where the trivial color structure is neglected and the Debye mass

$$m_D^2 = -\frac{g^2}{2\pi^2}\int_0^\infty \mathrm{d}k\, k^2 \frac{\mathrm{d}f_{\rm eq}(k)}{\mathrm{d}k}\,. \tag{2.46}$$

Using Eqs. (2.43) and (2.28), we find the Debye mass in the isotropic QCD plasma is

$$m_D^2 = g^2 T^2 \frac{N_f + 2N_c}{6}\,. \tag{2.47}$$

In the isotropic case there is only one distinct spatial direction in the system [2], the direction of $\mathbf{p}$, we can then decompose the self-energy into two *structure functions* α and β

$$\Pi^{ij} = \alpha A^{ij} + \beta B^{ij} \,. \tag{2.48}$$

Here, we define the two projectors [3]

$$A^{ij} = \delta^{ij} - p^i p^j / p^2 \,, \quad B^{ij} = p^i p^j / p^2 \,. \tag{2.49}$$

They obey the usual projector properties:

$$\begin{aligned} \mathbf{A}^2 = \mathbf{A} \,,\ \mathbf{B}^2 = \mathbf{B} \,, \\ \mathbf{A}\,\mathbf{B} = \mathbf{B}\,\mathbf{A} = 0 \,. \end{aligned} \tag{2.50}$$

The two structure functions can be determined by taking the following contractions:

$$\begin{aligned} p^i \Pi^{ij} p^j &= p^2 \beta \,, \\ \mathrm{Tr}\, \Pi^{ij} &= 2\alpha + \beta \,. \end{aligned} \tag{2.51}$$

In general, the self-energy tensor is defined by the following projections, for which the integrals in Eq. (2.45) can be solved analytically:

$$\Pi_T = \alpha = \frac{m_D^2}{2} \frac{\omega^2}{p^2} \left[1 - \frac{\omega^2 - p^2}{2\omega p} \ln \left(\frac{\omega + p}{\omega - p} \right) \right] \,, \tag{2.52}$$

$$\Pi_L = \frac{p^2}{\omega^2} \beta = m_D^2 \left[-1 + \frac{\omega}{2p} \ln \left(\frac{\omega + p}{\omega - p} \right) \right] \,. \tag{2.53}$$

Note that for real-valued ω, the two projections are real if P is a time-like four-vector ($P^2 > 0$), while for space-like P ($P^2 < 0$), the two projections are complex. They are real-valued for imaginary values of ω.

With these structure functions we can calculate the propagator $D^{ij}(P)$ explicitly. According to Eq. (2.41), the inverse propagator can be expressed as

$$\mathbf{D}^{-1}(P) = (p^2 - \omega^2 + \alpha)\mathbf{A} + (\beta - \omega^2)\mathbf{B} \,. \tag{2.54}$$

Upon inversion, we obtain the expression for the propagator in temporal axial gauge with gauge parameter being zero

$$\mathbf{D}(P) = \frac{1}{p^2 - \omega^2 + \alpha} \mathbf{A} + \frac{1}{\beta - \omega^2} \mathbf{B} \,. \tag{2.55}$$

Now, the dispersion relations of the transverse and longitudinal modes can be determined separately by finding the poles in the propagator [63]. For the transverse dispersion relations, we have

$$p^2 - \omega_T^2 + \Pi_T(\omega = \omega_T) = 0 \,, \tag{2.56}$$

and the longitudinal ones are determined by

$$\Pi_L(\omega = \omega_L) - p^2 = 0 \,. \tag{2.57}$$

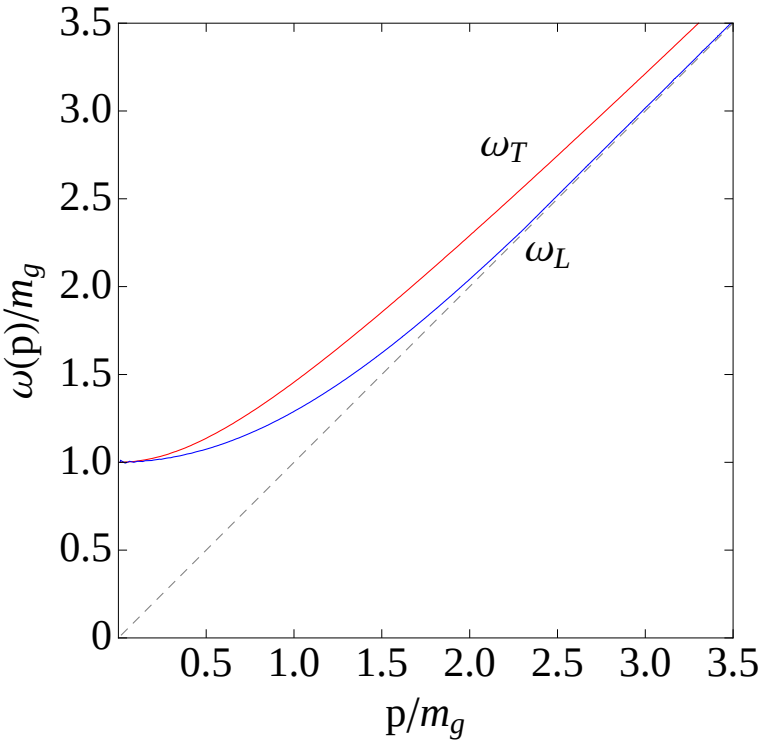

Figure 2.1: Dispersion relations for transverse and longitudinal gluons in units of $m_g = m_D/\sqrt{3}$. The light-gray line is the light-cone which is plotted as a visual aide.

Using the explicit expressions for the transverse and longitudinal projections, the poles in the propagator are given by

$$x^2 - 1 - \frac{m_D^2}{2p^2}\left[x^2 - x\frac{x^2-1}{2}\ln\left(\frac{x+1}{x-1}\right)\right] = 0\,, \tag{2.58}$$

and

$$\frac{m_D^2}{p^2}\left[1 - \frac{x}{2}\ln\left(\frac{x+1}{x-1}\right)\right] + 1 = 0\,, \tag{2.59}$$

respectively. Here, $x \equiv \omega_{T(L)}/p$. It is possible to find the analytical solutions approximately for small and large values of p. For small p, we have

$$\omega_T^2 \approx \frac{1}{3}m_D^2 + \frac{6}{5}p^2\,, \quad \omega_L^2 \approx \frac{1}{3}m_D^2 + \frac{3}{5}p^2\,. \tag{2.60}$$

For large p, the approximate solutions are

$$\omega_T^2 \approx \frac{m_D^2}{2} + p^2\,, \quad \omega_L^2 \approx p^2 + 4p^2\exp\left(-\frac{2p^2}{m_D^2}\right)\,. \tag{2.61}$$

[2] In local rest frame, the heat bath direction is $(1,0,0,0)$. For the spatial components we consider here, there is no explicit dependence on the heat bath direction.

[3] In addition, we have $A^{00} = A^{0i} = 0$ and $B^{00} = p^2/\omega^2$, $B^{0i} = p^i/\omega$ which can be obtained using the transversality of the self-energy.

The *stable modes* which have poles at real-valued $\omega > p$ only exist above the lowest frequency $\omega_{\rm p}$. Note that

$$\lim_{p\to 0}\omega_T^2 = \lim_{p\to 0}\omega_L^2 = \frac{m_D^2}{3}\,, \tag{2.62}$$

the lowest frequency $\omega_{\rm p}$ with which modes can propagate is $\frac{m_D}{\sqrt{3}}$. For large momenta the transverse modes tend to a mass hyperboloid with asymptotic mass $m_\infty^2 = m_D^2/2$, whereas the longitudinal ones approach the light-cone with exponentially vanishing residue. In general, the dispersion relations can be determined numerically and we show the dispersion relations in units of $m_g = m_D/\sqrt{3}$ in Fig. 2.1. As we can see in this figure, both longitudinal and transverse modes start from the point $(0, 1)$ according to the units we choose.

Taking the static limit, we find

$$\lim_{\omega\to 0}\Pi_T = 0\,, \quad \lim_{\omega\to 0}\frac{1}{p^2}\Pi_L = -\frac{m_D^2}{p^2}\,. \tag{2.63}$$

For the transverse modes, Π_T which is related to the inverse screening length vanishes. This corresponds to the absence of magnetostatic screening. On the other hand, Π_L for the longitudinal modes reaches the DEBYE mass which corresponds to the electrostatic screening. Note that for $0 < \omega < \omega_{\rm p}$, p becomes imaginary and there are no stable modes [80]. However, there is a collective behavior which corresponds to dynamical screening both in the electric and magnetic sector as long as $\omega > 0$.

3 Gluon self-energy from finite-temperature field theory

A QCD diagrammatic analysis of the collective phenomena will be reviewed in this chapter. It is equivalent to the transport theory approach as discussed in Chapter 2 [82, 75]. With the *hard-loop approximation*, namely the internal momenta are much larger than the external ones, it is shown explicitly that the exactly same result of the gluon self-energy tensor is obtained by computing the corresponding FEYNMAN diagrams. In *finite-temperature field theory*, the calculation of FEYNMAN diagrams can be performed in both imaginary time formalism and real time formalism [62, 63, 83]. When dealing with a non-equilibrium situation, the latter is more appropriate [83, 84]. We calculate the gluon self-energy within both imaginary and real time formalism. The result from the imaginary time formalism coincides with the one obtained from the real time formalism when the equilibrium distributions, i.e. FERMI-DIRAC or BOSE-EINSTEIN distributions are considered.

3.1 The basic points of finite-temperature field theory

The calculation of FEYNMAN amplitudes at finite temperature has two different methods: *imaginary time formalism* and *real time formalism*. With imaginary time arguments, the thermal perturbation theory has the same structure as the perturbation theory in the vacuum, the only difference being that the integrals over the loop energies are replaced by sums over the MATSUBARA frequencies. An analytic continuation is needed to obtain real time green functions in the imaginary time formalism. The complication of the real time formalism is the doubling of degrees of freedom. As a consequence, an n-point function has 2^n components. In spite of the difficulty, the real time formalism can be generalized to the non-equilibrium situations.

In the real time formalism, the propagator is given by a 2×2 matrix

$$G = \begin{pmatrix} G_{11} & G_{12} \\ G_{21} & G_{22} \end{pmatrix} . \tag{3.1}$$

The four components can be written as

$$\begin{aligned} G_{11}(X-Y) &= -i\langle \mathrm{T}(\psi(X)\psi^\dagger(Y))\rangle \,, \\ G_{12}(X-Y) &= \mp i\langle \psi^\dagger(Y)\psi(X)\rangle \,, \\ G_{21}(X-Y) &= -i\langle \psi(X)\psi^\dagger(Y)\rangle \,, \\ G_{22}(X-Y) &= -i\langle \tilde{\mathrm{T}}(\psi(X)\psi^\dagger(Y))\rangle \,, \end{aligned} \tag{3.2}$$

where $\psi(X)$ is a complex field operator in HEISENBERG picture and T is the usual time ordering operator, $\tilde{\mathrm{T}}$ is the anti-chronological time ordering operator. The upper sign is

taken for bosons and the lower sign is for fermions. Here G_{11} is the usual FEYNMAN causal propagator, whereas the other three are new in the real time formalism. Using the step-function

$$\Theta(X,Y) = \begin{cases} 1\,, & t_X > t_Y \\ 0\,, & \text{otherwise} \end{cases}\,, \tag{3.3}$$

we can rewrite the "11" and "22" components of the propagator as

$$\begin{aligned} G_{11}(X-Y) &= -i\,\Theta(X,Y)\langle(\psi(X)\psi^\dagger(Y))\rangle \mp i\,\Theta(Y,X)\langle(\psi^\dagger(Y)\psi(X))\rangle\,, \\ G_{22}(X-Y) &= -i\,\Theta(Y,X)\langle(\psi(X)\psi^\dagger(Y))\rangle \mp i\,\Theta(X,Y)\langle(\psi^\dagger(Y)\psi(X))\rangle\,. \end{aligned} \tag{3.4}$$

These four components of the propagator are not independent, but fulfill the relation

$$G_{11} - G_{12} - G_{21} + G_{22} = 0\,, \tag{3.5}$$

as a consequence of the identity $\Theta(X,Y) + \Theta(Y,X) = 1$.

For example, the bare scalar propagator can be written as

$$\begin{aligned} D(K) &= \begin{pmatrix} \frac{1}{K^2-m^2+i\epsilon} & 0 \\ 0 & \frac{-1}{K^2-m^2-i\epsilon} \end{pmatrix} - 2\pi i\,\delta(K^2-m^2) \\ &\quad \times \begin{pmatrix} N(\mathbf{k}) & \Theta(-k_0)+N(\mathbf{k}) \\ \Theta(k_0)+N(\mathbf{k}) & N(\mathbf{k}) \end{pmatrix}. \end{aligned} \tag{3.6}$$

Here we use the following notation: $K = (k_0, \mathbf{k})$. In equilibrium the distribution function $N(\mathbf{k})$ is given by BOSE-EINSTEIN distribution $N_{\rm eq}(\mathbf{k}) = 1/[\exp(k/T) - 1]$. For fermions the bare propagator reads

$$\begin{aligned} S(K) &= \begin{pmatrix} \frac{(\not{K}+m)}{K^2-m^2+i\epsilon} & 0 \\ 0 & \frac{-(\not{K}+m)}{K^2-m^2-i\epsilon} \end{pmatrix} + 2\pi i\,(\not{K}+m)\delta(K^2-m^2) \\ &\quad \times \begin{pmatrix} n(\mathbf{k}) & -\Theta(-k_0)+n(\mathbf{k}) \\ -\Theta(k_0)+n(\mathbf{k}) & n(\mathbf{k}) \end{pmatrix}, \end{aligned} \tag{3.7}$$

where the distribution function is given by FERMI-DIRAC distribution, i.e. $n_{\rm eq}(\mathbf{k}) = 1/[\exp(k/T) + 1]$ in equilibrium. Out of equilibrium the BOSE-EINSTEIN or FERMI-DIRAC distributions should be replaced by the non-equilibrium distributions which depend on the four momentum and the space-time coordinate [1].

In KELDYSH *representation* [85], it is more useful to write the propagator in terms of the three independent components

$$\begin{aligned} G_R &= G_{11} - G_{12}\,, \\ G_A &= G_{11} - G_{21}\,, \\ G_F &= G_{11} + G_{22}\,. \end{aligned} \tag{3.8}$$

[1] Throughout this dissertation, we consider the case where the distribution functions depend only on the momentum $\mathbf{k}$. However, they are not necessary to be isotropic.

G_R and G_A are the usual retarded and advanced propagators, satisfying

$$G_R(X-Y) - G_A(X-Y) = -i\langle[\psi(X), \psi^\dagger(Y)]_\mp\rangle\,, \tag{3.9}$$

and G_F is the symmetric combination

$$G_F(X-Y) = -i\langle[\psi(X), \psi^\dagger(Y)]_\pm\rangle\,. \tag{3.10}$$

In this definition, $[\psi(X), \psi^\dagger(Y)]_-$ is the usual commutator while $[\psi(X), \psi^\dagger(Y)]_+$ is the anti-commutator. The inverted relations read

$$\begin{aligned} G_{11} &= \frac{1}{2}\,(G_F + G_A + G_R)\,, \\ G_{12} &= \frac{1}{2}\,(G_F + G_A - G_R)\,, \\ G_{21} &= \frac{1}{2}\,(G_F - G_A + G_R)\,, \\ G_{22} &= \frac{1}{2}\,(G_F - G_A - G_R)\,. \end{aligned} \tag{3.11}$$

In momentum space these three bare propagators are given by

$$\begin{aligned} D_R(K) &= \frac{1}{K^2 - m^2 + i\,\mathrm{sgn}(k_0)\epsilon}\,, \\ D_A(K) &= \frac{1}{K^2 - m^2 - i\,\mathrm{sgn}(k_0)\epsilon}\,, \\ D_F(K) &= -2\pi i\,(1 + 2N(\mathbf{k}))\,\delta(K^2 - m^2)\,, \end{aligned} \tag{3.12}$$

for scalar bosons and

$$\begin{aligned} S_R(K) &= \frac{\not{K} + m}{K^2 - m^2 + i\,\mathrm{sgn}(k_0)\epsilon}\,, \\ S_A(K) &= \frac{\not{K} + m}{K^2 - m^2 - i\,\mathrm{sgn}(k_0)\epsilon}\,, \\ S_F(K) &= -2\pi i\,(\not{K} + m)\,(1 - 2n(\mathbf{k}))\,\delta(K^2 - m^2)\,, \end{aligned} \tag{3.13}$$

for fermions.

In real time formalism, similar relations hold for the self-energies:

$$\Pi_{11} + \Pi_{12} + \Pi_{21} + \Pi_{22} = 0\,, \tag{3.14}$$

and

$$\begin{aligned} \Pi_R &= \Pi_{11} + \Pi_{12}\,, \\ \Pi_A &= \Pi_{11} + \Pi_{21}\,, \\ \Pi_F &= \Pi_{11} + \Pi_{22}\,, \end{aligned} \tag{3.15}$$

where Π stands for the self-energy of a boson or fermion.

3.2 The calculation of gluon self-energy in imaginary time formalism

In this section, we review the calculation of the gluon self-energy in the *imaginary time formalism* [63]. We start with the calculation of photon self-energy. This will be done at the one-loop approximation and in the high-temperature limit, which means that the temperature is much larger than the electron mass and the external momenta. In the end, we continued these results analytically to Minkowski space. We also generalize these calculations to the QCD case. It turns out the gluonic contributions to the self-energy have the same structure as the quark ones except the trivial color factor. Since the one-loop photon self-energy contains no gauge boson propagator, it is gauge independent. Consequently, the same holds for the gluon self-energy. We also show that the results obtained in the diagrammatic approach is equivalent to those obtained in the transport theory approach as we discussed in Chapter 2.

The one-loop photon self-energy can be expressed as

$$\begin{aligned}\Pi_{\mu\nu} &= e^2 \sum\!\!\!\!\!\!\int_{\tilde{K}} \frac{\mathrm{d}^4\tilde{K}}{(2\pi)^4} \mathrm{Tr}\left[\gamma_\nu \not{\tilde{K}} \gamma_\mu (\not{\tilde{K}} - \not{\tilde{P}})\right] \tilde{\Delta}(\tilde{K})\tilde{\Delta}(\tilde{K}-\tilde{P}) \\ &= e^2 \sum\!\!\!\!\!\!\int_{\tilde{K}} \frac{\mathrm{d}^4\tilde{K}}{(2\pi)^4} (8\tilde{K}_\mu \tilde{K}_\nu - 4\tilde{K}^2\delta_{\mu\nu})\tilde{\Delta}(\tilde{K})\tilde{\Delta}(\tilde{K}-\tilde{P})\,. \end{aligned} \tag{3.16}$$

Note that in imaginary time formalism, we use Euclidean metric $\delta_{\mu\nu}$ which is a diagonal matrix defined by $\delta_{\mu\nu} = \mathrm{diag}(1,1,1,1)$ with $\mu,\nu = 1,\ldots,4$. To distinguish the notations in Minkowski space, we denote Euclidean momentum with a tilde. In Eq. (3.16) the four-momentum $\tilde{P}_\mu = (p_4, \mathbf{p}) = (-\tilde{\omega}, \mathbf{p})$ and $\tilde{K}_\mu = (k_4, \mathbf{k}) = (-\tilde{\omega}_n, \mathbf{k})$ [2]. The unit vector is defined as $\hat{\mathbf{k}} = \mathbf{k}/k$. Our convention for DIRAC matrices is that γ-matrices in Euclidean space obey anti-commutation relations: $\{\gamma_\mu, \gamma_\nu\} = -2\delta_{\mu\nu}$ with $\gamma_4 = i\gamma_0$. As a result, $\not{\tilde{K}} = \gamma_4 k_4 + \gamma\cdot\mathbf{k} = -\gamma_4\tilde{\omega}_n + \gamma\cdot\mathbf{k}$. The thermal sum-integral $\sum\!\!\!\!\!\!\int_{\tilde{K}} = T\sum_n \int \mathrm{d}^3\mathbf{k}/(2\pi)^3$. The inverse $\tilde{\Delta}(\tilde{K})$ equals to $\tilde{K}^2 = k_4^2 + k^2 = \tilde{\omega}_n^2 + k^2$. In the second line of the above equation, we use the HTL approximation. The loop momentum $\tilde{K}$ is assumed at the order of T, while the external momentum $\tilde{P}$ is at the order of gT. In the weak-coupling limit, we have $\tilde{K} \gg \tilde{P}$.

One important step of the calculation in imaginary time formalism is to perform the MATSUBARA *sums*. Here we will encounter the following three sums:

$$\begin{aligned} T\sum_n \tilde{\Delta}(\tilde{K})\tilde{\Delta}(\tilde{K}-\tilde{P}) &= -\frac{1}{4E_1E_2}\Big[(1-n_1-n_2)\Big(\frac{1}{i\tilde{\omega}-E_1-E_2} - \frac{1}{i\tilde{\omega}+E_1+E_2}\Big) \\ &- (n_1-n_2)\Big(\frac{1}{i\tilde{\omega}+E_1-E_2} - \frac{1}{i\tilde{\omega}-E_1+E_2}\Big)\Big]\,, \end{aligned} \tag{3.17}$$

[2] Note that in imaginary time formalism, the so-called MATSUBARA frequencies have discrete values. The loop momenta for which we should perform the frequency sum, is labeled by $(\tilde{\omega}_n, \mathbf{k})$. For fermions, the MATSUBARA frequencies are given by $\tilde{\omega}_n = (2n+1)\pi T$ with integer n. We don't need to perform the frequency sum for the external momentum $\tilde{P}$, however, we still label its frequency as $\tilde{\omega}$ without the index n.

$$T\sum_n \omega_n \tilde{\Delta}(\tilde{K})\tilde{\Delta}(\tilde{K}-\tilde{P}) = \frac{i}{4E_2}\Big[(1-n_1-n_2)(\frac{1}{i\tilde{\omega}-E_1-E_2}+\frac{1}{i\tilde{\omega}+E_1+E_2}) + (n_1-n_2)(\frac{1}{i\tilde{\omega}+E_1-E_2}-\frac{1}{i\tilde{\omega}-E_1+E_2})\Big], \tag{3.18}$$

$$T\sum_n \tilde{\Delta}(\tilde{K}) = \frac{1}{2k}(1+2n_1)\,, \tag{3.19}$$

where the subscripts "11" and "22" correspond to the momentum $\mathbf{k}$ and $\mathbf{k}-\mathbf{p}$, respectively. $E_1 = k$, $E_2 = |\mathbf{k}-\mathbf{p}|$ and n_1, n_2 are the equilibrium distribution functions as defined in Eq. (2.43). For example, $n_1 = n_{\rm eq}(\mathbf{k})$.

The calculation of the second term in Eq. (3.16) which we denote as $\Pi^2_{\mu\nu}$, is straightforward once we carry out the MATSUBARA sums

$$\Pi^2_{\mu\nu} = -4e^2 \not\int_{\tilde{K}} \frac{\mathrm{d}^4\tilde{K}}{(2\pi)^4}\tilde{K}^2\tilde{\Delta}(\tilde{K})\tilde{\Delta}(\tilde{K}-\tilde{P})\delta_{\mu\nu} = \frac{e^2T^2}{6}\delta_{\mu\nu}\,. \tag{3.20}$$

In fact, this integral is divergent. However, this divergence is temperature independent and it is absorbed into the zero temperature renormalization.

The calculation of the first term in Eq. (3.16) denoted as $\Pi^1_{\mu\nu}$ is more complicated than the second term. For simplicity, we will consider the calculation in high temperature limit and use the HTL approximation, $E_1 - E_2 \approx \mathbf{p}\cdot\hat{\mathbf{k}}$ and $n_1 - n_2 \approx \frac{\mathrm{d}n_{\rm eq}(k)}{\mathrm{d}k}\mathbf{p}\cdot\hat{\mathbf{k}}$. Firstly, we consider the spatial components of $\Pi^1_{\mu\nu}$

$$\Pi^1_{ij} = -\frac{e^2}{\pi^2}\int \frac{k^2\mathrm{d}k\mathrm{d}\Omega}{4\pi}\hat{k}_i\hat{k}_j\Big[(\frac{i\tilde{\omega}}{\tilde{P}\cdot\hat{\tilde{K}}}+\frac{i\tilde{\omega}}{\tilde{P}\cdot\hat{\tilde{K}}'}-2)\frac{\mathrm{d}n_{\rm eq}(k)}{\mathrm{d}k}+2\frac{n_{\rm eq}(k)}{k}\Big]. \tag{3.21}$$

Here, the light-like four-vectors are defined as $\hat{\tilde{K}} \equiv (-i,\hat{\mathbf{k}})$ and $\hat{\tilde{K}}' \equiv (-i,-\hat{\mathbf{k}})$. In the above expression, we use Eq. (3.17) for frequency sum and the temperature independent divergence is absorbed into the zero temperature renormalization as before. Note that, at high temperature, the leading contribution to the photon self-energy is proportional to T^2, so the subleading terms have been neglected. For example, there should be such a term $\int k\mathrm{d}k\frac{\mathrm{d}n_{\rm eq}(k)}{\mathrm{d}k}$ in Eq. (3.21). However, this term is only proportional to T which can be neglected in the high temperature limit.

For the integral over the solid angle, it is easy to show that

$$\int \mathrm{d}\Omega\hat{k}_i\hat{k}_j = \frac{4\pi}{3}\delta_{ij}\,, \quad \int \mathrm{d}\Omega\hat{k}_i\hat{k}_j\frac{1}{\tilde{P}\cdot\hat{\tilde{K}}'} = \int \mathrm{d}\Omega\hat{k}_i\hat{k}_j\frac{1}{\tilde{P}\cdot\hat{\tilde{K}}}\,. \tag{3.22}$$

After performing the integral over k, we get

$$\Pi_{ij} = \frac{e^2T^2}{3}\int\frac{\mathrm{d}\Omega}{4\pi}\frac{i\tilde{\omega}}{\tilde{P}\cdot\hat{\tilde{K}}}\hat{k}_i\hat{k}_j\,, \tag{3.23}$$

where the contribution from the second term in Eq. (3.16) was included.

Using the mass-shell constraint for the massless hard particles, $\tilde{\omega}_n^2 = -k^2$, the temporal component of $\Pi^1_{\mu\nu}$ can be calculated similarly as the spatial components. The result can be expressed as

$$\Pi_{44} = \frac{e^2T^2}{3}\left(1 - \int \frac{\mathrm{d}\Omega}{4\pi}\frac{i\tilde{\omega}}{\tilde{P}\,.\,\hat{\tilde{K}}}\right). \tag{3.24}$$

For the "4i" components, we have

$$\Pi_{4i} = \frac{e^2T^2}{3}\int \frac{\mathrm{d}\Omega}{4\pi}\frac{\tilde{\omega}}{\tilde{P}\,.\,\hat{\tilde{K}}}\hat{k}_i\,, \tag{3.25}$$

where the Eq. (3.18) is used for the MATSUBARA sums.

Combining all the expressions above, the final result for the photon self-energy is of the form

$$\Pi_{\mu\nu} = \frac{e^2T^2}{3}\int \frac{\mathrm{d}\Omega}{4\pi}\left(\delta_{\mu4}\delta_{\nu4} + \frac{i\tilde{\omega}\hat{\tilde{K}}_\mu\hat{\tilde{K}}_\nu}{\tilde{P}\,.\,\hat{\tilde{K}}}\right). \tag{3.26}$$

The symmetry of the self-energy tensor is obvious. It is also easy to show this tensor is transverse, i.e. $\tilde{P}_\mu\Pi_{\mu\nu} = \frac{e^2T^2}{3}\int\frac{\mathrm{d}\Omega}{4\pi}(i\tilde{\omega}\hat{\tilde{K}}_\nu - \tilde{\omega}\delta_{4\nu}) = 0$ [3].

As we did in Chapter 2, we can decompose the self-energy with the transverse and longitudinal projectors. In Euclidean space, the two projectors read

$$\begin{aligned} &\mathrm{A}_{44} = \mathrm{A}_{4i} = 0\,,\ \ \mathrm{A}_{ij} = \delta_{ij} - p_ip_j/p^2\,,\\ &\mathrm{B}_{\mu\nu} = \frac{\tilde{P}^2}{\tilde{\omega}^2}\left(\delta_{\mu\nu} - \frac{\tilde{P}_\mu\tilde{P}_\nu}{\tilde{P}^2} - \mathrm{A}_{\mu\nu}\right), \end{aligned} \tag{3.27}$$

and

$$\Pi_{\mu\nu} = \Pi_T\mathrm{A}_{\mu\nu} - \frac{\tilde{\omega}^2}{p^2}\Pi_L\mathrm{B}_{\mu\nu}\,. \tag{3.28}$$

The corresponding transverse and longitudinal projections are related to the "xx" and "4z" components of the self-energy. We can perform the integration over the solid angle by taking $\mathbf{p}$ parallel to the z-axis. As a result, we have

$$\begin{aligned} \Pi_{4z} &= \frac{e^2T^2}{3}\int\frac{\mathrm{d}\Omega}{4\pi}\frac{\tilde{\omega}}{i\tilde{\omega} + p\hat{k}_z}\hat{k}_z \\ &= \frac{e^2T^2}{3}\frac{\tilde{\omega}}{p}\left[1 - \frac{i\tilde{\omega}}{2p}\ln\left(\frac{i\tilde{\omega}+p}{i\tilde{\omega}-p}\right)\right], \end{aligned} \tag{3.29}$$

$$\begin{aligned} \Pi_{xx} &= \frac{e^2T^2}{3}\int\frac{\mathrm{d}\Omega}{4\pi}\frac{i\tilde{\omega}}{i\tilde{\omega} + p\hat{k}_z}\hat{k}_x\hat{k}_x \\ &= \frac{e^2T^2}{6}\frac{i\tilde{\omega}}{p}\left[\frac{i\tilde{\omega}}{p} + \frac{1}{2}\left(1 - \left(\frac{i\tilde{\omega}}{p}\right)^2\right)\ln\left(\frac{i\tilde{\omega}+p}{i\tilde{\omega}-p}\right)\right]. \end{aligned} \tag{3.30}$$

[3] Alternatively, one can prove the transversality directly form Eq. (3.16) by using $\tilde{P}\cdot\tilde{K} = [\tilde{K}^2 - (\tilde{P}-\tilde{K})^2]/2$ within the HTL approximation.

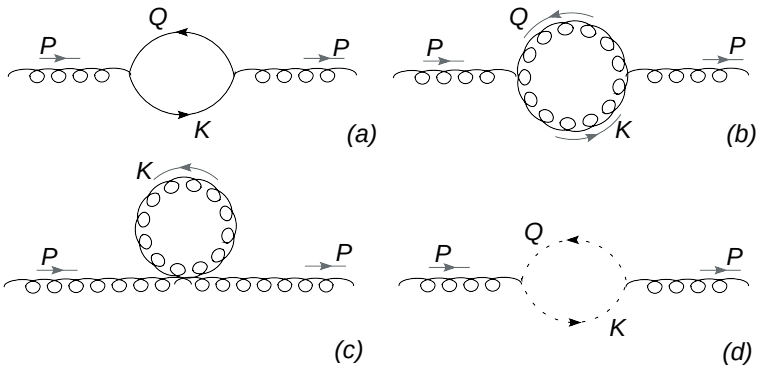

Figure 3.1: FEYNMAN diagrams contribute to gluon self-energy at one-loop approximation. The solid lines: quarks; The curly lines: gluons; The dashed lines: ghosts; The gray solid lines indicate the momentum direction of gluons.

It is easy to show that the corresponding projections in Euclidean space are

$$\Pi_L = -\frac{p}{\tilde{\omega}}\Pi_{4z} = \frac{e^2T^2}{3}\left[-1 + \frac{i\tilde{\omega}}{2p}\ln\left(\frac{i\tilde{\omega}+p}{i\tilde{\omega}-p}\right)\right], \tag{3.31}$$

$$\Pi_T = \Pi_{xx} = \frac{e^2T^2}{6}\frac{i\tilde{\omega}}{p}\left[\frac{i\tilde{\omega}}{p} + \frac{1}{2}\left(1-\left(\frac{i\tilde{\omega}}{p}\right)^2\right)\ln\left(\frac{i\tilde{\omega}+p}{i\tilde{\omega}-p}\right)\right]. \tag{3.32}$$

Finally, we should analytically continue Eqs. (3.31) and (3.32) from Euclidean space to Minkowski space. This continuation is performed by making the substitutions $i\tilde{\omega} \to \omega + i\epsilon$ [4] and $\tilde{P}^2 \to -P^2$. We find that after the continuation Eqs. (3.31) and (3.32) coincide with Eqs. (2.53) and (2.52) which are obtained in the transport theory approach.

Contrary to the photon self-energy, in principle, the gluon self-energy is not gauge-fixing independent. However, we find that in HTL approximation, the gluon self-energy does not depend on the choice of gauge. Here, we compute the gluon self-energy in Euclidean space in FEYNMAN gauge. There are four diagrams contribute at one-loop order as shown in Fig. 3.1. Adding the contributions from gluon and ghost loops, we have

$$\Pi^{(g)}_{\mu\nu}(\tilde{P}) = -g^2N_c\sum\!\!\!\!\!\!\int_{\tilde{K}}\frac{\mathrm{d}^4\tilde{K}}{(2\pi)^4}(4\tilde{K}_\mu\tilde{K}_\nu - 2\tilde{K}^2\delta_{\mu\nu})\tilde{D}(\tilde{K})\tilde{D}(\tilde{K}-\tilde{P}), \tag{3.33}$$

where $\tilde{D}(\tilde{K})$ is related to the gauge boson propagator in FEYNMAN gauge. The inverse $\tilde{D}(\tilde{K})$ equals to $\tilde{\omega}_n^2 + k^2$ with $\tilde{\omega}_n = 2\pi nT$. The fermion loop gives the similar expression as in QED

$$\Pi^{(f)}_{\mu\nu}(\tilde{P}) = \frac{g^2}{2}N_f\sum\!\!\!\!\!\!\int_{\tilde{K}}\frac{\mathrm{d}^4\tilde{K}}{(2\pi)^4}(8\tilde{K}_\mu\tilde{K}_\nu - 4\tilde{K}^2\delta_{\mu\nu})\tilde{\Delta}(\tilde{K})\tilde{\Delta}(\tilde{K}-\tilde{P}). \tag{3.34}$$

[4] Such a substitution corresponds to the retarded solution in Minkowski space.

Note that when performing the frequency sums, one goes from a bosonic to a fermionic loop by the substitution $N(E) \to -n(E)$. In HTL approximation, we have the following relations

$$\begin{aligned} \sum\!\!\!\!\!\!\int_{\tilde{K}} \frac{\mathrm{d}^4\tilde{K}}{(2\pi)^4}\tilde{\Delta}(\tilde{K}) &= -\frac{1}{2}\sum\!\!\!\!\!\!\int_{\tilde{K}} \frac{\mathrm{d}^4\tilde{K}}{(2\pi)^4}\tilde{D}(\tilde{K})\,, \\ \sum\!\!\!\!\!\!\int_{\tilde{K}} \frac{\mathrm{d}^4\tilde{K}}{(2\pi)^4}\tilde{\Delta}(\tilde{K})\tilde{\Delta}(\tilde{K}-\tilde{P}) &= -\frac{1}{2}\sum\!\!\!\!\!\!\int_{\tilde{K}} \frac{\mathrm{d}^4\tilde{K}}{(2\pi)^4}\tilde{D}(\tilde{K})\tilde{D}(\tilde{K}-\tilde{P})\,, \end{aligned} \tag{3.35}$$

where we make use of these equations

$$\int_0^\infty k\mathrm{d}k\, n_{\mathrm{eq}}(k) = \frac{1}{2}\int_0^\infty k\mathrm{d}k\, N_{\mathrm{eq}}(k)\,, \quad \int_0^\infty k\mathrm{d}k\frac{\mathrm{d}n_{\mathrm{eq}}(k)}{\mathrm{d}k} = \frac{1}{2}\int_0^\infty k\mathrm{d}k\frac{\mathrm{d}N_{\mathrm{eq}}(k)}{\mathrm{d}k}\,. \tag{3.36}$$

Taking the above equations into account, we find the expression for the gluon self-energy has the similar structure as that we have for photon in QED [86]

$$\begin{aligned} \Pi_{\mu\nu}(\tilde{P}) &= \Pi^{(f)}_{\mu\nu}(\tilde{P}) + \Pi^{(g)}_{\mu\nu}(\tilde{P}) \\ &= g^2(2C_A + N_f)\sum\!\!\!\!\!\!\int_{\tilde{K}} \frac{\mathrm{d}^4\tilde{K}}{(2\pi)^4}(4\tilde{K}_\mu\tilde{K}_\nu - 2\tilde{K}^2\delta_{\mu\nu})\tilde{\Delta}(\tilde{K})\tilde{\Delta}(\tilde{K}-\tilde{P})\,. \end{aligned} \tag{3.37}$$

The final result then takes the same form as the photon self-energy except the color factor and coupling constant:

$$\Pi_{\mu\nu} = \frac{g^2T^2}{3}(N_c + \frac{1}{2}N_f)\int\frac{\mathrm{d}\Omega}{4\pi}(\delta_{\mu4}\delta_{\nu4} + \frac{i\tilde{\omega}\hat{\tilde{K}}_\mu\hat{\tilde{K}}_\nu}{\tilde{P}\cdot\hat{\tilde{K}}})\,. \tag{3.38}$$

The only modification to the QED result in Eq. (3.26) is a change of the DEBYE mass. Again, the gluon self-energy obeys the WARD identity $\tilde{P}_\mu\Pi_{\mu\nu} = 0$.

3.3 The calculation of gluon self-energy in real time formalism

In this section, we proceed to calculate explicitly the *retarded gluon self-energy* in the *real time formalism*. As we mentioned before, the perturbative approach within the real time field theory provides a natural framework to study weakly interacting quantum field systems in and out of equilibrium. When employing the diagrammatic hard-loop approach in the real time formalism, we don't need to specify the form of the distribution functions. Here, we will consider the retarded self-energy and show that the results we obtain here are exactly the same as those derived in the transport theory approach and when the equilibrium FERMI-DIRAC and BOSE-EINSTEIN distributions are considered, we can reproduce the equilibrium self-energy which we have computed in the imaginary time formalism.

The contribution from the quark-loop to the gluon self-energy as shown in Fig. 3.1 is of the form

$$\Pi^{\mu\nu}(P) = -\frac{i}{2}N_f g^2\int\frac{\mathrm{d}^4K}{(2\pi)^4}\mathrm{Tr}\left[\gamma^\mu S(Q)\gamma^\nu S(K)\right]\,, \tag{3.39}$$

where S denotes the bare quark propagator as defined in Eq. (3.7) and $Q = K - P$. The trace over the color matrices gives $\delta_{ab}/2$ which indicates the self-energy is proportional to a

unit matrix in the color space. In the following, we will suppress the color indices. Summing the "11" and "12" components of the KELDYSH representation leads to

$$\begin{aligned}\Pi^{\mu\nu}(P) &= \Pi^{11}(P)+\Pi^{12}(P)\\ &= -\frac{i}{2}N_f g^2\int\frac{\mathrm{d}^4K}{(2\pi)^4}\left(\mathrm{Tr}\left[\gamma^\mu S_{11}(Q)\gamma^\nu S_{11}(K)\right]-\mathrm{Tr}\left[\gamma^\mu S_{21}(Q)\gamma^\nu S_{12}(K)\right]\right),\end{aligned} \tag{3.40}$$

where the minus sign in front of the second term comes from the vertex of the type 2 fields [83]. In this calculation, we will neglect the fermion mass and write the fermion propagator as $S(K)\equiv \not{K}\tilde{\Delta}(K)$. Performing the trace over the γ-matrices and using Eq. (3.11), we get

$$\begin{aligned}\Pi^{\mu\nu}(P) &= -iN_f g^2\int\frac{\mathrm{d}^4K}{(2\pi)^4}\Big[\tilde{\Delta}_F(Q)\tilde{\Delta}_R(K)+\tilde{\Delta}_A(Q)\tilde{\Delta}_F(K)\\ &+ \tilde{\Delta}_A(Q)\tilde{\Delta}_A(K)+\tilde{\Delta}_R(Q)\tilde{\Delta}_R(K)\Big]\left[Q^\mu K^\nu+K^\mu Q^\nu-g^{\mu\nu}(K\cdot Q)\right].\end{aligned} \tag{3.41}$$

Similarly, we have $S_{R,A,F}(K)\equiv \not{K}\tilde{\Delta}_{R,A,F}(K)$. Note that the distribution function which appears in the symmetric propagator is not necessary to be equilibrium. Terms containing $\tilde{\Delta}_A(Q)\tilde{\Delta}_A(K)$ and $\tilde{\Delta}_R(Q)\tilde{\Delta}_R(K)$ vanish after integration over k_0 [87, 75]. Temperature independent terms will be dropped in the following. Shifting variables $K\to -K+P$ in the first term, we find that the two terms, $\tilde{\Delta}_F(Q)\tilde{\Delta}_R(K)$ and $\tilde{\Delta}_A(Q)\tilde{\Delta}_F(K)$ have the same contributions to the final result. This is still true for a non-equilibrium distribution which satisfies $n(\mathbf{k})=n(-\mathbf{k})$. Then, the retarded self-energy reads

$$\begin{aligned}\Pi^{ij}(P) &= 2N_f g^2\int_{\mathbf{k}}\frac{n(\mathbf{k})}{k}\Bigg[\frac{2k^ik^j-p^ik^j-k^ip^j+\delta^{ij}(-\omega k+\mathbf{k}\cdot\mathbf{p})}{P^2-2k\,\omega+2\mathbf{k}\cdot\mathbf{p}-i\,\mathrm{sgn}(k-\omega)\epsilon}\\ &+ \frac{2k^ik^j-p^ik^j-k^ip^j+\delta^{ij}(\omega k+\mathbf{k}\cdot\mathbf{p})}{P^2+2k\,\omega+2\mathbf{k}\cdot\mathbf{p}-i\,\mathrm{sgn}(-k-\omega)\epsilon}\Bigg].\end{aligned} \tag{3.42}$$

Here, we only consider the spatial components of the self-energy tensor. Other components can be obtained by using the transversality of the tensor. Adopting the *HL approximation*, we assume that the internal momenta are of order T and therefore much larger than the external momenta which are of order gT [5]. The integrand in the square bracket can then be expanded in powers of the coupling and the leading term is of the form

$$\frac{2k^ik^j}{-2k\,\omega+2\mathbf{k}\cdot\mathbf{p}-i\,\epsilon}+\frac{2k^ik^j}{2k\,\omega+2\mathbf{k}\cdot\mathbf{p}+i\,\epsilon}. \tag{3.43}$$

If we replace $\mathbf{k}$ by $-\mathbf{k}$ for the first term, it can be easily shown that after integrating over $\mathbf{k}$, it cancels the contribution from the second term provided $n(\mathbf{k})=n(-\mathbf{k})$. As a result, the leading contribution vanishes. However, without this condition, the above two terms will give contributions which dominate over the HL results and such contributions appear

[5] For an arbitrary anisotropic distribution, we have to require the HL condition for each component, i.e. $\omega, p^i \ll k^i$, whereas in the isotropic (equilibrium) case $\omega, p \ll k$ suffices [75].

to be gauge independent. The next to leading term comes from the following four terms in the expansion of the integrand in the square bracket

$$\begin{aligned}\frac{-p^ik^j-k^ip^j+\delta^{ij}(-\omega k+\mathbf{k}\cdot\mathbf{p})}{-2k\,\omega+2\mathbf{k}\cdot\mathbf{p}-i\,\epsilon} &+ \frac{-p^ik^j-k^ip^j+\delta^{ij}(\omega k+\mathbf{k}\cdot\mathbf{p})}{2k\,\omega+2\mathbf{k}\cdot\mathbf{p}+i\,\epsilon}\\ -\frac{2k^ik^jP^2}{(-2k\,\omega+2\mathbf{k}\cdot\mathbf{p}-i\,\epsilon)^2} &- \frac{2k^ik^jP^2}{(2k\,\omega+2\mathbf{k}\cdot\mathbf{p}+i\,\epsilon)^2}\,.\end{aligned} \tag{3.44}$$

In fact, the first two terms in Eq. (3.44) give the same result, the last two terms also contribute equally after integrating over $\mathbf{k}$. As a result, the retarded self-energy can be expressed as

$$\Pi^{ij}(P)=2N_fg^2\int_{\mathbf{k}}\frac{n(\mathbf{k})}{k}\frac{(p^ik^j+k^ip^j)(\omega k-\mathbf{k}\cdot\mathbf{p})+\delta^{ij}(\omega k-\mathbf{k}\cdot\mathbf{p})^2-k^ik^jP^2}{(\omega k-\mathbf{k}\cdot\mathbf{p}+i\,\epsilon)^2}\,. \tag{3.45}$$

As we discussed in Sec. 3.2, the gluonic contributions to the self-energy tensor have the same structure as the quark ones in HL approximation [86], we can simply replace $2N_fn(\mathbf{k})$ by $f(\mathbf{k})=N_f(n(\mathbf{k})+\bar{n}(\mathbf{k}))+2N_cN(\mathbf{k})$ to get the full results of the gluon self-energy.

Now, we are going to prove Eq. (3.45) is fully equivalent to Eq. (2.35). For the first term in Eq. (2.35), we have

$$g^2\int_{\mathbf{k}}v^i\frac{\partial f(\mathbf{k})}{\partial k^\beta}g^{j\beta}=g^2\int_{\mathbf{k}}f(\mathbf{k})\frac{\partial(k^i/k)}{\partial k^j}=g^2\int_{\mathbf{k}}\frac{f(\mathbf{k})}{k}(\delta^{ij}-v^iv^j)\,. \tag{3.46}$$

Similarly, the second term in Eq. (2.35) can be rewritten as

$$\begin{aligned}-\;& g^2\int_{\mathbf{k}}v^i\frac{\partial f(\mathbf{k})}{\partial k^l}\frac{v^jp^l}{P\cdot V}=g^2\int_{\mathbf{k}}f(\mathbf{k})p^l\frac{\partial(\frac{k^ik^j}{k(P\cdot K)})}{\partial k^l}\\ =\;& g^2\int_{\mathbf{k}}\frac{f(\mathbf{k})}{k}\frac{(p^ik^j+k^ip^j)(P\cdot K)-k^ik^j[\mathbf{p}\cdot\mathbf{v}(P\cdot V)+(\omega\mathbf{p}\cdot\mathbf{v}-p^2)]}{(P\cdot K+i\,\epsilon)^2}\,.\end{aligned} \tag{3.47}$$

In the above equations, we perform a partial integration and use the condition $f(\mathbf{k}\to\infty)=0$. Adding Eqs. (3.46) and (3.47) together, we can immediately get Eq. (3.45). Note that the reflection symmetry of the distribution function is not necessary in the transport theory approach. If the distribution function in Eq. (3.45) is isotropic, for example, the equilibrium Fermi-Dirac or Bose-Einstein distribution, the integrals over k and over the solid angle Ω are decoupled, we can easily reproduce the results we obtained in the imaginary time formalism.

The symmetry and the transversality of the self-energy tensor can be also proved in the real time formalism. The symmetry can be directly read out from Eq. (3.41). Now we will prove the transversality of the self-energy tensor. We start with $P_\mu\Pi^{\mu\nu}(P)$ by considering first the quark-loop contribution

$$P_\mu\Pi^{\mu\nu}(P)=-i\,N_f\,g^2\int\frac{\mathrm{d}^4K}{(2\pi)^4}\left[2(P\cdot K)K^\nu-K^2P^\nu\right]\left[\tilde{\Delta}_F(Q)\tilde{\Delta}_R(P)+\tilde{\Delta}_A(Q)\tilde{\Delta}_F(P)\right]. \tag{3.48}$$

Integrating over k_0 we get

$$P_\mu \Pi^{\mu 0}(P) = 2N_f\, g^2 \int_{\mathbf{k}} \frac{n(\mathbf{k})}{k} \left[\frac{2(\omega k - \mathbf{k}\cdot\mathbf{p})k - P^2 k}{-2\omega k + 2\mathbf{k}\cdot\mathbf{p} + P^2 - i\,\mathrm{sgn}(k-\omega)\epsilon} + \frac{-2(-\omega k - \mathbf{k}\cdot\mathbf{p})k + P^2 k}{2\omega k + 2\mathbf{k}\cdot\mathbf{p} + P^2 - i\,\mathrm{sgn}(-k-\omega)\epsilon} \right]. \tag{3.49}$$

The integrands in the square bracket can be expanded for small external momenta analogously to Eqs. (3.43) and (3.44). The leading term vanishes due to the reflection symmetry of the distribution function. We find that the next to leading term in the expansion which contributes in HL approximation is exactly zero. As a result, $P_\mu \Pi^{\mu 0}(P) = 0$ with the HL approximation. Similarly, we can show that $P_\mu \Pi^{\mu\, i}(P) = 0$. Due to the same structure of the gluonic contributions, the total gluon self-energy is transverse.

Finally, the time-like components can be obtained by using the transversality of the self-energy tensor

$$\Pi^{0m}(P) = p^l \Pi^{lm}(P)/\omega\,, \quad \Pi^{00}(P) = p^l p^m \Pi^{lm}(P)/\omega^2\,. \tag{3.50}$$

With the above discussions, we demonstrated that the gluon self-energy can be derived equivalently from both transport theory and QCD diagrammatic analysis. The HL approach has been generalized to systems out of equilibrium. However, up to now, only very specific forms of deviations from the equilibrium have been discussed: systems out of chemical equilibrium, which are relevant in the context of heavy-ion collisions [88], and such where the momentum distribution is isotropic but not of the Fermi-Dirac or Bose-Einstein form [89, 90, 87]. In the following chapters, we will concentrate on systems whose distributions are anisotropic in momentum space. Such a distribution is relevant for parton system generated in the heavy-ion collisions. Particularly, we study the effects due to a local anisotropy of the plasma in momentum space on the heavy-quark potential and the in-medium properties of quarkonium states.

4 The anisotropic quark-gluon plasma

In this chapter, we are going to consider a QCD plasma in which the parton distribution is anisotropic in momentum space. In general, an anisotropic plasma can be either in equilibrium or out of equilibrium. The state of equilibrium being static and homogeneous is sometimes anisotropic and the anisotropy appears due to the external fields, for example, the magnetized plasma. Anisotropic states are also common for systems which are out of equilibrium. One example is the quark-gluon plasma which is of particular interest for us. The parton system generated at the early stage in the ultra-relativistic heavy-ion collisions at RHIC or LHC has a strong anisotropy in its distribution in momentum space due to the different expanding rate of the transverse and longitudinal directions [91, 56].

It is interesting to study the effects due to the presence of an anisotropy. Such effects will change the properties of the QGP system and make differences when comparing with the usually studied isotropic QGP [1]. One of the effects is the so-called chromo-Weibel instability which we review in this chapter [92, 93, 94, 95, 59, 60, 96, 97]. Besides the stable modes we discussed in Chapter 2 for an isotropic QCD plasma, there are also unstable modes which appear when the parton distributions become anisotropic. In the original paper [52], Weibel showed the unstable transverse modes exist in electromagnetic plasmas with anisotropic momentum distributions and the rate of growth for these unstable modes was derived in linear response theory. In the QGP system, it is still worthwhile to investigate these instabilities which are characterized by exponential growth of the transverse chromo-magnetic fields and such unstable modes may play an important role in the thermalization of quark-gluon plasma from anisotropic, non-equilibrium initial conditions.

4.1 The anisotropy in momentum space

The introduction of an anisotropic distribution is necessary for descriptions of QGP created in the heavy-ion collisions. Immediately after the collision, the partons are produced from the incoming colliding nuclei at $\tau = \tau_0 \sim Q_s^{-1}$, at which time the partonic momentum distributions can be assumed to be isotropic (but not necessary to be equilibrium). Here, τ is the proper time and Q_s is the gluon saturation scale. The physics at early times is dominated by the hard gluons with momentum at the saturation scale which have occupation numbers of order $1/\alpha_s$ [98, 99, 100].

For $\tau > Q_s^{-1}$, the hard gluons would simply follow straight-line trajectories and segregate themselves in beam direction if there is no interaction. The expansion which is most relevant is the longitudinal expansion of the matter since at early times it is much larger than the radial expansion. The longitudinal expansion causes the system to quickly become much

[1] We consider an isotropic system which is described by the equilibrium Fermi-Dirac or Bose-Einstein distributions.

colder in the longitudinal direction than in the transverse (radial) direction, $k_\perp \gg k_z \sim 1/\tau$ and a local momentum *anisotropy* appears.

Using collisional mechanisms, the "bottom-up" thermalization shows that during the first stage of evolution hard gluons scatter out-of-plane counteracting the effect of the expansion of the system reducing the rate at which the longitudinal momentum decreases instead to $k_z \sim Q_s^{2/3}\tau^{-1/3}$ [56]. Although less extreme in terms of the rate at which the longitudinal momentum decreases this scenario still results in considerable momentum space anisotropies in the gluon distribution function.

Because the first stage of the "bottom-up" scenario is described by hard gluons with $k_z \ll k_T \sim Q_s$, in order to demonstrate the instability, we use such a distribution of hard partons that is approximately described by a class of anisotropic distribution functions. The anisotropic distribution can be obtained by stretching or squeezing an isotropic one along a certain direction, thereby preserving a cylindrical symmetry in momentum space. This particular class of distribution functions has been first discussed by Romatschke and Strickland which takes the following form [60, 96]

$$f(\mathbf{k}) = f_{\rm iso}\left(\sqrt{k^2 + \xi(\mathbf{k}\cdot\mathbf{n})^2}\right), \tag{4.1}$$

where $f_{\rm iso}$ is an arbitrary isotropic distribution function [2]. In real time approach, the distribution $f_{\rm iso}$ is not necessarily thermal. In the above equation, we denote the direction of anisotropy by a unit vector $\mathbf{n}$.

The parameter ξ which is an adjustable anisotropy parameter determines the degree of anisotropy,

$$\xi = \frac{1}{2}\langle k_\perp^2\rangle/\langle k_z^2\rangle - 1\,, \tag{4.2}$$

where $k_z \equiv \mathbf{k}\cdot\mathbf{n}$ and $\mathbf{k}_\perp \equiv \mathbf{k} - \mathbf{n}(\mathbf{k}\cdot\mathbf{n})$ denote the particle momentum along and perpendicular to the direction of anisotropy, respectively. $\xi > 0$ corresponds to a contraction of the distribution in $\mathbf{n}$ direction, whereas $-1 < \xi < 0$ represents a stretching of the distribution in $\mathbf{n}$ direction. Alternatively, positive ξ corresponds to removing particles with a large momentum component along $\mathbf{n}$ direction while the negative values correspond to adding particles with a large momentum component along $\mathbf{n}$ direction. If $f_{\rm iso}$ is a thermal ideal-gas distribution and ξ is small then ξ is also related to the shear viscosity of the plasma; for example, for one-dimensional Bjorken expansion in the Navier-Stokes limit [101]

$$\xi = \frac{10}{T\tau}\frac{\eta}{s}\,, \tag{4.3}$$

where η/s is the ratio of shear viscosity to entropy density [3]. In an expanding system, non-vanishing viscosity implies finite momentum relaxation rate and therefore an anisotropy of the particle momenta. For $\eta/s \simeq 0.1$– 0.2 and $\tau T \simeq 1$– 3, one finds that $\xi \simeq 1$. According to Eq. (4.2), if we choose $\mathbf{n}$ to be parallel to the beam direction, then $\xi > 0$ is the case relevant for the heavy-ion collisions.

For a certain anisotropy Fig. 4.1 shows how this procedure deforms the Fermi-Dirac distribution.

[2] The function $f_{\rm iso}(k)$ should decrease monotonically with k, so that the square of the Debye mass defined in Eq. (4.8) is guaranteed to be positive.

[3] Note that this expression only holds true in the Navier-Stokes limit. In the general case, one can relate ξ to the shear tensor. For more information, please see [102].

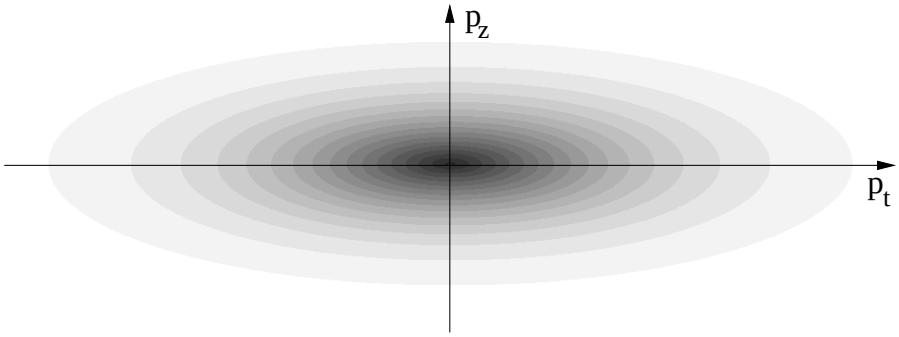

Figure 4.1: Contour plot of a squeezed FERMI-DIRAC distribution with anisotropy parameter $\xi = 10$. The anisotropy vector $\mathbf{n}$ is taken to be along the p_z direction. Figure taken from [78].

In such anisotropic systems it has been shown that the physics of the QCD collective modes changes dramatically as compared to the isotropic case and instabilities are present which can accelerate the thermalization and isotropization of the plasma. We will discuss the instabilities in Sec. 4.5.

4.2 The gluon self-energy in an anisotropic QCD plasma

The expression of the *retarded gluon self-energy* as derived in Chapter 2 contains a parton distribution function $f(\mathbf{k})$ which is completely arbitrary. With the specified anisotropic distribution function, we can compute the gluon self-energy analytically. Again we will restrict our consideration to the spatial part of $\Pi^{\mu\nu}$ for simplicity and the time-like components can be easily obtained by using the symmetry and transversality of the gluon self-energy tensor. The spatial components of the self-energy tensor reads

$$\Pi^{ij}(P) = -g^2 \int_{\mathbf{k}} v^i \frac{\partial f(\mathbf{k})}{\partial k^l} \left(\delta^{jl} + \frac{v^j p^l}{P \cdot V + i\epsilon} \right) . \tag{4.4}$$

According to the structure of the anisotropic distribution function introduced in Sec. 4.1, we can simplify the above expression by performing a change of variables to $\tilde{k}$, namely we introduce [60]

$$\tilde{k}^2 = k^2 \left(1 + \xi (\mathbf{v} \cdot \mathbf{n})^2 \right) . \tag{4.5}$$

Consequently, we have the following relations

$$\begin{aligned} \frac{\partial f(\mathbf{k})}{\partial k^l} &= \frac{v^l + \xi (\mathbf{v} \cdot \mathbf{n}) n^l}{\sqrt{1 + \xi (\mathbf{v} \cdot \mathbf{n})^2}} \frac{\partial f_{\text{iso}}(\tilde{k}^2)}{\partial \tilde{k}} , \\ \mathrm{d}^3 k &= \frac{\tilde{k}^2 \mathrm{d}\tilde{k} \mathrm{d}\Omega}{1 + \xi (\mathbf{v} \cdot \mathbf{n})^{3/2}} . \end{aligned} \tag{4.6}$$

Now it is possible to integrate out the $\tilde{k}$-dependence giving

$$\Pi^{ij}(P) = m_D^2 \int \frac{\mathrm{d}\Omega}{4\pi} v^i \frac{v^l + \xi (\mathbf{v} \cdot \mathbf{n}) n^l}{(1 + \xi (\mathbf{v} \cdot \mathbf{n})^2)^2} \left(\delta^{jl} + \frac{v^j p^l}{P \cdot V + i\epsilon} \right) , \tag{4.7}$$

where

$$m_D^2 = -\frac{g^2}{2\pi^2}\int_0^\infty \mathrm{d}k\, k^2 \frac{\mathrm{d}f_{\mathrm{iso}}(k^2)}{\mathrm{d}k}\,. \tag{4.8}$$

Comparing Eq. (2.46), we find that in our treatment the DEBYE mass doesn't change when the anisotropic distribution is considered. In QCD case, $m_D^2 = g^2T^2(N_f + 2N_c)/6$, while in QED case, we have $m_D^2 = e^2T^2/3$.

Note that in Eq. (4.7), there is an extra dependence on the preferred anisotropic direction $\mathbf{n}$ as compared to the corresponding isotropic result in Eq. (2.45). Therefore we can no longer decompose the self-energy into transverse and longitudinal parts. In general, the self-energy tensor depends on the soft momentum P, the anisotropic direction $\mathbf{n}$ as well as the heat bath direction [4]. We develop the following tensor bases for a symmetric three-tensor [60]:

$$\begin{aligned} A^{ij} &= \delta^{ij} - p^i p^j/p^2\,, \\ B^{ij} &= p^i p^j/p^2\,, \\ C^{ij} &= \tilde{n}^i\tilde{n}^j/\tilde{n}^2\,, \\ D^{ij} &= p^i\tilde{n}^j + p^j\tilde{n}^i\,, \end{aligned} \tag{4.9}$$

and decompose the self-energy tensor into four *structure functions*

$$\Pi^{ij} = \alpha A^{ij} + \beta B^{ij} + \gamma C^{ij} + \delta D^{ij}\,. \tag{4.10}$$

In Eq. (4.9), $\tilde{n}^i = A^{ij}n^j$ is the part of $\mathbf{n}$ that is orthogonal to p^i, i.e. $\tilde{\mathbf{n}}\cdot\mathbf{p} = 0$. Actually, the first two tensor bases A^{ij} and B^{ij} are exactly the same as those in the isotropic case. The isotropic results can be reproduced by setting $\xi = 0$. In this limit, the self-energy doesn't depend on $\mathbf{n}$ any more. We can immediately get the following results

$$\begin{aligned} \alpha(P,0) &= \Pi_T(P)\,, \\ \beta(P,0) &= \frac{\omega^2}{p^2}\Pi_L(P)\,, \\ \gamma(P,0) &= 0\,, \\ \delta(P,0) &= 0\,, \end{aligned} \tag{4.11}$$

where $\Pi_T(P)$ and $\Pi_L(P)$ are given by Eqs. (2.52) and (2.53), respectively.

For non-zero anisotropy parameter ξ, we determine the four structure functions by taking the contractions:

$$\begin{aligned} p^i\Pi^{ij}p^j &= p^2\,, \\ \tilde{n}^i\Pi^{ij}p^j &= \tilde{n}^2p^2\,, \\ \tilde{n}^i\Pi^{ij}\tilde{n}^j &= \tilde{n}^2(\alpha+\gamma)\,, \\ \mathrm{Tr}\,\Pi^{ij} &= 2\alpha+\beta+\gamma\,. \end{aligned} \tag{4.12}$$

Besides the dependence on DEBYE mass, the strength of the anisotropy ξ, and the four momentum P, the four structure functions also depend on the angle between the spatial

[4] As before, we work in the local rest frame and the heat bath direction is given by $(1,0,0,0)$. For the spatial components, there is no explicit dependence on this direction.

momentum and the anisotropy direction. If we choose $\mathbf{n} = \hat{\mathbf{z}}$, the dependence on the spatial momentum $\mathbf{p}$ is no longer independent on the polar angle, but it has a symmetry in the transverse plane (transverse to $\mathbf{n}$). Then we can choose $\mathbf{p}$ to lie in the x-z plane which immediately follows by $\mathbf{p}\cdot\mathbf{v} = p_x\cos\phi\sin\theta' + p_z\cos\theta'$ [5]. With the above setup, we can perform the solid angle integral in Eq. (4.7). For example, we consider the structure function β

$$\begin{aligned}
\beta &= \frac{m_D^2}{p^2}\int\frac{\mathrm{d}\Omega}{4\pi}\mathbf{p}\cdot\mathbf{v}\frac{v^l+\xi\cos\theta' n^l}{(1+\xi\cos^2\theta')^2}(p^l+\frac{\mathbf{p}\cdot\mathbf{v}p^l}{\omega-\mathbf{p}\cdot\mathbf{v}+i\,\epsilon}) \\
&= \frac{m_D^2}{p^2}\int\frac{\mathrm{d}\Omega}{4\pi(1+\xi\cos^2\theta')^2}\left(\omega(\mathbf{p}\cdot\mathbf{v}+\xi\cos\theta' p_z)+\omega^2(\frac{\omega+\xi\cos\theta' p_z}{\omega-\mathbf{p}\cdot\mathbf{v}+i\,\epsilon}-1)\right) \\
&= \frac{-m_D^2\omega^2}{p^2}\int\frac{\mathrm{d}(\cos\theta')}{2(1+\xi\cos^2\theta')^2}\left(1-(\omega+\xi\cos\theta' p_z)R(w-p_z\cos\theta', p_x\sin\theta')\right),
\end{aligned} \tag{4.13}$$

where the new function $R(a,b)$ is defined as

$$R(a,b) = \int_0^{2\pi}\frac{d\phi}{2\pi}\frac{1}{a-b\cos\phi+i\epsilon} = \frac{1}{\sqrt{a+b+i\epsilon}\sqrt{a-b+i\epsilon}}\,. \tag{4.14}$$

When a and b are real-valued R can be simplified to

$$R(a,b) = \frac{\mathrm{sgn(a)}\Theta(\mathrm{a}^2-\mathrm{b}^2)}{\sqrt{a^2-b^2}} - \frac{i\Theta(b^2-a^2)}{\sqrt{b^2-a^2}}\,, \tag{4.15}$$

with $\Theta(x)$ being the usual step-function. The calculation for other three structure functions is straightforward but tedious. We only list the results here [60]

$$\begin{aligned}
\alpha(P,\xi) &= \frac{m_D^2}{p^2\tilde{n}^2}\int\frac{\mathrm{d}(\cos\theta')}{2}\frac{\omega+\xi p_z\cos\theta'}{(1+\xi(\cos\theta')^2)^2}\Big[\omega-p_z\cos\theta' \\
&\qquad +p^2(s^2-(\cos\theta'-\frac{\omega p_z}{p^2})^2)R(\omega-p_z\cos\theta', p_x\sin\theta')\Big], \\
\gamma(P,\xi) &= m_D^2\int\frac{\mathrm{d}(\cos\theta')}{2}\frac{1}{p^2(1+\xi\cos^2\theta')^2}\Big[\omega^2+\xi p^2\cos^2\theta'-2\frac{p^2}{p_x^2}(\omega^2-\xi p_z^2\cos^2\theta') \\
&+ \frac{(\omega+\xi p_z\cos\theta')p^4}{p_x^2}\left(2(\cos\theta'-\frac{\omega p_z}{p^2})^2-s^2\right)R(\omega-p_z\cos\theta', p_x\sin\theta')\Big], \\
\delta(P,\xi) &= \frac{m_D^2\omega}{p^4\tilde{n}^2}\int\frac{\mathrm{d}(\cos\theta')}{2}\frac{\omega+\xi p_z\cos\theta'}{(1+\xi\cos^2\theta')^2}\Big[p_z+(p^2\cos\theta'-\omega p_z) \\
&\qquad \times R(\omega-p_z\cos\theta', p_x\sin\theta')\Big],
\end{aligned} \tag{4.16}$$

where $s^2 = (1-\omega^2/p^2)(p_x^2/p^2)$. The remaining integration over θ' can also be done analytically. However, we don't list the rather cumbersome explicit expressions here. In the above results we assume $\mathbf{p}$ lies in the x-z plane. In the general case, p_x should be replaced by $\mathbf{p}_\perp$.

[5] We use the notation $\mathrm{d}\Omega = \mathrm{d}(\cos\theta')\mathrm{d}\phi$

Although the four structure functions have much more complicated expressions at finite ξ than the isotropic case, they share the same features as the corresponding isotropic structure functions Π_L and Π_T. There is a cut in the complex ω plane which we can choose to run along the real ω axis from $-p < \omega < p$. For real-valued ω the structure functions are complex when $\omega < p$ and real when $\omega > p$. For imaginary-valued ω all the structure functions are real-valued.

For the sake of the studies of quarkonium states in an anisotropic QCD plasma in the next chapters, we are going to analyze the four structure functions in two special cases which are of particular interest for our work. Firstly, we consider the four structure functions in the static limit by taking $\omega \to 0$. As we will see later, the values in static limit are relevant for the calculation of the heavy-quark potential where the quark pairs are almost at rest due to the large quark masses and the non-relativistic limit will be considered.

As ω approaches to zero along the real axis, the leading term of α and γ is at the order of $\sim \mathcal{O}(\omega^0)$ and we can define the corresponding *mass scales* as

$$\begin{aligned} m_\alpha^2 &= \lim_{\omega\to 0} \alpha\,, \\ m_\gamma^2 &= \lim_{\omega\to 0} \gamma\,. \end{aligned} \tag{4.17}$$

For β and δ, the leading contribution is at the order of $\sim \mathcal{O}(\omega^2)$ and $\sim \mathcal{O}(i\omega)$, respectively. Similarly, we define another two mass scales as

$$\begin{aligned} m_\beta^2 &= \lim_{\omega\to 0} -\frac{p^2}{\omega^2}\beta\,, \\ m_\delta^2 &= \lim_{\omega\to 0} \frac{\tilde{n}p^2}{\omega}\mathrm{Im}\,\delta\,. \end{aligned} \tag{4.18}$$

According to Eq. (4.15), if the integrands contain the function R, the interval of the integration over $\cos\theta'$ should be divided into three small intervals at static limit,

$$\int_{-1}^{1} \mathrm{d}(\cos\theta') = \int_{-1}^{-p_x/p} \mathrm{d}(\cos\theta') + \int_{-p_x/p}^{p_x/p} \mathrm{d}(\cos\theta') + \int_{p_x/p}^{1} \mathrm{d}(\cos\theta')\,. \tag{4.19}$$

Note that function R is imaginary-valued when $-p_x/p < \cos\theta' < p_x/p$. In this interval, we can easily check that in Eqs. (4.13) and (4.16), integrands which contain R are odd functions of $\cos\theta'$ for α, β/ω^2 and γ. As a result, $\int_{-1}^{1} \mathrm{d}(\cos\theta') \to \int_{-1}^{-p_x/p} \mathrm{d}(\cos\theta') + \int_{p_x/p}^{1} \mathrm{d}(\cos\theta')$ [6]. While for δ/ω, it is an even function of $\cos\theta'$, only $\int_{-p_x/p}^{p_x/p} \mathrm{d}(\cos\theta')$ contributes. In addition, integrands without function R are real-valued therefore their contributions to the mass scales are also real. Especially, for δ/ω such a contribution is zero.

The above discussion shows in the static limit, δ/ω is imaginary while the other three mass scales are real. The analytical results for the four mass scales can be obtained after

[6] Note that the sum of these two terms are not simply zero because of the sign function in Eq. (4.15). In the calculation, we assume p_x and p_z are positive due to the symmetry and there is no ambiguity.

we perform the integration over θ'. Explicitly, we have

$$\begin{aligned}
m_\alpha^2 &= -\frac{m_D^2}{2p_\perp^2\sqrt{\xi}}\left(p_z^2\arctan\sqrt{\xi}-\frac{p_z p^2}{\sqrt{p^2+\xi p_\perp^2}}\arctan\frac{\sqrt{\xi}p_z}{\sqrt{p^2+\xi p_\perp^2}}\right),\\
m_\beta^2 &= m_D^2\frac{(\sqrt{\xi}+(1+\xi)\arctan\sqrt{\xi})(p^2+\xi p_\perp^2)+\xi p_z\left(p_z\sqrt{\xi}+\frac{p^2(1+\xi)}{\sqrt{p^2+\xi p_\perp^2}}\arctan\frac{\sqrt{\xi}p_z}{\sqrt{p^2+\xi p_\perp^2}}\right)}{2\sqrt{\xi}(1+\xi)(p^2+\xi p_\perp^2)},\\
m_\gamma^2 &= -\frac{m_D^2}{2}\left(\frac{p^2}{\xi p_\perp^2+p^2}-\frac{1+\frac{2p_z^2}{p_\perp^2}}{\sqrt{\xi}}\arctan\sqrt{\xi}+\frac{p_z p^2(2p^2+3\xi p_\perp^2)}{\sqrt{\xi}(\xi p_\perp^2+p^2)^{\frac{3}{2}}p_\perp^2}\arctan\frac{\sqrt{\xi}p_z}{\sqrt{p^2+\xi p_\perp^2}}\right),\\
m_\delta^2 &= -\frac{\pi m_D^2\xi p_z p_\perp p}{4(\xi p_\perp^2+p^2)^{\frac{3}{2}}},
\end{aligned}\tag{4.20}$$

and

$$p^2 = p_\perp^2 + p_z^2\,. \tag{4.21}$$

The above expressions apply when $\mathbf{n}=(0,0,1)$ points along the z-axis. In the general case, p_z and $\mathbf{p}_\perp$ get replaced by $\mathbf{p}\cdot\mathbf{n}$ and $\mathbf{p}-\mathbf{n}(\mathbf{p}\cdot\mathbf{n})$, respectively. Note that besides the dependence on the DEBYE mass and anisotropy parameter ξ, the four mass scales depend on the angle between $\mathbf{p}$ and $\mathbf{n}$. When the isotropic limit is considered, the only non-vanishing mass scale is $m_\beta^2 = m_D^2$.

The other special case we will discuss here is the small but non-zero anisotropy because small ξ is more relevant to the quarkonium studies. In heavy-ion collisions quarkonium states are expected to form when the temperature has dropped to (1– 2) T_c, by then, the plasma may have equilibrated at least partly. In this case, the plasma distribution is close to the ideal FERMI-DIRAC or BOSE-EINSTEIN distribution. In the small-ξ limit it is possible to obtain analytic expressions for all of the structure functions order by order in ξ. To linear order in ξ [60]

$$\begin{aligned}
\alpha &= \Pi_T(z)+\xi\left[\frac{z^2}{12}(3+5\cos 2\theta_n)m_D^2-\frac{1}{6}(1+\cos 2\theta_n)m_D^2\right.\\
&\qquad\left.+\frac{1}{4}\Pi_T(z)\left((1+3\cos 2\theta_n)-z^2(3+5\cos 2\theta_n)\right)\right],\\
z^{-2}\beta &= \Pi_L(z)+\xi\left[\frac{1}{6}(1+3\cos 2\theta_n)m_D^2+\Pi_L(z)\left(\cos 2\theta_n-\frac{z^2}{2}(1+3\cos 2\theta_n)\right)\right],\\
\gamma &= \frac{\xi}{3}(3\Pi_T(z)-m_D^2)(z^2-1)\sin^2\theta_n\,,\\
\delta &= \frac{\xi}{3p}(4z^2m_D^2+3\Pi_T(z)(1-4z^2))\cos\theta_n\,,
\end{aligned}\tag{4.22}$$

where $z=\omega/p$ and θ_n is the angle between $\mathbf{p}$ and $\mathbf{n}$.

Using Eq. (2.41), we can obtain the anisotropic gluon propagator in temporal axial gauge

$$\mathbf{D}(P) = \Delta_A\mathbf{A}+(p^2-\omega^2+\alpha+\gamma)\Delta_G\mathbf{B}+[(\beta-\omega^2)\Delta_G-\Delta_A]\mathbf{C}-\delta\Delta_G\mathbf{D}\,, \tag{4.23}$$

with

$$\Delta_A^{-1}(P) = p^2 - \omega^2 + \alpha\,, \tag{4.24}$$
$$\Delta_G^{-1}(P) = (p^2 - \omega^2 + \alpha + \gamma)(\beta - \omega^2) - p^2\tilde{n}^2\delta^2\,. \tag{4.25}$$

4.3 Stable modes

Now we will discuss the collective modes in an anisotropic plasma. Firstly, we consider the *stable modes* which have poles at real-valued $\omega > p$. This is similar as what we did in the isotropic case except that extra modes may appear for non-zero anisotropy. Consider zeros of Δ_G^{-1}, we can make use of the following factorization [60]:

$$\Delta_G^{-1} = (\omega^2 - \Omega_+^2)(\omega^2 - \Omega_-^2)\,, \tag{4.26}$$

where

$$2\Omega_\pm^2 = \bar{\Omega}^2 \pm \sqrt{\bar{\Omega}^4 - 4((\alpha + \gamma + p^2)\beta - p^2\tilde{n}^2\delta^2)}\,, \tag{4.27}$$

and

$$\bar{\Omega}^2 = \alpha + \beta + \gamma + p^2\,. \tag{4.28}$$

Note that the quantity under the square root in Eq. (4.27) is always positive for real $\omega > p$. It can be easily shown by rewriting this quantity as $(\alpha - \beta + \gamma + p^2)^2 + 4p^2\tilde{n}^2\delta^2$. In the case of real $\omega > p$, all the structure functions are real. Therefore there are at most two stable modes coming from Δ_G.

The remaining stable collective modes come from the zeros of Δ_A^{-1}. The *dispersion relations* for all of the collective modes are then given by the solutions

$$\omega_\pm^2 = \Omega_\pm^2(\omega_\pm)\,,$$
$$\omega_\alpha^2 = p^2 + \alpha(\omega_\alpha)\,. \tag{4.29}$$

In the isotropic limit ($\xi \to 0$), there are only two modes as we discussed before, namely $\omega_\alpha = \omega_+ = \omega_T$ and $\omega_- = \omega_L$. For finite ξ, there are three stable quasi-particle modes with dispersion relations that depend on the angle of propagation with respect to the anisotropy direction, θ_n. Similarly, the dispersion relations can be determined numerically. For simplicity, we plot the dispersion relations at non-zero anisotropy in the case where the propagation direction is parallel to the direction of anisotropy, i. e. $\theta_n = 0$. In this case, there are only two modes appear at non-zero anisotropy [7] and we denote them as transverse and longitudinal modes. The comparison with the corresponding isotropic modes is shown in Fig. 4.2. The dispersion relations for all three modes for different angles θ_n are shown in Ref. [60].

4.4 Unstable modes

For a finite ξ, there are also some collective modes whose dispersion relations can be determined by taking imaginary-valued ω. These modes are either exponentially decaying which corresponds to poles of the propagator along the negative imaginary ω axis, or exponentially

[7] Note that for this angle of propagation the structure function γ and $\tilde{n}^2$ vanish [96].

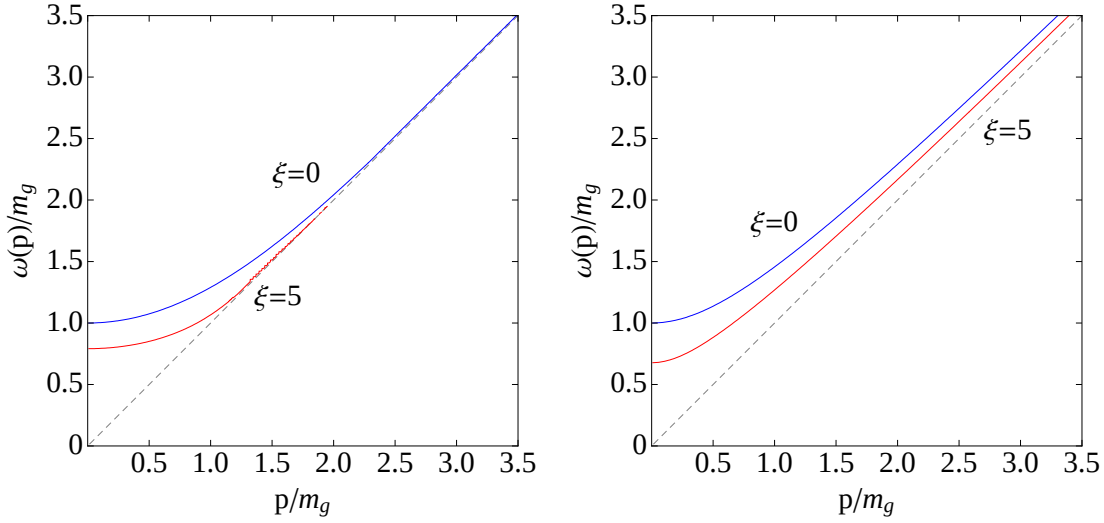

Figure 4.2: Dispersion relations for transverse and longitudinal gluons in units of $m_g = m_D/\sqrt{3}$ in both isotropic plasma and anisotropic plasma with $\xi = 5$, $\theta_n = 0$. The light-gray line is the light-cone which is plotted as a visual aide.
Left: The dispersion relations for longitudinal modes. Right: The dispersion relations for transverse modes.

growing which corresponds to poles along the positive imaginary ω axis. The existence of poles along the imaginary ω axis is one of the most interesting features of the anisotropic quark-gluon plasma. We are especially interested in the presence of *unstable modes* that, instead of being damped, grow exponentially with time. The qualitative explanation of the origin of these so-called chromo-Weibel instabilities will be discussed in Sec. 4.5. In addition, poles at complex ω (not purely imaginary) have been checked numerically but none were found [60].

To study the unstable modes of the system we can write $\omega \to i\Gamma$, with Γ being the real-valued solution to the equations

$$\begin{aligned} \Delta_G^{-1} &= (\Gamma^2 + \Omega_+^2)(\Gamma^2 + \Omega_-^2) = 0\,, \\ \Delta_A^{-1} &= (\Gamma^2 + p^2 + \alpha) = 0\,. \end{aligned} \tag{4.30}$$

With imaginary-valued ω, numerically one finds that $\Omega_+^2 > 0$ for all $\Gamma > 0$. As a result, there is at most one solution for $\Delta_G^{-1} = 0$. We can also check that $\Delta_A^{-1}(\omega = i\Gamma) = 0$ has only solutions for $\xi > 0$. It turns out that for $\xi > 0$, there are two unstable modes in the system which can be found by solving [60]

$$\begin{aligned} \Gamma_-^2 &= -\Omega_-^2(i\Gamma_-)\,, \\ \Gamma_\alpha^2 &= -p^2 - \alpha(i\Gamma_\alpha)\,. \end{aligned} \tag{4.31}$$

We denote these two unstable modes as minus-mode and α-mode respectively. We should point out only the positive solutions correspond to the instability, while those negative solutions correspond to the decaying ones. For simplicity, we only consider the case where

$\mathbf{p} \parallel \mathbf{n}$ ($\theta_n = 0$). There is only one unstable mode, α-mode in this special case. We show a plot of the growth rate Γ_α for different anisotropy parameters in Fig. 4.3. For solutions for arbitrary angles, please see Ref. [60]. It turns out that the growth rate is largest for $\theta_n = 0$, which we will explain on physical grounds in Sec. 4.5. From the plot, one can also see that the growth rate and the maximal value of p for the unstable modes become larger with increasing anisotropy.

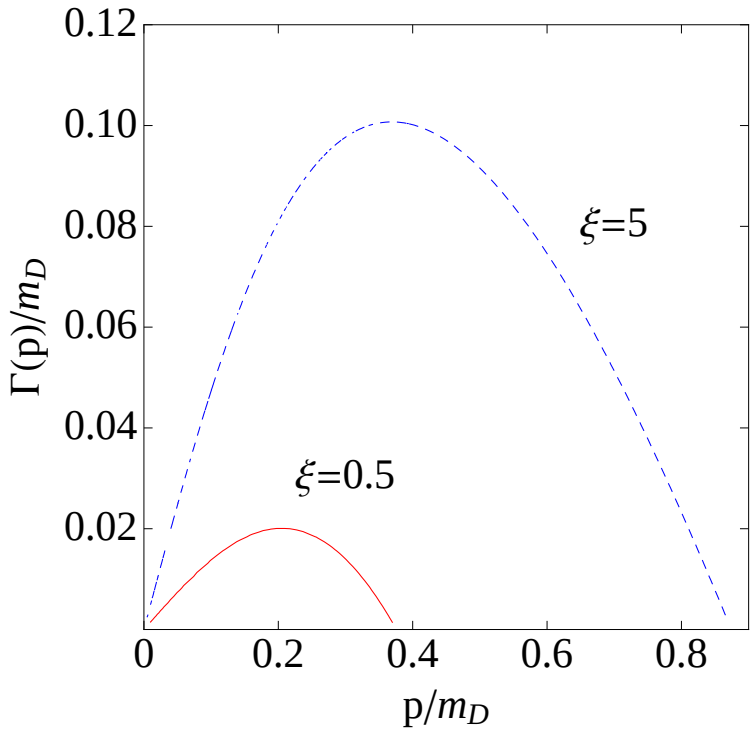

Figure 4.3: Growth rate of the unstable α-mode for $\mathbf{p} \parallel \mathbf{n}$ and different anisotropy parameters.

4.5 Qualitative origin of instabilities

Since the characteristic time of instability growth is shorter than (or at least comparable to) other time scales of the parton system evolution, plasma instabilities may play an important role in the thermalization of quark-gluon plasma from anisotropic, non-equilibrium initial conditions. They can drive the system towards isotropy, thus speeding up its equilibration. The importance of the plasma instabilities has been extensively discussed in the last few years. For example, according to Arnold, Lenaghan and Moore [55], the early stage of quark-gluon plasma evolution in the "bottom-up" thermalization scenario has been drastically modified by such instabilities. Although a somewhat extreme condition, i.e. the infinitely large anisotropy was considered, we can expect the original "bottom-up" scenario should be replaced by a different scheme during the early time in the presence of

instabilities.

Here, we will give a qualitative review of the origin of the magnetic *instabilities* [55]. A magnetic unstable mode known as the filamentation or WEIBEL instability can possibly appear in such an anisotropic plasma as we introduced in Sec. 4.1. However, the electric instabilities are absent in our anisotropic system. For simplicity, we consider a gas of non-interacting hard particles in zero field. Due to the reflection symmetry of the distribution function $f(\mathbf{k}) = f(-\mathbf{k})$, there is no current associated with these particles because, for all the particles going in one direction, there are just as many particles going in the other direction. Now turn on a small magnetic field $\mathbf{B}$ with wave-vector $\mathbf{p}$, which we shall take to point in the z direction. Take $\mathbf{B}$ to be in the $\pm y$ direction with $\mathbf{B} = B\mathbf{e}_y \sin(pz)$, where $\mathbf{e}_y$ is the unit vector in the y direction. We will take the vector field $\mathbf{A}$ to be in the $\pm x$ direction, with $\mathbf{A} = A\mathbf{e}_x \cos(pz)$ and $\mathbf{B} = \nabla \times \mathbf{A}$. Magnetic forces from the small $\mathbf{B}$ field will make charged particles slightly wiggle around straight-line trajectories. The small wiggles in direction will cause the x-component of the current to be larger in some places and smaller in others, compared to the value obtained from the straight-line trajectory.

With the above setup, firstly we consider particles whose initial velocities are very close to being orthogonal to the propagation direction $\mathbf{p}$. The curvature of trajectories caused by the magnetic field will trap the z-motion of such particles. These particles which positively contribute to the current in a given filament, are focused in the filament center while those, which negatively contribute, are moved to the neighboring one. Thus, both the initial current and the magnetic field generated by this current are growing which will contribute to instabilities. On the other hand, particles whose initial velocities are very close to being parallel to the propagation direction $\mathbf{p}$ will give an opposite effect to the initial current and the magnetic field as compared to the trapped particles. As a result, these untrapped particles stabilize against the growth of the current and magnetic field. For a detailed discussion, please see Ref. [55].

In the case of isotropic hard distributions, the contributions of trapped and untrapped particles must cancel and there are no instabilities in such a system. If we start with an isotropic distribution and, for a given $\mathbf{p}$, remove some of the untrapped particles, then we must have magnetic instability. If we instead add untrapped particles, we must have stability. As we mentioned in Sec. 4.4, if we choose the direction of anisotropy $\mathbf{n}$ to be parallel to the propagation direction, for a given anisotropy ξ, the effect of the trapped particles becomes most important and we can expect the growth rate of the instabilities is largest in the case. In an anisotropic system, the kinetic energy related to a motion of particles along the direction of the momentum surplus (trapped particles) is used to generate the magnetic fields which drives the distribution to be isotropic.

Finally, we should point out that the self-energy was derived in a linear approximation. As we mentioned before, this approximation holds in QCD as long as the mean-field four-potential is much smaller than the temperature. However, whenever there is truly exponential growth of the fields in the presence of the anisotropy, the linear approximation will break down very quickly. Actually, unstable modes cannot grow to infinity and even in the electromagnetic plasma there are several possible mechanisms which stop the instability growth [103, 104]. In the case of the quark-gluon plasma, the non-linear terms in the transport equations may play an important role and probably regulate the growth of the modes which have become unstable.

5 Heavy-quark potential in an anisotropic QCD plasma

Properties of heavy quarkonia at finite temperature can play an important role to study the in-medium modification of inter-quark forces and help to understand the phenomenon of non-Abelian Debye screening in quark-gluon plasma. Information on quarkonium spectral functions at high temperature has started to emerge from lattice QCD simulations [105, 106] which has motivated a number of attempts to understand the lattice measurements within non-relativistic potential models including finite-temperature effects such as screening [107, 47]. There are different potential models on the market. However, all of these models are restricted to a plasma in which the parton distributions are isotropic in momentum space. For such a system, the screening effect is described by the Debye mass which has a form of $m_D = g^2T^2(N_f + 2N_c)/6$ in leading perturbative calculation. When there is some deviation from the ideal isotropic distribution, one can expect that the effective screening mass should be modified, thus the properties of quarkonium states will also change due to the anisotropic momentum distribution. Here, we make the first attempt to consider the effects due to a local anisotropy of the plasma in momentum space on the *heavy-quark potential*. Such deviations from perfect isotropy are expected for a real plasma as created in high-energy heavy-ion collisions, which undergoes expansion [1].

The basic idea of the potential model is that a short-range attractive color-Coulomb interaction with a long-range confining interaction provides an adequate account of the interaction between a quark and anti-quark. The long-range confining interaction is non-perturbative and in this chapter, we will employ the perturbative approach to study only the Coulomb interaction. When the isotropic distribution is considered, the leading behavior of the potential in the perturbative expansion which arises due to one-gluon exchange is known as the Debye screened potential. Such a potential can be obtained by the Fourier transform of the static gluon propagator. We will study the perturbative potential with an anisotropic parton distribution introduced in Sec. 4.1 and compare our results with the usually studied isotropic ones.

5.1 Perturbative potential due to one-gluon exchange

Perturbatively the heavy-quark potential can be related to the scattering amplitude corresponding to one-gluon exchange and in the non-relativistic limit it is given by the temporal part of the static propagator in momentum space. As an simple example, we consider the potential between two charges in QED, i.e. the electron-positron pair in vacuum and show that the Coulomb potential can be obtained when comparing the scattering amplitude

[1] This chapter is based on the work published in [108].

calculated in QED with that in non-relativistic quantum mechanics with Born approximation [109].

For electron-positron scattering, the leading order contribution comes from the Feynman diagram as shown in Fig. 5.1. The S-matrix element for this process can be expressed as

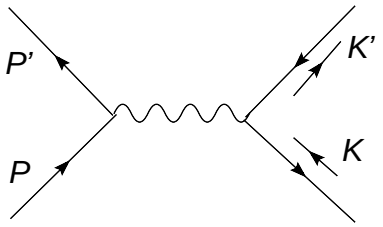

Figure 5.1: Feynman diagram at leading order for electron-positron scattering.

$$\begin{aligned} i\,\mathcal{M} &= -(-i\,e)^2 \bar{u}(P')\gamma^\mu u(P) i D_{\mu\nu} \bar{v}(K)\gamma^\nu v(K') \\ &= -i\,e^2 \bar{u}(P')\gamma^\mu u(P) \frac{g_{\mu\nu}}{(P'-P)^2} \bar{v}(K)\gamma^\nu v(K')\,. \end{aligned} \tag{5.1}$$

Note that in order to untangle the contractions, it requires three operator interchanges. As a result, an overall minus sign appears. However, in the case of electron-electron scattering or positron-positron scattering, we don't have such an overall minus sign.

To evaluate the amplitude in the non-relativistic limit, we keep terms only to lowest order in the three-momenta. Thus, we have

$$\begin{aligned} P = (m_e, \mathbf{p})\,, \quad K = (m_e, \mathbf{k})\,, \\ P' = (m_e, \mathbf{p}')\,, \quad K' = (m_e, \mathbf{k}')\,. \end{aligned} \tag{5.2}$$

Here, we use $E_P = \sqrt{m_e^2 + p^2} = m_e + p^2/(2m_e) + \mathcal{O}(p^4)$. Terms at the order of $\mathcal{O}(p^2)$ or higher have been neglected in Eq. (5.2). m_e is the mass of electron or positron. Similarly, we have

$$\begin{aligned} (P'-P)^2 &= -|\mathbf{p}'-\mathbf{p}|^2 + \mathcal{O}(p^4)\,, \\ u^s(P) &= \sqrt{m_e} \begin{pmatrix} \kappa^s \\ \kappa^s \end{pmatrix}\,, \end{aligned} \tag{5.3}$$

where κ is a two-component constant spinor normalized to $\kappa^{s'\dagger}\kappa^s = \delta^{ss'}$.

In non-relativistic limit, we have

$$\bar{u}(P')\gamma^0 u(P) = u^\dagger(P')u(P) \approx 2m_e \kappa'^\dagger \kappa\,. \tag{5.4}$$

Other terms, $\bar{u}(P')\gamma^i u(P)$ can be neglected as compared to $\bar{u}(P')\gamma^0 u(P)$ in non-relativistic limit. For positrons, similar result holds

$$\bar{v}(K)\gamma^0 v(K') = v^\dagger(K)v(K') \approx 2m_e \kappa^\dagger \kappa'\,. \tag{5.5}$$

Actually, the normalization condition of the two-component spinor indicates that the spin of each particle is separately conserved in this non-relativistic scattering interaction. Thus

we have

$$\begin{aligned} i\mathcal{M} &\approx -(-i\,e)^2(2m_e\kappa'^{\dagger}\kappa)_{\mathbf{p}}iD_{00}(2m_e\kappa^{\dagger}\kappa')_{\mathbf{k}} \\ &= -i\,e^2\frac{1}{-|\mathbf{p}'-\mathbf{p}|^2}(2m_e\kappa'^{\dagger}\kappa)_{\mathbf{p}}(2m_e\kappa^{\dagger}\kappa')_{\mathbf{k}}\,. \end{aligned} \tag{5.6}$$

The above result should be compared with the Born approximation to the scattering amplitude in non-relativistic quantum mechanics, written in terms of the potential V

$$\langle P'|i\,\mathcal{T}|P\rangle = -i\tilde{V}(\mathbf{q})(2\pi)\delta(E_{p'}-E_p)\,, \tag{5.7}$$

where $\mathbf{q}=\mathbf{p}'-\mathbf{p}$. So the corresponding potential in momentum space reads

$$\tilde{V}(\mathbf{q}) = \frac{e^2}{-|\mathbf{p}'-\mathbf{p}|^2}\,. \tag{5.8}$$

The factors of $2m_e$ in Eqs. (5.4) and (5.5) arise from the relativistic normalization conventions and must be dropped when comparing to Eq. (5.7) which assumes conventional non-relativistic normalization of states. The additional $\delta^3(\mathbf{p}'-\mathbf{p})$ goes away when we integrate over the momentum of the target.

Performing the Fourier transform, we get the Coulomb potential as expected

$$\begin{aligned} V(\mathbf{r}) &= -e^2\int\frac{\mathrm{d}^3q}{(2\pi)^3}\frac{1}{q^2}e^{i\mathbf{q}\cdot\mathbf{r}} \\ &= -\frac{e^2}{4\pi r}\,. \end{aligned} \tag{5.9}$$

This is an attractive potential. However, for electron-electron and positron-positron scatterings, we don't have an overall minus sign when untangling the contractions and a repulsive potential appears. We have just verified that, in quantum field theory, when a vector particle is exchanged, like charges repel while unlike charges attract. In general, when the exchanged particle is a scalar or tensor boson, there is a universally attractive potential. One example is the feature of gravitational forces.

According to the above discussion, we find the non-relativistic potential is essentially determined by the temporal component of the photon propagator in the static limit. Generally, we have

$$V(\mathbf{r}) = -e^2\int\frac{\mathrm{d}^3q}{(2\pi)^3}D^{00}(q^0=0,\mathbf{q})e^{i\mathbf{q}\cdot\mathbf{r}}\,. \tag{5.10}$$

Here, the momentum of the exchanged photon is denoted as $Q=(q^0,\mathbf{q})$. In fact, when the hard-loop resummed photon propagator in an isotropic plasma is considered, the above definition gives the well-known Debye screened potential with Debye mass $m_D^2=e^2T^2/3$. However, such an definition is not gauge invariant because the gauge boson propagator is gauge dependent. The above definition works well in covariant gauge and Coulomb gauge. The temporal axial gauge is not appropriate since $D^{00}\equiv 0$ as a consequence of the gauge fixing condition $A^0=0$. In Sec. 5.2, we will compute the anisotropic gluon propagator in all three linear gauges explicitly and we find there is a gauge invariant quantity which can be used to define the non-relativistic potential. Our results can be easily generalized to the isotropic medium by setting $\xi=0$.

5.2 Gluon propagator in an anisotropic QCD plasma

In Sec. 4.2, we have derived the gluon propagator in an anisotropic plasma in temporal axial gauge. However, as we mentioned above, this gauge is not appropriate to define the potential from the FOURIER transform of the temporal component of the static propagator. In this section, we will consider the *retarded gluon propagator* in *general linear gauges*: covariant gauge, COULOMB gauge and temporal axial gauge. The starting point is the expression of the *retarded gluon self-energy* which we derived in both transport theory approach and QCD diagrammatic approach

$$\Pi^{\mu\nu}_{ab}(P) = g^2\delta_{ab}\int_{\mathbf{k}} V^\mu \frac{\partial f(\mathbf{k})}{\partial K^\beta}\left(g^{\nu\beta} - \frac{V^\nu P^\beta}{P\cdot V + i\epsilon}\right). \tag{5.11}$$

As we show in Sec. 4.2, in a suitable tensor basis the components of $\Pi^{\mu\nu}$ can be determined explicitly. Since the temporal component becomes important in our consideration, we extend the tensor bases used in Sec. 4.2 to four-tensor bases appropriate for use in general covariant gauges. Specifically,

$$\begin{aligned}
A^{\mu\nu} &= -g^{\mu\nu} + \frac{P^\mu P^\nu}{P^2} + \frac{\tilde{M}^\mu \tilde{M}^\nu}{\tilde{M}^2}\,,\\
B^{\mu\nu} &= -\frac{P^2}{(M\cdot P)^2}\frac{\tilde{M}^\mu \tilde{M}^\nu}{\tilde{M}^2}\,,\\
C^{\mu\nu} &= \frac{\tilde{M}^2 P^2}{\tilde{M}^2P^2 + (N\cdot P)^2}[\tilde{N}^\mu\tilde{N}^\nu - \frac{\tilde{M}\cdot\tilde{N}}{\tilde{M}^2}(\tilde{M}^\mu\tilde{N}^\nu + \tilde{M}^\nu\tilde{N}^\mu) + \frac{(\tilde{M}\cdot\tilde{N})^2}{\tilde{M}^4}\tilde{M}^\mu\tilde{M}^\nu]\,,\\
D^{\mu\nu} &= \frac{P^2}{M\cdot P}\left[2\frac{\tilde{M}\cdot\tilde{N}}{\tilde{M}^2}\tilde{M}^\mu\tilde{M}^\nu - \left(\tilde{N}^\mu\tilde{M}^\nu + \tilde{M}^\mu\tilde{N}^\nu\right)\right].
\end{aligned} \tag{5.12}$$

Here, M^μ is the heat-bath vector, which in the local rest frame is given by $M^\mu = (1,0,0,0)$ and

$$\tilde{M}^\mu = M^\mu - \frac{M\cdot P}{P^2}P^\mu\,, \tag{5.13}$$

is the part that is orthogonal to P^μ. The direction of anisotropy in momentum space is given by the vector

$$N^\mu = (0,\mathbf{n})\,, \tag{5.14}$$

where $\mathbf{n}$ is a three-dimensional unit vector as we used before. Similarly, we define

$$\tilde{N}^\mu = N^\mu - \frac{N\cdot P}{P^2}P^\mu\,, \tag{5.15}$$

which satisfies $P\cdot\tilde{N} = 0$. Then, we can decompose the self-energy as

$$\Pi^{\mu\nu} = \alpha A^{\mu\nu} + \beta B^{\mu\nu} + \gamma C^{\mu\nu} + \delta D^{\mu\nu}\,. \tag{5.16}$$

With the above definition of the tensor bases, it is easy to show that the self-energy is symmetric and transverse.

In principle, the tensor basis $C^{\mu\nu}$ and $D^{\mu\nu}$ could be chosen differently, such that the individual tensors have a simpler structure. For example, one could choose

$$\begin{aligned} C^{\mu\nu} &= \tilde{N}^\mu \tilde{N}^\nu - \frac{\tilde{M}\cdot\tilde{N}}{2\tilde{M}^2}(\tilde{M}^\mu \tilde{N}^\nu + \tilde{M}^\nu \tilde{N}^\mu)\,, \\ D^{\mu\nu} &= \frac{(\tilde{M}\cdot\tilde{N})^2}{\tilde{M}^4}\tilde{M}^\mu \tilde{M}^\nu - \tilde{N}^\mu \tilde{N}^\nu\,. \end{aligned} \tag{5.17}$$

However, in the bases defined in Eq. (5.12) the spatial components are identical to those from Eq. (4.9). The advantage of choosing the tensor bases Eq. (5.12) is to avoid the rather tedious re-evaluation of the four structure functions. Note that the self-energy tensor is symmetric and transverse, not all of its components are independent. We can therefore restrict our considerations to the spatial parts. As a result, for a specified anisotropic distribution, i.e. Eq. (4.1), the analytical expressions of the four structure functions are given by Eqs. (4.13) and (4.16).

Now, we can use the Dyson-Schwinger *equation* [2] to determine the hard-loop resummed gluon propagator

$$iD^* = iD + iD\left(-i\Pi\right)iD^*\,, \tag{5.18}$$

and the inverse propagator [3] has an explicit form

$$(D^{*-1})^{\mu\nu} = (D^{-1})^{\mu\nu} - \Pi^{\mu\nu}\,. \tag{5.19}$$

In the following, we use D^* and D to denote the resummed and bare propagators, respectively. The propagator is diagonal in color and so color indices will be suppressed.

We consider the retarded propagator in covariant, Coulomb and temporal axial gauges. The bare propagators read

$$\begin{aligned} D^{\mu\nu}_{\text{cova}} &= \frac{-g^{\mu\nu}}{P^2} + (1-\eta)\frac{P^\mu P^\nu}{P^4}\,, \\ D^{\mu\nu}_{\text{Coul}} &= \frac{M^\mu M^\nu}{p^2} + \frac{A^{\mu\nu}}{P^2} - \eta\frac{P^\mu P^\nu}{p^4}\,, \\ D^{\mu\nu}_{\text{temp}} &= \frac{A^{\mu\nu}}{P^2} + \frac{((M\cdot P)M^\mu - P^\mu)((M\cdot P)M^\nu - P^\nu)}{(M\cdot P)^2\,p^2} - \eta\frac{P^\mu P^\nu}{(M\cdot P)^2}\,, \end{aligned} \tag{5.20}$$

where η is the gauge parameter. Because the self-energy is gauge independent in one-loop approximation, the inverse resummed propagators can be expressed as

$$\begin{aligned} (D^{*-1})^{\mu\nu}_{\text{cova}} &= -P^2 g^{\mu\nu} + P^\mu P^\nu - \Pi^{\mu\nu} - \frac{1}{\eta}P^\mu P^\nu\,, \\ (D^{*-1})^{\mu\nu}_{\text{Coul}} &= -P^2 g^{\mu\nu} + P^\mu P^\nu - \Pi^{\mu\nu} - \frac{1}{\eta}(P^\mu - M\cdot P M^\mu)(P^\nu - M\cdot P M^\nu)\,, \\ (D^{*-1})^{\mu\nu}_{\text{temp}} &= -P^2 g^{\mu\nu} + P^\mu P^\nu - \Pi^{\mu\nu} - \frac{1}{\eta}M^\mu M^\nu\,. \end{aligned} \tag{5.21}$$

[2] In real time formalism, the propagator and self energy are both 2×2 matrices. Here, we consider the retarded propagator whose Fourier transform in the static limit is related to the real part of the heavy-quark potential in the non-relativistic limit. The advanced and symmetric propagators will be discussed in Chapter 7.

[3] Here, the inverse propagator is defined as $(D^{*-1})^{\mu\sigma} D^{*\ \nu}_{\sigma} = g^{\mu\nu}$ in Minkowski space.

Firstly, we consider the retarded propagator in covariant gauge. With the four-tensor bases, we have

$$\begin{aligned}\left(D^{*-1}\right)^{\mu\nu}_{\rm cova}(P,\xi) &= -P^2 g^{\mu\nu} + P^\mu P^\nu - \Pi^{\mu\nu}(P,\xi) - \frac{1}{\eta}P^\mu P^\nu \\ &= (P^2-\alpha)A^{\mu\nu} + (\omega^2-\beta)B^{\mu\nu} - \gamma C^{\mu\nu} - \delta D^{\mu\nu} - \frac{1}{\eta}P^\mu P^\nu\,. \end{aligned} \tag{5.22}$$

Upon inversion, the propagator is written as

$$D^{*\mu\nu}_{\rm cova}(P,\xi) = \alpha' A^{\mu\nu} + \beta' B^{\mu\nu} + \gamma' C^{\mu\nu} + \delta' D^{\mu\nu} + \lambda P^\mu P^\nu\,. \tag{5.23}$$

Using $(D^{*-1})^{\mu\sigma} D^{*\ \nu}_{\sigma} = g^{\mu\nu}$ it follows that the coefficient of $g^{\mu\nu}$ in $(D^{*-1})^{\mu\sigma} D^{*\ \nu}_{\sigma}$ should equal 1 while the coefficients of the other tensor structures, for example of $N^\mu N^\nu$, $N^\mu P^\nu$ and $P^\mu P^\nu$ should vanish. Hence, we can determine the coefficients in the propagator from the following equations

$$\begin{aligned} \alpha' &= \frac{1}{P^2-\alpha}\,, \\ (P^2-\alpha-\gamma)\gamma' - \delta\,\delta'\frac{P^2(p^2-(N\cdot P)^2)}{\omega^2} &= \frac{\gamma}{P^2-\alpha}\,, \\ (P^2-\alpha-\gamma)\delta' &= \delta\,\beta'\frac{P^2}{\omega^2}\,, \\ \frac{\delta}{P^2-\alpha} + \delta\,\gamma' &= (\omega^2-\beta)\delta'\frac{P^2}{\omega^2}\,, \\ \frac{1}{P^2} + \frac{\lambda}{\eta}P^2 &= 0\,. \end{aligned} \tag{5.24}$$

Solving the above equations, we find that in *covariant gauge* the propagator in an anisotropic plasma is given by

$$\begin{aligned} D^{*\mu\nu}_{\rm cova} &= \frac{1}{P^2-\alpha}\left[A^{\mu\nu} - C^{\mu\nu}\right] + \Delta_G\Bigg[(P^2-\alpha-\gamma)\frac{\omega^4}{P^4}B^{\mu\nu} \\ &+ (\omega^2-\beta)C^{\mu\nu} + \delta\frac{\omega^2}{P^2}D^{\mu\nu}\Bigg] - \frac{\eta}{P^4}P^\mu P^\nu\,, \end{aligned} \tag{5.25}$$

where

$$\Delta_G^{-1} = (P^2-\alpha-\gamma)(\omega^2-\beta) - \delta^2\left[p^2-(N\cdot P)^2\right]\,. \tag{5.26}$$

For $\xi = 0$, we recover the isotropic propagator in covariant gauge

$$D^{*\mu\nu}_{\rm iso} = \frac{1}{P^2-\alpha}A^{\mu\nu} + \frac{1}{(\omega^2-\beta)}\frac{\omega^4}{P^4}B^{\mu\nu} - \frac{\eta}{P^4}P^\mu P^\nu\,. \tag{5.27}$$

In Coulomb *gauge*, it has a similar expression

$$\begin{aligned} D^{*\mu\nu}_{\rm Coul} &= \frac{1}{P^2-\alpha}\left[A^{\mu\nu} - C^{\mu\nu}\right] + \Delta_G\Bigg[(P^2-\alpha-\gamma)\frac{\omega^2}{p^2}\bar{B}^{\mu\nu} \\ &+ (\omega^2-\beta)C^{\mu\nu} + \delta\frac{\omega^2}{P^2}\bar{D}^{\mu\nu}\Bigg] - \frac{\eta}{p^4}P^\mu P^\nu\,, \end{aligned} \tag{5.28}$$

where the two new projectors $\bar{B}^{\mu\nu}$ and $\bar{D}^{\mu\nu}$ are defined as

$$\begin{aligned}\bar{B}^{\mu\nu} &= M^\mu M^\nu, \\ \bar{D}^{\mu\nu} &= \frac{P^2}{M\cdot P}\left[2\frac{\tilde{M}\cdot\tilde{N}}{\tilde{M}^2}M^\mu M^\nu - \left(\bar{N}^{*\mu}M^\nu + M^\mu \bar{N}^{*\nu}\right)\right],\end{aligned} \tag{5.29}$$

with

$$\bar{N}^{*\mu} = N^\mu + \frac{N\cdot P}{p^2}P^\mu\,. \tag{5.30}$$

For $\xi = 0$, we recover the isotropic propagator in COULOMB gauge

$$D^{*\,\mu\nu}_{\rm iso} = \frac{1}{P^2-\alpha}A^{\mu\nu} + \frac{1}{(\omega^2-\beta)}\frac{\omega^2}{p^2}\bar{B}^{\mu\nu} - \frac{\eta}{p^4}P^\mu P^\nu\,. \tag{5.31}$$

In *temporal axial gauge*, we have

$$\begin{aligned}D^{*\,\mu\nu}_{\rm temp} &= \frac{1}{P^2-\alpha}\left[A^{\mu\nu} - C^{\mu\nu}\right] + \Delta_G\Big[(P^2-\alpha-\gamma)\tilde{B}^{\mu\nu} \\ &+ (\omega^2-\beta)C^{\mu\nu} + \delta\tilde{D}^{\mu\nu}\Big] - \frac{\eta}{\omega^2}P^\mu P^\nu\,,\end{aligned} \tag{5.32}$$

where the two new projectors $\tilde{B}^{\mu\nu}$ and $\tilde{D}^{\mu\nu}$ are defined as

$$\begin{aligned}\tilde{B}^{\mu\nu} &= \frac{(\omega M^\mu - P^\mu)(\omega M^\nu - P^\nu)}{p^2}, \\ \tilde{D}^{\mu\nu} &= (P^\mu - \omega M^\mu)\tilde{N}^{*\nu} + \tilde{N}^{*\mu}(P^\nu - \omega M^\nu)\,,\end{aligned} \tag{5.33}$$

with

$$\tilde{N}^{*\mu} = N^\mu - \frac{N\cdot P}{p^2}(\omega M^\mu - P^\mu)\,. \tag{5.34}$$

For $\xi = 0$, we recover the isotropic propagator in temporal axial gauge

$$D^{*\,\mu\nu}_{\rm iso} = \frac{1}{P^2-\alpha}A^{\mu\nu} + \frac{1}{(\omega^2-\beta)}\tilde{B}^{\mu\nu} - \frac{\eta}{\omega^2}P^\mu P^\nu\,. \tag{5.35}$$

The basic idea of the calculation in COULOMB and temporal axial gauges is essentially the same as what we did in covariant gauge. Although the above calculations are tedious, we can still easily check some basic properties of the propagators in these linear gauges with different *gauge fixing conditions*, i.e.

$$\begin{cases} P_\mu D^{*\mu\nu}(P) = 0\,, & \partial^\mu A_\mu = 0 \text{ (cova)} \\ P_i D^{*\mu i}(P) = 0\,, & \partial^i A_i = 0 \text{ (Coul)} \\ D^{*0i} = D^{*00} = 0\,, & A_0 = 0 \text{ (temp)} \end{cases}. \tag{5.36}$$

Note that, when the isotropic distribution is considered, in COULOMB gauge, we have $D^{0i}(P) = 0$.

In fact, no matter the plasma is isotropic or anisotropic, the definition of the potential in Eq. (5.10) is equivalent in covariant gauge and COULOMB gauge. The temporal components of the propagator in static limit are given by

$$\begin{aligned} D^{*\,00}_{\rm iso}(\omega=0) &= \frac{1}{p^2+m_D^2}\,, \\ D^{*\,00}_{\rm aniso}(\omega=0) &= \frac{p^2+m_\alpha^2+m_\gamma^2}{(p^2+m_\alpha^2+m_\gamma^2)(p^2+m_\beta^2)-m_\delta^4}\,, \end{aligned} \tag{5.37}$$

for isotropic and anisotropic medium, respectively. The four mass scales m_α^2, m_β^2, m_γ^2 and m_δ^2 are defined in Eqs. (4.17) and (4.18) and the explicit expressions are given by Eq. (4.20). In temporal axial gauge, due to the fact that $A_0 = 0$, it fails to define the potential. However, there is a simple relation among these three gauges

$$\lim_{\omega\to 0}\frac{\omega^2}{p^2}\mathrm{Tr}\,D^{*\,ij}_{\rm temp} = D^{*\,00}_{\rm cova}(\omega=0) = D^{*\,00}_{\rm Coul}(\omega=0)\,. \tag{5.38}$$

Note that the above equation holds when the gauge fixing term vanishes, i.e. $\eta = 0$. In general, we find that the quantity $|\frac{\omega^2}{p^2}\mathrm{Tr}\,D^{*\,ij} - D^{*\,00}|$ in static limit is gauge independent which might be used as a more general definition of the potential [110].

5.3 Heavy-quark potential in an anisotropic QCD plasma

We determine the *real part* [4] *of the potential* in non-relativistic limit, at leading order, from the FOURIER transform of the static gluon propagator,

$$V(\mathbf{r},\xi) = -g^2C_F\int\frac{\mathrm{d}^3\mathbf{p}}{(2\pi)^3}\,e^{i\mathbf{p}\cdot\mathbf{r}}D^{*\,00}(\omega=0,\mathbf{p},\xi) \tag{5.39}$$

$$= -g^2C_F\int\frac{\mathrm{d}^3\mathbf{p}}{(2\pi)^3}\,e^{i\mathbf{p}\cdot\mathbf{r}}\frac{p^2+m_\alpha^2+m_\gamma^2}{(p^2+m_\alpha^2+m_\gamma^2)(p^2+m_\beta^2)-m_\delta^4}\,. \tag{5.40}$$

In order to get some analytical results, we first check some limiting cases. When $\xi = 0$ then $m_\beta^2 = m_D^2$ while all other mass scales in the static propagator vanish. Hence, we recover the isotropic DEBYE potential

$$V(\mathbf{r},\xi=0) = V_{\rm iso}(r) = -g^2C_F\int\frac{\mathrm{d}^3\mathbf{p}}{(2\pi)^3}\frac{e^{i\mathbf{p}\cdot\mathbf{r}}}{p^2+m_D^2} = -\frac{g^2C_F}{4\pi r}\,e^{-\hat{r}}\,, \tag{5.41}$$

where $\hat{r}\equiv rm_D$ is a dimensionless quantity.

Consider, on the other hand, the limit $r\to 0$ for arbitrary ξ. The phase factor in Eq. (5.40) is essentially constant up to momenta of order $p\sim 1/r$ and since the masses are bounded as $p\to\infty$ they can be neglected. The potential then coincides with the vacuum COULOMB potential

$$V(\mathbf{r}\to 0,\xi) = V_{\rm vac}(r) = -g^2C_F\int\frac{\mathrm{d}^3\mathbf{p}}{(2\pi)^3}\frac{e^{i\mathbf{p}\cdot\mathbf{r}}}{p^2} = -\frac{g^2C_F}{4\pi r}\,. \tag{5.42}$$

[4] In fact, there is also an imaginary part of the potential which is related to the "decay width" and we will discuss this part later.

The same potential emerges for extreme anisotropy since all mass scales approach to zero as $\xi \to \infty$:

$$V(\mathbf{r}, \xi = \infty) = -\frac{g^2 C_F}{4\pi r}\,. \tag{5.43}$$

This is due to the fact that at $\xi = \infty$ the phase space density $f(\mathbf{k})$ from Eq. (4.1) has support only in a two-dimensional plane orthogonal to the direction $\mathbf{n}$ of anisotropy. As a consequence, the density of the medium vanishes in this limit.

For an anisotropic distribution, one of the most important features of the potential is that the angular dependence appears, namely, the potential depends on the angle between $\mathbf{r}$ and $\mathbf{n}$. This can be seen analytically for small but non-zero ξ. To linear order in ξ the potential can be expressed as

$$V(\mathbf{r}, \xi \ll 1) = V_{\rm iso}(r) - g^2 C_F\, \xi m_D^2 \int \frac{\mathrm{d}^3\mathbf{p}}{(2\pi)^3}\, e^{i\mathbf{p}\cdot\mathbf{r}}\, \frac{\frac{2}{3} - (\mathbf{p}\cdot\mathbf{n})^2/p^2}{(p^2 + m_D^2)^2}\,. \tag{5.44}$$

A convenient way to perform the integration is to choose a spherical coordinate system where $\mathbf{r}$ is parallel the z component of $\mathbf{p}$. Furthermore, we can assume $\mathbf{n}$ lies in the p_z-p_y plane according to the cylindrical symmetry in momentum space.

The potential at leading order in ξ then takes the following form

$$V(\mathbf{r}, \xi \ll 1) = V_{\rm iso}(r)\,[1 - \xi \mathcal{F}(\hat{r}, \theta)]\,. \tag{5.45}$$

The function

$$\mathcal{F}(\hat{r}, \theta) \equiv f_0(\hat{r}) + f_1(\hat{r})\cos(2\theta)\,, \tag{5.46}$$

with

$$\begin{aligned} f_0(\hat{r}) &= \frac{6(1 - e^{\hat{r}}) + \hat{r}[6 - \hat{r}(\hat{r} - 3)]}{12\hat{r}^2}\,, \\ f_1(\hat{r}) &= \frac{6(1 - e^{\hat{r}}) + \hat{r}[6 + \hat{r}(\hat{r} + 3)]}{4\hat{r}^2}\,, \end{aligned} \tag{5.47}$$

and θ is the angle between $\mathbf{r}$ and $\mathbf{n}$. This expression does not apply for $\hat{r}$ much larger than 1, which is a shortcoming of the direct Taylor expansion of $V(\mathbf{r}, \xi)$ in powers of ξ.

There are two cases which are especially interesting for discussion. Firstly, we consider the case where $\mathbf{r}$ is parallel to the direction $\mathbf{n}$ of anisotropy,

$$V(\mathbf{r} \parallel \mathbf{n}, \xi \ll 1) = V_{\rm iso}(r) \left[1 + \xi \left(2\frac{e^{\hat{r}} - 1}{\hat{r}^2} - \frac{2}{\hat{r}} - 1 - \frac{\hat{r}}{6}\right)\right]\,, \tag{5.48}$$

where $\hat{r} \equiv r m_D$, as before. For $\hat{r} \simeq 1$ where the result is reliable, the coefficient of ξ is positive, $(\cdots) = 0.27$ for $\hat{r} = 1$, and thus a slightly deeper potential than in an isotropic plasma emerges at distance scales $r \sim 1/m_D$.

The other case is to consider that $\mathbf{r} \perp \mathbf{n}$, we have

$$V(\mathbf{r} \perp \mathbf{n}, \xi \ll 1) = V_{\rm iso}(r) \left[1 + \xi \left(\frac{1 - e^{\hat{r}}}{\hat{r}^2} + \frac{1}{\hat{r}} + \frac{1}{2} + \frac{\hat{r}}{3}\right)\right]\,. \tag{5.49}$$

The same limitations for $\hat{r}$ apply as in Eq. (5.48). Here, too, the coefficient of the anisotropy parameter is positive, $(\cdots) = 0.115$ for $\hat{r} = 1$, but smaller than for $\mathbf{r} \parallel \mathbf{n}$. Hence, a $Q\bar{Q}$ pair

aligned along the direction of momentum anisotropy and separated by a distance $r \sim 1/m_D$ is expected to attract more strongly than a pair aligned in the transverse plane.

For general ξ and $\hat{r}$, the integral in Eq. (5.40) has to be performed numerically. In fact, we can rewrite the denominator of the integrand as

$$(p^2 + m_\alpha^2 + m_\gamma^2)(p^2 + m_\beta^2) - m_\delta^4 = (p^2 + m_+^2)(p^2 + m_-^2)\,, \tag{5.50}$$

where

$$2m_\pm^2 = M^2 \pm \sqrt{M^4 - 4(m_\beta^2(m_\alpha^2 + m_\gamma^2) - m_\delta^4)}\,, \tag{5.51}$$

with

$$M^2 = m_\alpha^2 + m_\beta^2 + m_\gamma^2\,. \tag{5.52}$$

Since the mass scales could be negative, the integrand then becomes divergent at some points. However, they are simple first-order poles and we can evaluate this integral using a principal part prescription. Numerical results are shown in Figs. 5.2 and 5.3. In Fig. 5.2, we show the potential in the region $\hat{r} \sim 1$ for various degrees of plasma anisotropy. In this region of $\hat{r}$, the medium effect is relatively important. At very small $\hat{r}$, the states are basically COULOMB states and they are not affected too much by the medium. One observes that in general screening is reduced, i.e. that the potential at $\xi > 0$ is deeper and closer to the vacuum potential than for an isotropic medium. This is partly caused by the lower density of the anisotropic plasma. However, the effect is not uniform in the polar angle, as shown in Fig. 5.3: the angular dependence disappears more rapidly at small $\hat{r}$, while at large $\hat{r}$ there is stronger binding for $\mathbf{r}$ parallel to the direction of anisotropy. Overall, one may therefore expect that quarkonium states whose wave-functions are sensitive to the regime $\hat{r} \sim 1$ are bound more strongly in an anisotropic medium, in particular if the $Q\bar{Q}$ pair is aligned along $\mathbf{n}$. For other θ between 0 and $\pi/2$, the anisotropic effect is expected to be smaller than the special case where $\mathbf{r} \parallel \mathbf{n}$ but larger than the other one where $\mathbf{r} \perp \mathbf{n}$.

5.4 Discussions

We have determined the HL gluon propagator in an anisotropic (viscous) plasma in general linear gauges. Its FOURIER transform at vanishing frequency defines a non-relativistic potential for static sources. This definition is feasible in covariant and COULOMB gauges. A possible gauge invariant definition of the potential was also discussed. We found that, generically, screening is weaker than in isotropic media and so the potential is closer to that in vacuum, in particular if the $Q\overline{Q}$ pair is aligned along the direction of anisotropy.

Actually, in Ref. [111], the authors determined finite-temperature corrections to the static heavy-quark potential as a function of the shear viscosity to entropy density ratio in a strongly coupled, large N_c conformal field theory dual to five-dimensional GAUSS-BONNET gravity. It is shown that their results are qualitatively the same as ours. However, these corrections are even smaller than our perturbative QCD calculation at distances relevant for small bound states in a deconfined plasma.

When we use the potential to study the properties of quarkonium states in medium, for example, to determine the binding energy of the bound states, the non-perturbative

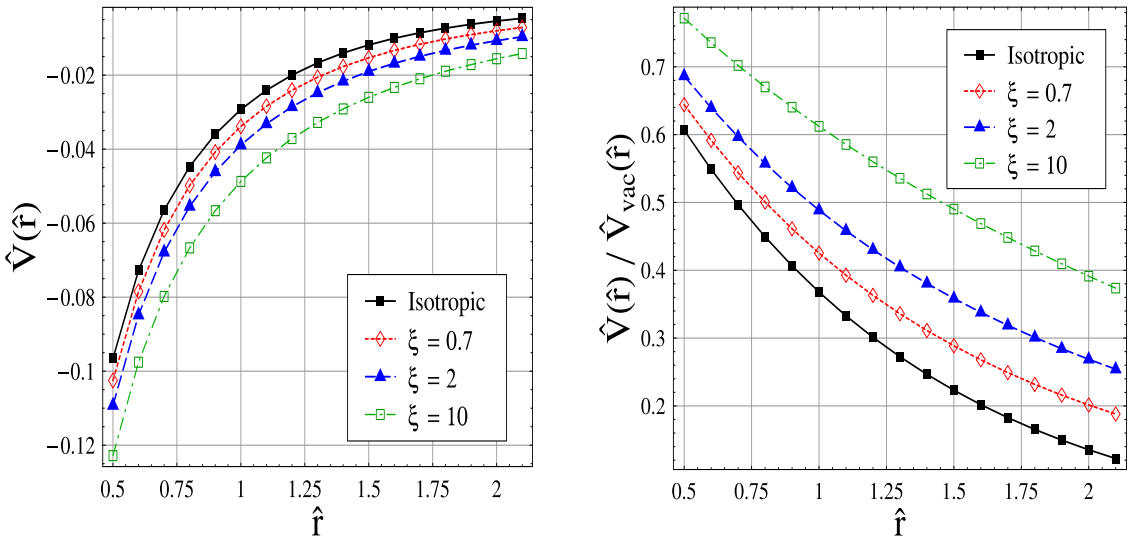

Figure 5.2: Heavy-quark potential at leading order as a function of distance ($\hat{r} \equiv rm_D$) for $\mathbf{r}$ parallel to the direction $\mathbf{n}$ of anisotropy. The anisotropy parameter of the plasma is denoted by ξ.
Left: the potential divided by the DEBYE mass and by the coupling, $\hat{V} \equiv V/(g^2 C_F m_D)$.
Right: potential relative to that in vacuum.

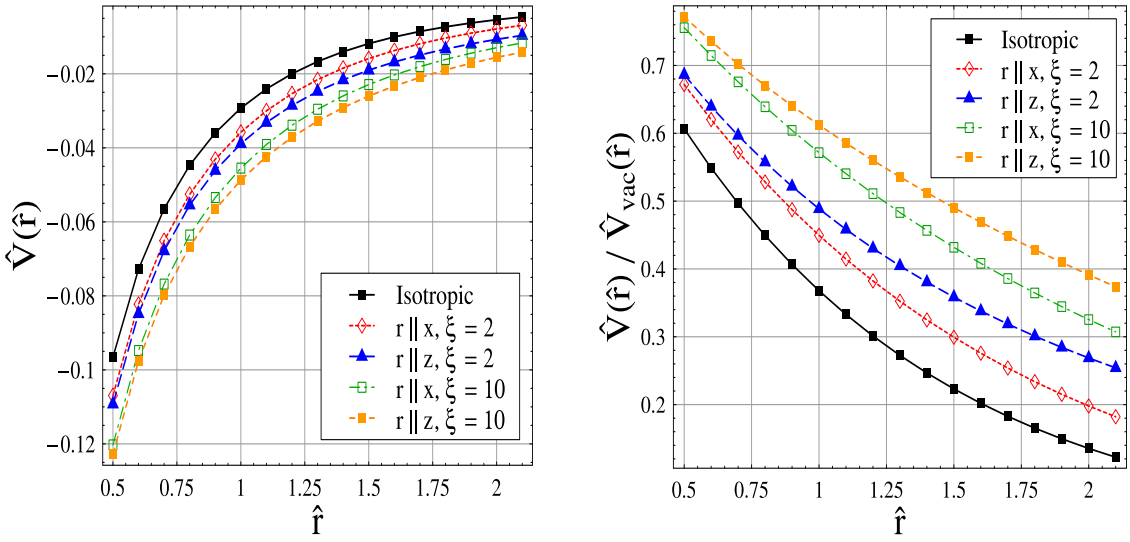

Figure 5.3: Comparison of $\hat{V}(\mathbf{r} \parallel \mathbf{n}, \xi)$ and $\hat{V}(\mathbf{r} \perp \mathbf{n}, \xi)$.

part (string part) also plays an important role in general cases. Actually, our results are applicable when the momentum of the exchanged gluon is on the order of the DEBYE mass m_D or higher, i.e. for distances on the order of $\lambda_D = 1/m_D$ or less. For realistic values of the coupling, $\alpha_s \approx 0.3$, λ_D coincides with the scale $r_{\rm med}(T) \approx 0.5\,(T_c/T)\,\mathrm{fm}$ introduced in Refs. [47, 112], where medium-induced effects appear.

Following the discussion in [47], at short distances, $r < r_{\rm med}(T)$, the potential is given by

$$V(r) \simeq -\frac{\alpha}{r} + \sigma r\,, \tag{5.53}$$

where $\sigma \simeq 1$ GeV/fm is the SU(3) string tension; color factors have been absorbed into the couplings. Since $r_{\rm med}(T) \sim 1/T$, it follows that at sufficiently high temperature $r_{\rm med}(T)$ is smaller than $\sqrt{\alpha/\sigma}$ and so the perturbative COULOMB contribution dominates over the linear confining potential at the length scale λ_D. Roughly, this holds for $T \geq 2T_c$. In this case, our result is directly relevant for quarkonium states with wave-functions which are sensitive to the length scale $\lambda_D \simeq r_{\rm med}$.

On the other hand, for lower T the scale $r_{\rm med}(T)$ where medium-induced effects appear may grow larger than $\simeq \sqrt{\alpha/\sigma}$. In this regime, quarkonium states are either unaffected by the medium; namely, if the quark mass is very large and the typical momentum component in the wave-function is $\gg 1/r_{\rm med}(T)$. Conversely, states with a root-mean-square (RMS) radius $\geq r_{\rm med}(T)$ do experience medium modifications. For such states, however, it is insufficient to consider only the (screened) COULOMB part of the potential which arises from one-gluon exchange. Rather, one should then sum the medium-dependent contributions due to one-gluon exchange and due to the string [47]. The modification to the non-perturbative string part due to the anisotropy effect will be discussed in Chapter 6 where the KARSCH-MEHR-SATZ potential model at finite temperature will be considered.

Finally, as a simple application of the above results, we consider the $Q\bar{Q}$ pair in an anisotropic plasma where the temperature is assumed to be high enough and the quark mass is very large [5]. As a result, the string part in the potential can be neglected and the state is basically a COULOMB state. In this case, the medium effect can be treated as a perturbation. In particular, we will concentrate on the shift of the *binding energy* due to the medium effect. An analytic estimate can be obtained from non-relativistic perturbation theory (to first order) for states with a BOHR radius times DEBYE mass small as compared to the anisotropy parameter ξ [113]. For weak anisotropy, $\xi \ll 1$, and distances $\hat{r} \ll 1$, we expand the potential as

$$\begin{aligned} V(\mathbf{r}) &\approx V_{\rm iso}(r) - 4\pi\alpha\xi m_D^2 \int \frac{\mathrm{d}^3\mathbf{p}}{(2\pi)^3}\, e^{i\mathbf{p}\cdot\mathbf{r}}\, \frac{\frac{2}{3} - (\mathbf{p}\cdot\mathbf{n})^2/p^2}{(p^2+m_D^2)^2} \\ &= V_{\rm iso}(r)\,[1 - \xi\mathcal{F}(\hat{r},\theta)] \\ &= V_{\rm iso}(r)\left[1 - \xi(-\frac{\hat{r}}{6} - \frac{\hat{r}^2}{48}(1+3\cos 2\theta) + \dots)\right] \\ &= V_{\rm vac}(r) + \alpha m_D - \frac{\alpha\xi m_D}{6} + \dots\,, \end{aligned} \tag{5.54}$$

where $\alpha \equiv g^2 C_F/4\pi$. Using the assumption $\frac{m_D}{\alpha M_Q} \ll \xi \ll 1$, the vacuum potential dominates. In our approximation, the medium corrections to the vacuum potential are independent of

[5] According to the lattice based potential models, the potential at infinite distance is proportional to the inverse temperature which we will neglect at high temperature limit.

r and θ. Then the binding energy for such small-size states can be expressed as

$$E_{\text{bin}} \approx E_{\text{vac}} + \alpha m_D - \frac{\alpha \xi m_D}{6} \,. \tag{5.55}$$

Note that $E_{\text{vac}} < 0$. The relative shift of the binding energy due to the presence of the (weakly anisotropic) medium is therefore given by

$$\frac{\delta E}{E_{\text{vac}}} \approx \frac{4 m_D}{\alpha M_Q} \left[-1 + \frac{\xi}{6} + \cdots \right] , \qquad \left(\text{for } \frac{m_D}{\alpha M_Q} \ll \xi \ll 1 \right) . \tag{5.56}$$

The first term corresponds to the reduced binding due to screening by the medium while the second term is the correction due to the non-zero anisotropy which indicates a increasing binding. The restriction to $m_D/\alpha M_Q \ll \xi$ is necessary because terms of order $\mathcal{O}(m_D/\alpha M_Q)$ inside the brackets have been neglected.

The above analysis applies also to excited states, provided that their size (in units of the DEBYE length) is small as compared to ξ. The shift of the binding energy for the n^{th} state is

$$\frac{\delta E}{E_{\text{vac}}} \approx \frac{4 m_D}{\alpha M_Q} \, n^2 \left[-1 + \frac{\xi}{6} + \cdots \right] . \tag{5.57}$$

However, it should be clear that for realistic cases (i.e. temperatures, quark masses and coupling constant), our above assumption that $m_D/\alpha M_Q \ll \xi$ is too extreme. Here, we only consider a theoretically clean limit in order to see how the anisotropy could affect the binding energy of the bound state. For states with a intermediate size, we must solve exactly the three-dimensional SCHRÖDINGER equation with a suitable anisotropic potential including both COULOMB and string contributions.

6 Quarkonium states in an anisotropic QCD plasma

In Quantum Chromodynamics with small T' HOOFT coupling (which equals $g^2 N_c$) at short distances non-relativistic quarkonium states exist. Their binding energies are much smaller than the quark mass $M_Q \gg \Lambda_{\rm QCD}$ ($Q = c, b$), and their size is much larger than $1/M_Q$. At zero temperature, since the velocity of the quarks in the bound state is small, $v_Q \ll 1$, quarkonium can be understood in terms of non-relativistic potential models [114] using the CORNELL potential [38]. The potential model can actually be derived directly from QCD as an effective field theory by integrating out modes above the scales M_Q and then $M_Q v_Q$, respectively [25, 115].

At high temperatures, the deconfined phase of QCD exhibits screening of static color-electric fields [116, 117]. It is expected that this screening leads to the dissociation of quarkonium states, which can serve as a signal for the formation of a deconfined quark-gluon plasma in heavy-ion collisions [32]. Inspired by the success at zero temperature, potential model descriptions have also been applied to understand quarkonium properties at finite temperature. The pioneering paper of MATSUI and SATZ [32] was followed by the work of KARSCH, MEHR and SATZ (KMS) [40], which presented the first quantitative calculation. In recent works more involved calculations of quarkonium spectral functions and meson current correlators obtained from potential models have been performed [107, 118, 119, 120, 121, 122, 123, 47]. The results have been compared to first-principle QCD calculations performed numerically on lattices [44, 105, 106, 124]. A summary and review of the current understanding of these potential models is presented in Ref. [33], and different aspects of quarkonium in collider experiments can be found in Refs. [125, 29]. More recently the imaginary part of the potential due to LANDAU damping has been calculated [126, 127, 128]. Also, the derivation of potential models from QCD via effective field theory methods has been extended to finite T [41]. All of these works, however, have been performed with the assumption of an isotropic thermal medium.

Since the anisotropic distribution is a more realistic description of the parton system generated in heavy-ion collisions, it is worthwhile to consider the properties of quarkonia such as the binding energy, decay width and dissociation temperature, in such a system and make a comparison with the corresponding results in the isotropic plasma. As we have seen in Chapter 5, the effect of the anisotropic distribution will reduce the screening, thus a more binding of quarkonium states is expected in such a plasma. However, for charmonium and bottomonium which are most interesting for the bound states studies, our previous analysis is no longer applicable because the string potential is not negligible now. In order to determine the binding energy for such bound states, we need to consider how the string part of potential behaves in the anisotropic plasma. Since this part is non-perturbative, we will consider it based on the potential model. In this chapter, we attempt a first assessment of the properties of quarkonium states in a QCD plasma which exhibits an anisotropy in

momentum space due to a locally anisotropic hydrodynamic expansion with non-vanishing shear viscosity [1]. We note that the non-equilibrium effect described here arises beyond the linear response approximation in that the operators corresponding to various properties of quarkonium states need to be evaluated in an ensemble of anisotropic (in momentum space) gauge field configurations.

We stress that in this work we restrict to solving the time-independent SCHRÖDINGER equation, i.e. we assume that the plasma is at a constant temperature T and anisotropy ξ. This approximation is useful if the time scale associated with the bound state, $\sim 1/|E_{\rm bind}|$, is short compared to the time scales over which T and ξ vary. Indeed, for sufficiently large quark mass M_Q this condition should be satisfied.

6.1 The Karsch-Mehr-Satz potential model at finite temperature

Lacking knowledge of the exact heavy-quark potential at finite temperature, different phenomenological potentials, as well as lattice-QCD based potentials have been used in potential models to study quarkonium.

The KMS model [40] assumes the following form of the heavy-quark potential at finite temperature in an isotropic plasma with $\xi = 0$:

$$F(r,T) = -\frac{\alpha}{r}\exp\left(-m_D\, r\right) + \frac{\sigma}{m_D}\left[1 - \exp\left(-m_D\, r\right)\right] . \tag{6.1}$$

Here, $\alpha \approx 0.385$ is an effective COULOMB coupling at (moderately) short distances, $\sigma = 0.223$ GeV^2 is the string tension and $m_D(T)$ is the DEBYE screening mass.

Eq. (6.1) is a model for the action of a WILSON loop of size $1/T$ and r in the temporal and spatial directions, respectively (see Ref. [130] and references therein). This potential has been used before to study quarkonium bound states [107, 118]. However, it was realized shortly after that Eq. (6.1) cannot be taken directly as the heavy-quark potential because it contains an entropy contribution; see, for example, the discussion in Refs. [47, 131, 130, 33]. Rather, Eq. (6.1) corresponds to the free energy due to the presence of a $Q\bar{Q}$ in the medium. We emphasize that the entropy term in the lattice data is merely a perturbative entropy contribution present at large distances [2], $r \to \infty$, and it is absent at short distances [130]. One can remove this entropy term from the lattice data by parameterizing $F(r \to \infty, T) \equiv F_\infty(T)$ in the form $F_\infty(T) = a/T - bT$ and then adding the term bT to $F(r,T)$ at large distance, thereby obtaining what has been called the *physical potential* in Refs. [47, 123].

Alternatively, one could calculate the full entropy $S = -\partial F/\partial T$ and add it to the free energy, which leads to the internal energy $U = F + TS$. The internal energy calculated in lattice QCD [132] shows a large increase in U_∞ near T_c, due to the large increase of the entropy near T_c. Furthermore, at temperatures $T \simeq T_c$ a potential model based on the internal energy becomes much more binding than the $T = 0$ CORNELL potential (we refer to this as "overshooting"). For these reasons, the internal energy $U(r,T)$ obtained on the lattice should neither be identified with the heavy-quark potential, although it has been used in potential models before [131, 122, 107, 118]. Nevertheless, the internal energy provides a useful upper limit for the potential at finite T. A version of the internal energy in

[1] This chapter is based on the work published in [129].

[2] We evaluate it in anisotropic HL resummed perturbation theory in Sec. 6.2.

which the overshooting problem was eliminated, was designed in Refs. [47, 123] and called the *most confining potential*.

In this work we also construct a model for a potential which could be viewed as an upper limit for the heavy-quark potential, i.e. $V_\infty \simeq U_\infty$. Our present model is very simple and contains a minimum number of parameters, as the primary goal is to generalize the finite temperature potential to anisotropic media. In our model we add the full entropy contribution to the KMS *ansatz* (6.1):

$$\begin{aligned} V(r,T) &= F(r,T) - T\frac{\partial F(r,T)}{\partial T} \\ &\approx -\frac{\alpha}{r}\,(1+m_D\,r)\exp\left(-m_D\,r\right) + 2\frac{\sigma}{m_D}\left[1-\exp\left(-m_D\,r\right)\right] \\ &- \sigma\,r\,\exp(-m_D\,r)\,. \end{aligned} \tag{6.2}$$

In the second line we have used that m_D is approximately proportional to T at high temperatures. Since the effect of the running of the coupling is important only at distances less than 0.1 fm, not relevant for quarkonium studies, here we do not consider running-coupling corrections. Fig. 6.1 compares the potential at finite temperature to that at $m_D = 0$ which is a CORNELL potential.

This potential, just as its original form Eq. (6.1), essentially represents an interpolation from the well-known CORNELL potential at short distances to an exponentially DEBYE-screened string attraction at large r. With $g \simeq 2$, $m_D \simeq gT$ and $T_c \simeq 200$ MeV, the length scale where medium effects become large is roughly given by $r_{\rm med}(T) \simeq T_c/(2T)$ fm, in approximate agreement with lattice results from Ref. [112]. In Eq. (6.2) corrections to the CORNELL potential are suppressed at distances $r < 1/m_D$, i.e. they appear only at order $(m_D\,r)^2$. This is due to the fact that we subtracted the derivative $\partial F/\partial \log T$ even at intermediate distances; it appears to give a better representation of the lattice potential at $r < r_{\rm med}(T)$, which in fact coincides with the CORNELL *ansatz*. One can see in Fig. 6.1 that our potential $V(r)$ is very close to the CORNELL potential for distances up to $r \simeq 0.4$ fm, in agreement with lattice results [112]. The finite-temperature potential (6.2) does not overshoot the CORNELL potential significantly at any r [123], at least up to temperatures on the order of $1.5\,T_c$. This is actually the temperature range where most bound states (except perhaps 1S bottomonium) are expected to dissociate in an isotropic medium [47, 123]. On the other hand, Fig. 6.1 shows that at rather high temperatures of order $3T_c$, the model (6.2) does overshoot the CORNELL potential at short distances. This indicates that this simple form of the finite-temperature potential is not appropriate when the DEBYE mass m_D is large. However, this regime is not of interest here since even the $b\bar{b}$ states are no longer bound. Overall, the potential (6.2) appears to provide a reasonable model for the inter-quark potential in the deconfined phase at (moderately) high temperatures.

At $r \to \infty$ the potential (6.2) approaches

$$V_\infty(T) = 2\frac{\sigma}{m_D} \simeq \frac{0.16\ \text{GeV}^2}{T}\,. \tag{6.3}$$

Again, this is in approximate agreement with the $V_\infty \simeq 1/T$ *ansatz* used in Ref. [123]. Note, in particular, that Eq. (6.3) is about the same as the internal energy $U_\infty(T)$ obtained from

the lattice data [123]. We take this as an indication that our potential (6.2) represents an upper limit for the possible finite-temperature potentials.

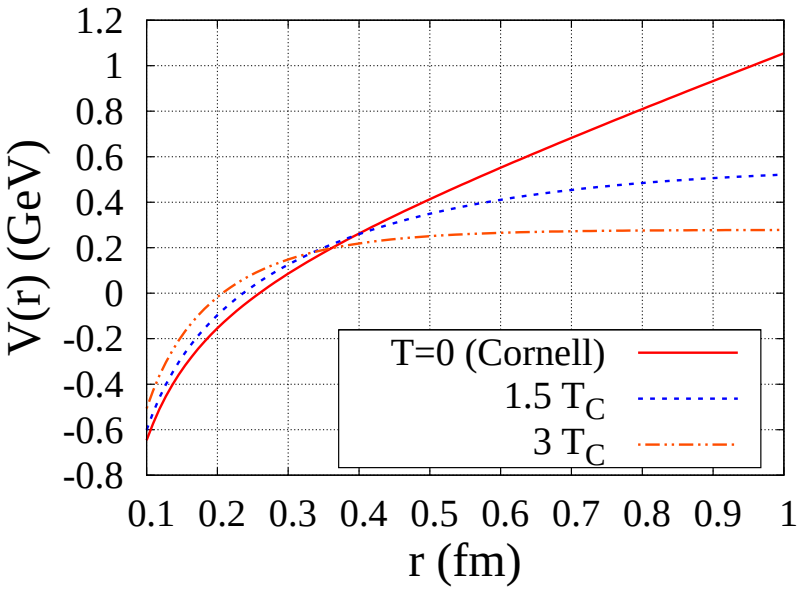

Figure 6.1: The model potential from Eq. (6.2) at zero and at finite temperature as a function of distance. Temperature is normalized to $T_c = 192$ MeV and the temperature dependence of the DEBYE mass is parameterized as given in Eq. (6.24) below.

The main assumption of the KMS model is that the very same screening scale m_D which emerges in the DEBYE-COULOMB potential also appears in the non-perturbative, long-distance contribution due to the string. In the following, we take over this assumption to anisotropic plasmas.

It is interesting to note that the KMS *ansatz* for the free energy from Eq. (6.1) can be obtained in the usual way from the FOURIER transform of the static propagator, provided that a non-perturbative contribution

$$\frac{m_G^2}{(p^2 + m_D^2)^2}\,, \tag{6.4}$$

is added to the standard HL resummed propagator [133, 134]. Here, m_G^2 is a constant of dimension two which can be related to the string tension σ by matching onto a CORNELL potential at small $m_D\, r$. The presence of such an additional dimensional scale (besides T) also leads to a non-vanishing trace of the energy-momentum tensor [135].

6.2 The potential model in quark-gluon plasma with small anisotropy

Our fundamental assumption is that the modified KMS potential (6.2), which provides a reasonable upper-limit model for the heavy-quark potential in isotropic media, retains its

basic form also when the local momentum distribution of the plasma particles is anisotropic ($\xi > 0$). However, the isotropic DEBYE mass $m_D(T)$ is now replaced by an angular dependent screening scale $\mu(\theta;\xi,T)$ which we will discuss in the following.

6.2.1 Angular dependence of the potential at short distances

Perturbatively we can evaluate the potential from one-gluon exchange at short distance. At tree level the potential corresponds to the FOURIER transform of the static gluon propagator which resums screening effects at high temperature [3]. For $\xi > 0$ the potential depends not only on the distance between the Q and $\bar{Q}$ but also on the angle θ between their separation $\mathbf{r}$ and the direction $\mathbf{n}$ of anisotropy [108].

As discussed in Sec. 4.2, quarkonium states are expected to form when the temperature has dropped to $(1-2)T_c$, by then, the plasma distribution is close to the ideal FERMI-DIRAC and BOSE-EINSTEIN distributions since it has equilibrated at least partly. As a result, small anisotropy will be considered in the following and we can expand the potential to linear order in ξ. With such simplifications, an analytical approximation of the potential can be obtained. Recall that the potential up to linear order in ξ can be expressed as

$$\begin{aligned} V(\mathbf{r},\xi) &= V_{\rm iso}(r) - g^2 C_F\, \xi m_D^2 \int \frac{\mathrm{d}^3\mathbf{p}}{(2\pi)^3}\, e^{i\mathbf{p}\cdot\mathbf{r}}\, \frac{\frac{2}{3} - (\mathbf{p}\cdot\mathbf{n})^2/p^2}{(p^2+m_D^2)^2} \\ &= V_{iso}(r)\,[1 - \xi\mathcal{F}(\hat{r},\theta)] \\ &= V_{\rm iso}(r)\bigg(1 - \xi f_0(\hat{r}) - \xi f_1(\hat{r})\cos(2\theta)\bigg)\,, \end{aligned} \tag{6.5}$$

where $\hat{r} \equiv r\, m_D$ and $m_D(T)$ denotes the screening mass in the isotropic medium at a given temperature T, as before. Also, $V_{\rm iso}(r)$ is the DEBYE-screened COULOMB potential in an isotropic medium, as given by the first term in Eq. (6.1), and the function

$$\begin{aligned} f_0(\hat{r}) &= \frac{6(1-e^{\hat{r}}) + \hat{r}[6 - \hat{r}(\hat{r}-3)]}{12\hat{r}^2} = -\frac{\hat{r}}{6} - \frac{\hat{r}^2}{48} + \cdots\,, \\ f_1(\hat{r}) &= \frac{6(1-e^{\hat{r}}) + \hat{r}[6 + \hat{r}(\hat{r}+3)]}{4\hat{r}^2} = -\frac{\hat{r}^2}{16} + \cdots\,. \end{aligned} \tag{6.6}$$

We have already mentioned that Eqs. (6.5) and (6.6) do not apply at large distances $\hat{r} \gg 1$, which is a shortcoming of the TAYLOR expansion of the full potential in powers of ξ. Actually, this is of no importance in the following because these expressions are used at short distances only in order to determine the angular dependence of the screening scale, which will then replace m_D in Eq. (6.2).

We can now define the θ-dependent screening mass in the anisotropic medium as the inverse of the distance scale $r_{\rm med}(\theta)$ over which $|rV(r)|$ drops by a factor of e:

$$\log \frac{-\alpha}{r_{\rm med}\, V(r_{\rm med},\theta;\xi,T)} = 1\,, \tag{6.7}$$

$$\mu(\theta;\xi,T) = r_{\rm med}^{-1}(\theta;\xi,T)\,. \tag{6.8}$$

[3] In this part we are only interested in distances up to $\sim 1/\mu$. It is therefore not crucial to distinguish carefully whether the potential is identified with the FOURIER transform of the propagator or with the internal energy. We shall add the entropy contribution later, c.f. Eqs. (6.11) and (6.12), to suppress corrections to the CORNELL potential at short distances.

In Eq. (6.7) we have used the fact that $rV \to -\alpha$ as $r \to 0$. To leading order in ξ this leads to

$$\hat{r}_{\rm med} \;=\; 1 - \xi \mathcal{F}(\hat{r}_{\rm med}, \theta)\,. \tag{6.9}$$

An approximate solution to Eq. (6.9) is given by

$$\hat{r}_{\rm med} \simeq 1 + \xi \frac{3+\cos 2\theta}{16} \quad \Rightarrow \quad \frac{\mu}{m_D} \simeq 1 - \xi \frac{3+\cos 2\theta}{16}\,. \tag{6.10}$$

For $\xi = 0.5$ (1.0) this solution achieves a relative accuracy of $\leq 4\%$ ($\leq 18\%$) over the entire range of θ. The accuracy of this result can be improved systematically by going beyond $\mathcal{O}(\hat{r}^2)$ in the expansion of the functions f_0 and f_1 introduced in Eq. (6.6).

In the KMS model, all the temperature dependent information is contained in the DEBYE mass. Therefore, one can expect that the corresponding anisotropy corrections to the isotropic medium appear only in the screening mass which enables us to define an effect *anisotropic screening mass* $\mu(\theta;\xi,T)$ to describe the anisotropic medium effect. So the "minimal" extension of the KMS model to non-zero anisotropy consists of replacing $m_D(T)$ in Eq. (6.2) by $\mu(\theta;\xi,T)$ from above:

$$V(\mathbf{r}) = -\frac{\alpha}{r}\,(1+\mu\, r)\exp\left(-\mu\, r\right) + \frac{2\sigma}{\mu}\left[1-\exp\left(-\mu\, r\right)\right] - \sigma\, r\, \exp(-\mu\, r)\,. \tag{6.11}$$

At short distances this reduces to the CORNELL potential $V(r) = -\alpha/r + \sigma\, r$, as it should be.

Corrections to Eq. (6.11) due to the finite quark mass can be accounted for by adding a temperature- and spin-independent correction proportional to $\sigma/(m_Q^2\, r)$ [136]. This improves the accuracy of the wave-functions of quarkonium states obtained from the solution of the non-relativistic SCHRÖDINGER equation. The potential finally takes the form

$$V(\mathbf{r}) = -\frac{\alpha}{r}\,(1+\mu\, r)\exp\left(-\mu\, r\right) + \frac{2\sigma}{\mu}\left[1-\exp\left(-\mu\, r\right)\right] - \sigma\, r\, \exp(-\mu\, r) - \frac{0.8\,\sigma}{m_Q^2\, r}\,. \tag{6.12}$$

6.2.2 Perturbative heavy-quark free energy

In the limit of infinite mass, the free energy of a heavy quark in a hot plasma is related to the expectation value of POLYAKOV loops. At high temperature, this can be calculated within hard-loop resummed perturbation theory. The leading-order contribution is given by

$$F_Q(\xi,T) = -\frac{1}{2}(ig)^2\, C_F \int \frac{\mathrm{d}^3\mathbf{p}}{(2\pi)^3}\left[D^{00}(\mathbf{p}) - \frac{1}{p^2}\right], \tag{6.13}$$

where $D^{00}(\mathbf{p})$ is the hard-loop resummed propagator of static A_0 fields. We have subtracted the temperature-independent contribution to F_Q which is not of interest here. Also, this renders the integral ultraviolet-finite. For the case of an anisotropic medium, $D^{00}(\mathbf{p})$ is given in Eq. (5.37). The expression (6.13) then turns into

$$F_Q(\xi,T) = -\frac{1}{2}\alpha_s C_F m_D h(\xi)\,, \tag{6.14}$$

with a temperature-independent function $h(\xi)$. For small anisotropy the following expansion in ξ applies:

$$h(\xi) = 1 - \frac{1}{6}\xi + \frac{18 - \pi^2}{240}\xi^2 + \cdots . \tag{6.15}$$

However, beyond the quadratic term, a fractional power may appear. In Appendix B, we will discuss this expansion in ξ in more detail. Here, we identify this expression with the free energy of a quark due to its interaction with the medium (i.e. half the free energy of a $Q\bar{Q}$ pair at large separation). However, the perturbative entropy contribution $TS = -T\partial F_Q/\partial T$ should be added again in order to obtain the potential. Since Eq. (6.14) is linear in T (at fixed coupling), it follows that the perturbative contribution to V_∞ vanishes [4]. On the other hand, lattice data (for an isotropic medium) indicate that the free energy of a $Q\bar{Q}$ pair at infinite separation also contains a non-perturbative contribution of the form $V_\infty(T) = r_{\mathrm{med}}(T)\,\sigma$ [47], which agrees qualitatively with the prediction of the KMS model, $V_\infty \sim \sigma/m_D$. Within the framework of the KMS model, this implies that at $\xi \neq 0$, $V_\infty(\theta;\xi,T)$ depends on angle as screening becomes anisotropic.

6.3 Solving the three-dimensional Schrödinger equation

To determine the wave-functions of bound quarkonium states, we solve the Schrödinger equation

$$\begin{aligned} \hat{H}\psi_v(\mathbf{x}) &= E_v\,\psi_v(\mathbf{x})\,, \\ \hat{H} &= -\frac{\nabla^2}{2M_R} + V(\mathbf{x}) + M_1 + M_2\,, \end{aligned} \tag{6.16}$$

on a three-dimensional lattice in coordinate space with the potential given in Eq. (6.12). Here M_1 and M_2 are the masses of the two heavy quarks and M_R is the reduced mass: $M_R = M_1M_2/(M_1 + M_2)$. The index v on the eigenfunctions, ψ_v, and energies, E_v, represents a list of all relevant quantum numbers, e.g. n, l, and m for a radial Coulomb potential. Due to the anisotropic screening scale, the wave-functions are no longer radially symmetric if $\xi \neq 0$. Since we consider only small anisotropies we nevertheless label the states as $1S$ (ground state) and $1P$ (first excited state), respectively.

To solve Eq. (6.16) we use the finite difference time domain method (FDTD) [137, 138]. In this method we start with the time-dependent Schrödinger equation

$$i\frac{\partial}{\partial t}\phi(\mathbf{x},t) = \hat{H}\phi(\mathbf{x},t)\,, \tag{6.17}$$

which can be solved by expanding in terms of the eigenfunctions, ψ_v:

$$\phi(\mathbf{x},t) = \sum_v c_v\psi_v(\mathbf{x})e^{-iE_vt}\,. \tag{6.18}$$

If one is only interested in the lowest energy states (ground state and first few excited states) an efficient way to proceed is to transform Eqs. (6.17) and (6.18) to Euclidean time by a

[4] A term $F_Q \sim a/T$ could be generated by a non-perturbative contribution of the form $m_G^2/(p^2 + m_D^2)^2$ to the static gluon propagator, as already mentioned above. m_G^2 is a constant of dimension two [134].

WICK rotation, $\tau \equiv it$:

$$\frac{\partial}{\partial \tau}\phi(\mathbf{x},\tau) = -\hat{H}\phi(\mathbf{x},\tau)\,, \tag{6.19}$$

and

$$\phi(\mathbf{x},\tau) = \sum_{\upsilon} c_\upsilon \psi_\upsilon(\mathbf{x}) e^{-E_\upsilon \tau}\,. \tag{6.20}$$

For details of the algorithm we refer to Ref. [138].

6.3.1 Finding the ground state

By definition the ground state is the state with the lowest energy eigenvalue, E_0. Therefore, at late imaginary time the sum over eigenfunctions (6.20) is dominated by the ground state eigenfunction

$$\lim_{\tau\to\infty} \phi(\mathbf{x},\tau) \to c_0\psi_0(\mathbf{x})e^{-E_0\tau}\,. \tag{6.21}$$

Because of this one can obtain the ground state wave-function, ψ_0, and energy, E_0, by solving Eq. (6.19) starting from a random three-dimensional wave-function, $\phi_{\text{initial}}(\mathbf{x},0)$, and evolving forward in imaginary time. This initial wave-function should have non-zero overlap with all eigenfunctions of the Hamiltonian; however, due to the damping of higher-energy eigenfunctions at sufficiently late imaginary times we are left with only the ground state, $\psi_0(\mathbf{x})$. Once the ground state wave-function (or, in fact, any other wave-function) is found we can compute its energy eigenvalue via

$$E_\upsilon(\tau\to\infty) = \frac{\langle\psi_\upsilon|\hat{H}|\psi_\upsilon\rangle}{\langle\psi_\upsilon|\psi_\upsilon\rangle} = \frac{\int d^3\mathbf{x}\,\psi_\upsilon^*\,\hat{H}\,\psi_\upsilon}{\int d^3\mathbf{x}\,\psi_\upsilon^*\psi_\upsilon}\,. \tag{6.22}$$

To obtain the binding energy of a state, $E_{\upsilon,\text{bind}}$, we subtract the quark masses and the potential at infinity

$$E_{\upsilon,\text{bind}} \equiv E_\upsilon - M_1 - M_2 - \frac{\langle\psi_\upsilon|V(\theta,|\mathbf{r}|\to\infty)|\psi_\upsilon\rangle}{\langle\psi_\upsilon|\psi_\upsilon\rangle}\,. \tag{6.23}$$

For the isotropic KMS potential the last term is independent of the quantum numbers υ and equal to σ/m_D. In the anisotropic case, however, this is no longer true since the operator $V_\infty(\theta)$ carries angular dependence, as already discussed above. Its expectation value is of course independent of θ but does depend on the anisotropy parameter ξ.

6.3.2 Finding the excited states

The basic method for finding excited states is to first evolve the initially random wave-function to large imaginary times, find the ground state wave-function, ψ_0, and then project this state out from the initial wave-function and re-evolve the partial-differential equation in imaginary time. However, there are (at least) two more efficient ways to accomplish this. The first is to record snapshots of the three-dimensional wave-function at a specified interval τ_{snapshot} during a single evolution in τ. After having obtained the ground state wave-function, one can then go back and extract the excited states by projecting out the ground state wave-function from the recorded snapshots of $\phi(\mathbf{x},\tau)$.

An alternative way to select different excited states is to impose a symmetry condition on the initially random wave-function which cannot be broken by the Hamiltonian evolution [138]. For example, one can select the first excited state of the (anisotropic) potential by anti-symmetrizing the initial wave-function around either the x, y, or z axes. In the anisotropic case this trick can be used to separate the different polarizations of the first excited state of the quarkonium system and to determine their energy eigenvalues with high precision. This high precision allows one to more accurately determine the splitting between polarization states which are otherwise degenerate in the isotropic DEBYE-COULOMB potential.

Whichever method is used, once the wave-function of an excited state has been determined one can again use the general formulas (6.22) and (6.23) to determine its binding energy.

6.4 Numerical results

In this section we present the solutions of the three-dimensional SCHRÖDINGER equation (6.16) in a weakly anisotropic medium. In particular, we determine the temperature dependence of the binding energies of different charmonium and bottomonium states obtained with the anisotropic potential (6.12) that has been constructed from the most binding isotropic potential. The anisotropy- and temperature-dependent screening mass $\mu(\theta;\xi,T)$ is given in Eq. (6.10). To illustrate the effect of the anisotropy of the medium more clearly we shall also compare the results to those obtained for an isotropic medium. In the latter case $\xi = 0$ and so $\mu(\theta;\xi,T) = m_D(T)$, where the temperature dependence of the DEBYE mass is given by

$$m_D(T) = A\, gT \sqrt{(1 + N_f/6)}\,. \tag{6.24}$$

For $N_f = 2$ number of massless quark flavors the parameter $A = 1.4$ has been determined in lattice calculations [139]. We choose a fixed gauge coupling of $g = 1.72$ which yields $m_D(T)/T \approx 2.8$. This agrees approximately with lattice estimates of m_D/T for temperatures on the order of $T/T_c \sim 1.5$, and it also gives a reasonable estimate of the free energy at infinite separation [139]. The values of the charm and bottom quark masses are chosen such that at low temperature the correct masses of $M_{J/\psi} = 3.1$ GeV and $M_\Upsilon = 9.4$ GeV for the J/ψ and the Υ, respectively, are recovered. Accordingly,

$$M_c = 1.3 \text{ GeV} \qquad \text{and} \qquad M_b = 4.7 \text{ GeV}\,. \tag{6.25}$$

All of the results reported below were obtained from lattices with lattice spacings approximately 20 times smaller than the root-mean-square radius $\langle \mathbf{r}^2 \rangle_\upsilon^{1/2}(T,\xi,M_Q)$ of the state under consideration, defined by the quantum number υ. The lattice size L was chosen to be about 6 times larger than the root-mean-square radius [5]. Discretization errors and finite-size effects are thus expected to be reasonably small and nearly independent of T, ξ, M_Q, and υ. We stopped the time evolution when the energy $E_\upsilon(\tau)$ of the state had stabilized to within 10^{-8}. A more detailed investigation of numerical errors is beyond the scope of the present work. Our goal here is to show how quarkonium states may be affected by the anisotropy of the medium.

[5] Since we restrict the analysis to only weak medium anisotropies, we employ isotropic lattices with uniform lattice spacing in all three cartesian directions.

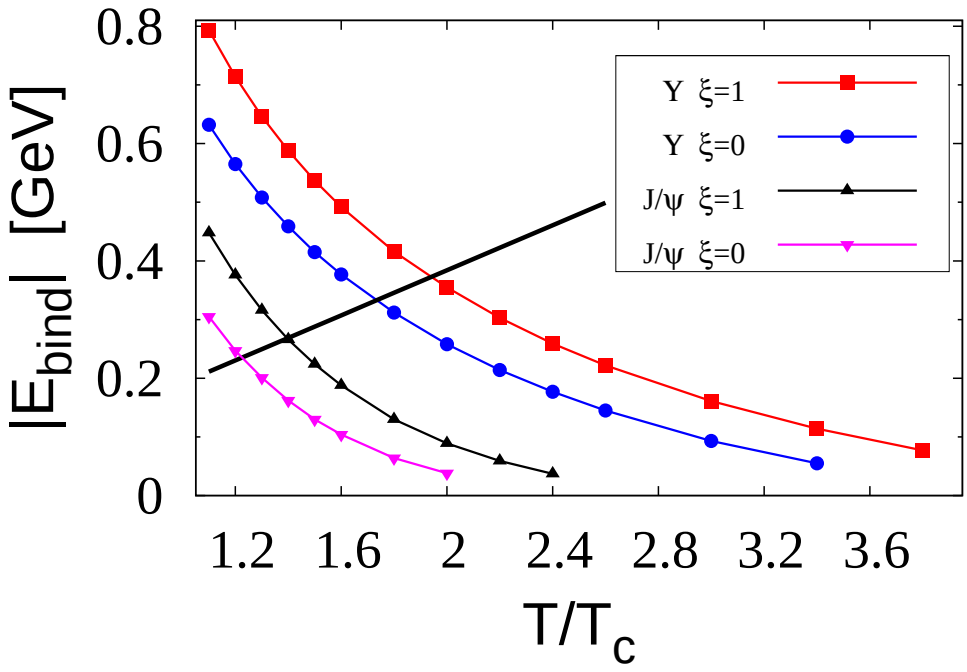

Figure 6.2: Temperature-dependence of the binding energies $|E_{\rm bind}|$ for the ground-states of charmonium (lower curves) and bottomonium (upper curves) in the vector channel for two values of the plasma anisotropy parameter ξ. The straight line corresponds to a binding energy equal to the temperature.

The temperature dependence of the *binding energies* of charmonium and bottomonium ground states in the vector channel [6] are depicted in Fig. 6.2. The figure shows the results obtained for isotropic $\xi = 0$ and anisotropic $\xi = 1$ media. The former are in agreement with those obtained in Ref. [123] with the so-called most confining isotropic potential. As expected, the binding energy decreases as the screening mass $m_D(T)$ increases with temperature T. This plot also indicates that $|E_{\rm bind}|$ increases with the anisotropy ξ. This can be understood from the fact that in an anisotropic plasma the screening scale $\mu(\theta)$ at a given temperature is smaller than the corresponding DEBYE mass m_D; see Eq. (6.10). As a consequence, the screening of the attractive COULOMB and string contributions is less accentuated in the anisotropic plasma and so quarkonium states are bound more strongly than in an isotropic medium. The magnitude of this effect is substantial even for the moderate anisotropy considered here. Near the critical temperature T_c, for example, the binding energy of the 1S vector $c\bar{c}$ ground state increases by about 50%, and that of the 1S $b\bar{b}$ ground state increases by roughly 30% compared to the binding energies calculated in an isotropic medium (the only case addressed previously in the literature).

It is important to highlight another aspect of the reduced screening. In our potential model the asymptotic value of the potential is intrinsically related to the screening mass via

[6] Spin effects are neglected in our treatment and the ground state could be identified with either the pseudoscalar or the vector state. For definitness, we shall refer to the vector channel.

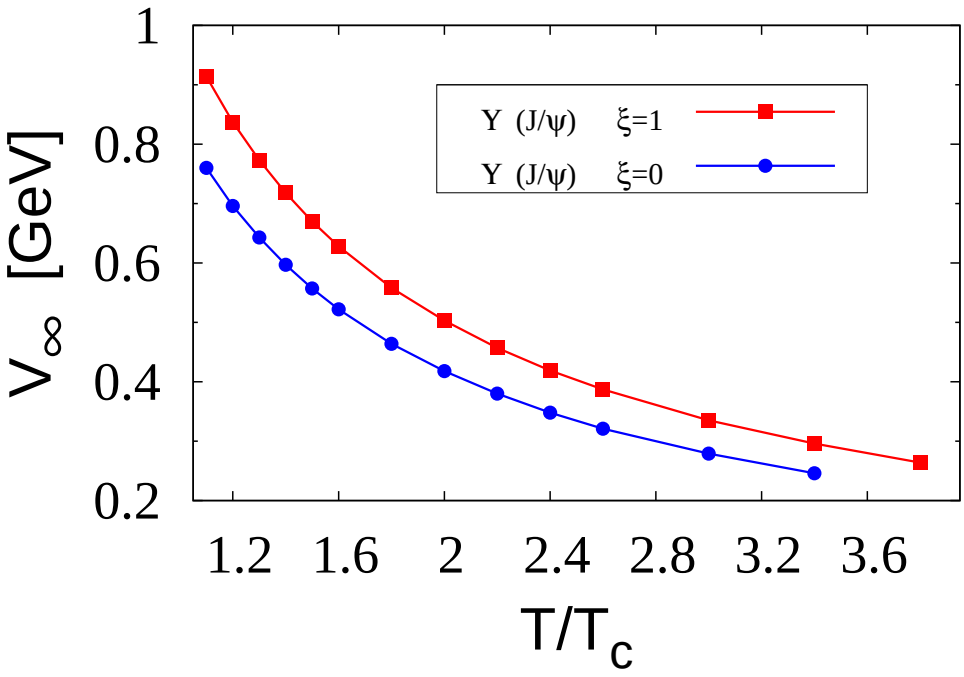

Figure 6.3: Expectation value of V_∞ in the J/Ψ or Υ states as a function of temperature for two values of the plasma anisotropy parameter ξ.

the relation $\langle V_\infty \rangle(T) = \langle v|2\sigma\mu^{-1}(\theta;\xi,T)|v\rangle$. This implies that in the anisotropic medium less screening translates into an increase of the potential at infinite separation, V_∞. The above is illustrated in Fig. 6.3 which shows the expectation value of V_∞ in the Υ state [7]. V_∞, in turn, determines the *continuum threshold*, which, at a given T is at higher energy than in the isotropic case. This implies that at a given temperature the energy gap between the bound state and the continuum, which is the binding energy, is increased compared to the isotropic case.

Comparing the behavior of $\langle V_\infty \rangle$ to that of the binding energy of the Υ from Fig. 6.2 shows that the decrease of $|E_{\rm bind}|$ with T is largely due to the decrease of the continuum threshold $\langle V_\infty \rangle$. The energy of the state is almost independent of T (for $T \leq 2T_c$) and ξ (for $\xi \leq 1$). This has interesting implications for phenomenology: On one hand, the center of the Υ-peak in the dilepton invariant mass distribution may not shift much (since $V_\infty = 0$ for decay into dileptons) even for temperatures larger than T_c where the binding energy is significantly lower than in vacuum. On the other hand, when $|E_{\rm bind}| \sim T$ we expect substantial broadening of the states due to direct thermal activation [140, 123]. The thermal width can be estimated from the binding energy [140]. When the width is larger than the binding energy, a state decays faster than it binds [123]. Note, that in the same temperature domain collisions with thermal particles of the medium would further broaden the width of a state. Thus, the dissociation of the bound states may be expected to occur

[7] We recall that V_∞ is proportional to the identity at $\xi = 0$ and hence its expectation value is the same for all states. At $\xi = 1$ we obtain a very small difference between $\langle J/\Psi|V_\infty|J/\Psi\rangle$ and $\langle \Upsilon|V_\infty|\Upsilon\rangle$.

roughly when $|E_{\rm bind}| \sim T$ [33]. With the potential investigated here, which likely represents an upper limit for the attractive interaction, the condition $|E_{\rm bind}| \sim T$ is met for the J/ψ by $1.2\,T_c$ for $\xi = 0$, in agreement with previous results [123], and by $1.4\,T_c$ for $\xi = 1$. We stress furthermore that the *thermal density* of a given state,

$$\rho \sim \exp\left(-\frac{E_{\rm bind}}{T}\right) , \tag{6.26}$$

is not enhanced significantly when $|E_{\rm bind}| < T$. In other words, since T decreases with time in a heavy-ion collision, quarkonium states with quantum numbers υ should appear at a temperature $T_\upsilon \sim |E_{\upsilon,\rm bind}|$ [8]. From Fig. 6.2 it is plausible that in a viscous plasma quarkonium synthesis occurs at higher temperature than in a perfectly equilibrated medium. For the J/Ψ for example, $\Delta T_{\rm synth}/T_c \simeq 20\%$ for $\xi = 1$ as compared to $\xi = 0$.

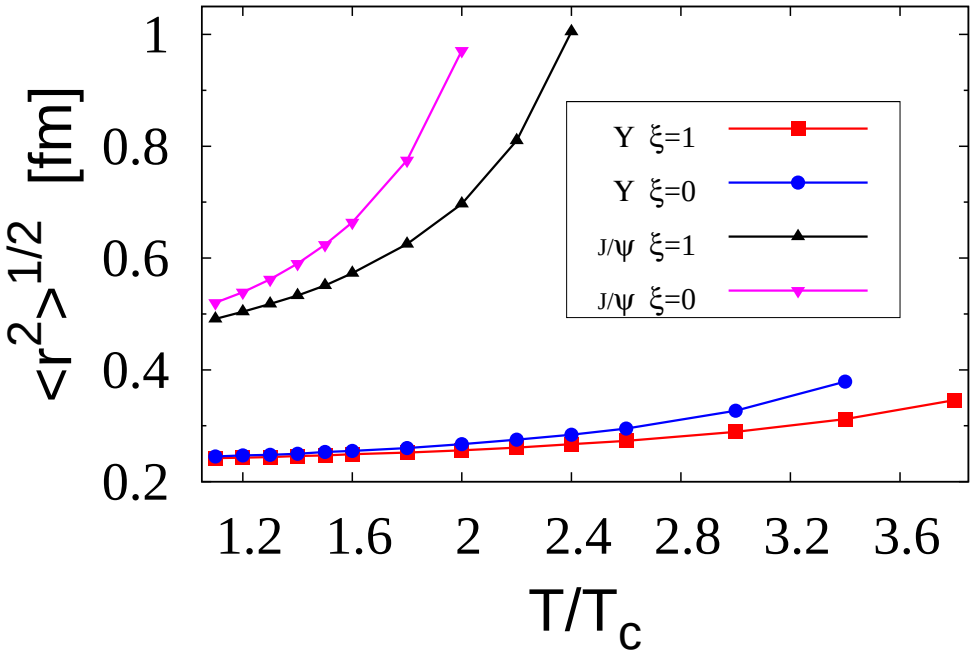

Figure 6.4: Root-mean-square radii of the $1S$ ground-states of charmonium (upper curves) and bottomonium (lower curves) as functions of temperature for two values of the plasma anisotropy parameter ξ.

In Fig. 6.4 we show the *root-mean-square radii* $\langle \mathbf{r}^2 \rangle^{1/2}(T, \xi)$ of the $c\bar{c}$ and $b\bar{b}$ ground states as functions of temperature. The former grows rather rapidly above the dissociation point where $|E_{\rm bind}| \sim T$. The size of the Υ, on the other hand, increases only little with temperature. We can understand these results, qualitatively, as follows: for charmonium the string part of the potential dominates, and the growth of its RMS radius with T indicates

[8] The total number of formed quarkonium states depends on how many heavy quarks are produced in the initial hard processes, and on what fraction thereof is bound in D- and B-mesons, respectively.

that screening of the string is strong [9]. We observe a similar behavior of the first $1P$ excited state of bottomonium. On the other hand, $1S$ bottomonium is too small to be affected strongly by screening (for $T \leq 2T_c$), it is essentially a COULOMB state. The weaker binding as compared to low temperature is largely due to a decrease of the continuum threshold V_∞, as already mentioned above.

Indeed, we can get the similar conclusions by studying the behavior of the wave-functions. In Figs. 6.5 and 6.6, it is shown that the *wave-functions* of the $b\bar{b}$ ground state is essentially unaffected by the medium for $T \leq 2T_c$ and $\xi \leq 1$. However, the wave-functions of J/Ψ have a visible deform when the temperature changes. For an anisotropic system with $\xi = 1$, we plot the wave-functions along two typical directions: $\mathbf{r} \perp \mathbf{n}$ and $\mathbf{r} \parallel \mathbf{n}$ at fixed temperature. However, the difference between the two directions is very small especially for the $b\bar{b}$ ground state.

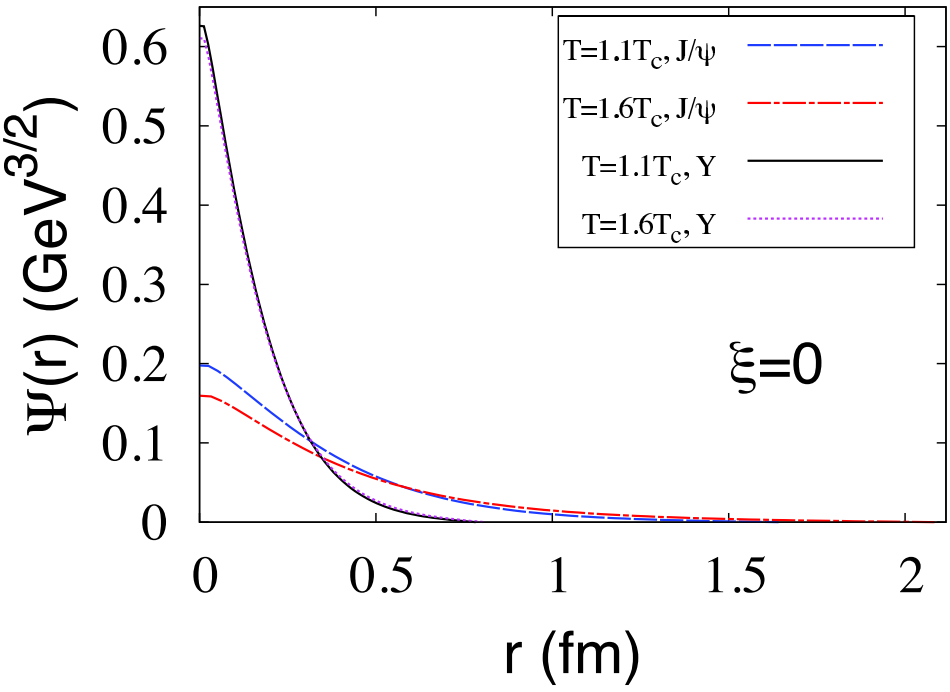

Figure 6.5: Wave-functions of the J/Ψ and Υ states at different temperature in an isotropic quark-gluon plasma.

In this vein, it is also instructive to look at the behavior of the *absolute energy* of the J/Ψ and Υ states versus temperature, shown in Fig. 6.7. We recall that $E - 2M_Q = \langle V_\infty \rangle + E_{\text{bind}}$. The energy of the Υ increases slightly with temperature as is expected for a small-size state bound mainly by the DEBYE-COULOMB part of the potential (plus a constant): the first term on the right hand side of Eq. (6.12) increases with the screening mass μ. On the other hand, $E_{J/\Psi}$ decreases with T because the second term in Eq. (6.12) decreases as μ increases.

Fig. 6.8 shows the temperature dependence of the binding energies of the $1P$ states of

[9] Recall that the in the KMS model the string tension enters with a factor of $1/m_D(T)$ at intermediate distances on the order of $r \sim 1/m_D(T)$.

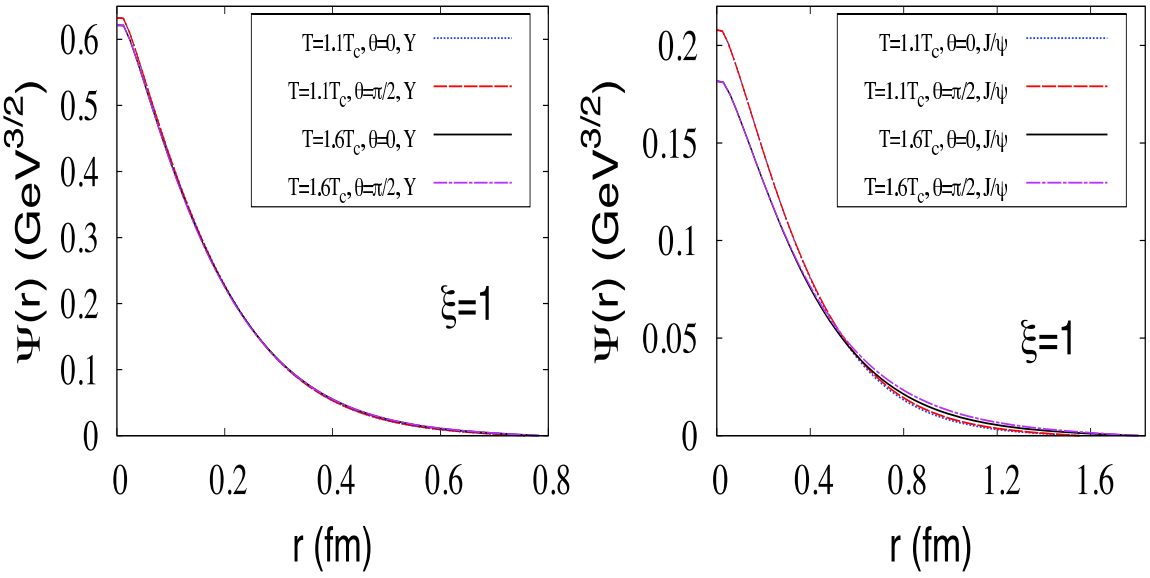

Figure 6.6: Wave-functions of the J/Ψ and Υ states at different temperature in an anisotropic quark-gluon plasma with $\xi = 1$.

bottomonium [10], identified with the χ_b. The anisotropy again leads to an increase of $|E_{\rm bind}|$ by about 50%, comparable to the behavior of the J/Ψ from above. It also leads to a preferred *polarization* of the χ_b, with about 50 MeV splitting between states with angular momentum $L_z = 0$ and $L_z = \pm 1$, respectively. At $T \sim T_c$, due to the BOLTZMANN factor (6.26), the population of the state with $L_z = 0$ is about 30% higher than that of either one of the $L_z = \pm 1$ states. Here, the polarization is with respect to the axis $\mathbf{n}$ of anisotropy, which coincides with the direction of expansion of the plasma. In addition, quarkonium states produced in high-energy collisions initially through semi-hard gluon fusion may exhibit polarization with respect to the particle velocity vector [141].

6.5 Discussions

In a viscous plasma, anisotropic expansion of a fluid element leads to an anisotropy of the quasi-particle momentum distributions. The hard-loop resummed propagator of static color-electric fields then carries angular dependence which leads to anisotropic screening.

In this chapter we have proposed the first model for the static potential between a very heavy quark and anti-quark in a hot anisotropic QCD plasma. Conceptually, we assume that the time scale $\sim 1/|E_{\rm bind}|$ associated with the bound state is short compared to the time scales over which the temperature and the anisotropy evolve.

At distances on the order of the DEBYE length the potential can be calculated from perturbative QCD (at high temperature). At larger distances it is, however, dominated by the non-perturbative string attraction. Lattice gauge theory simulations have shown that in the deconfined phase the string is screened at a similar scale $r_{\rm med}(T) \sim 1/m_D(T)$ and

[10] The $1P$ states of charmonium do not have binding energies which exceed the temperature significantly for $T \sim T_C$.

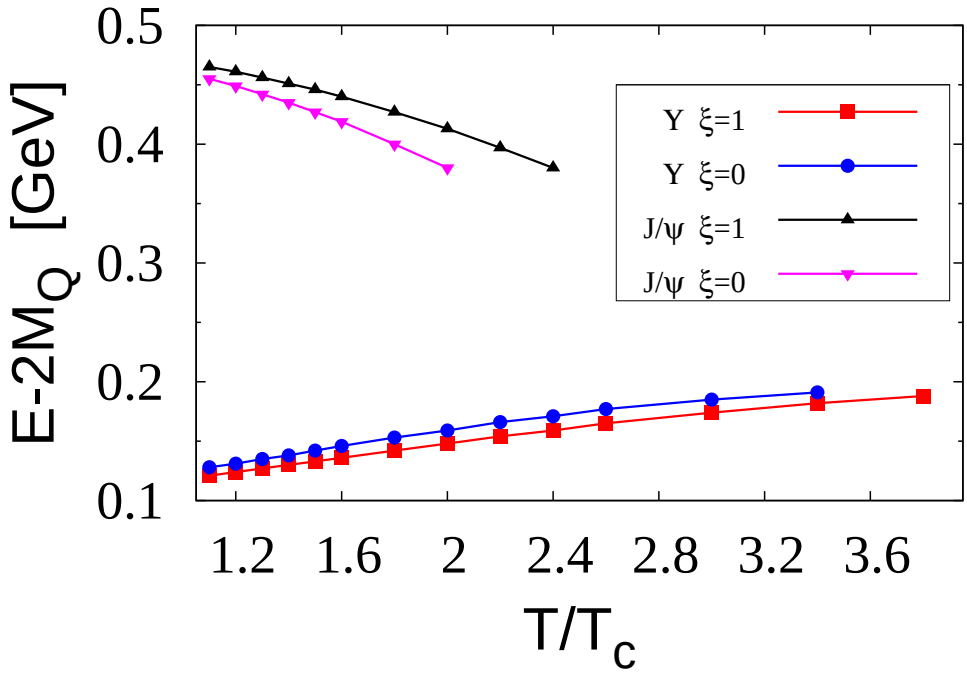

Figure 6.7: Absolute energy of the J/Ψ and Υ states, minus twice the corresponding quark mass, as a function of temperature.

that at infinite separation the free energy of a $Q\bar{Q}$ pair approaches a constant $V_\infty(T)$, equal to twice the free energy of a single heavy quark in the plasma.

The essential features appear to be in qualitative agreement with a model originally proposed by Karsch, Mehr and Satz [40]. However, to obtain the heavy-quark potential we subtract the entropy contribution from their *ansatz* for the free energy of a $Q\bar{Q}$ pair. We thereby obtain the internal energy of the $Q\bar{Q}$ pair which should be viewed as an upper limit for the physical potential. The latter may be less binding than the KMS internal energy used here. We note that in the relevant temperature region, up to about $2T_c$, the potential at short and intermediate distances follows the zero-temperature Cornell potential; i.e. the overshooting problem of the internal energy is eliminated, in accordance with lattice data on the free energy.

The KMS model correctly reproduces the Cornell potential at short distances and, moreover, does not introduce any new parameters besides the string tension. This is important for our present goal of extending the isotropic potential to anisotropic plasmas. Knowledge of the anisotropic screening scale obtained from the gluon propagator is sufficient to generalize the KMS model to anisotropic media.

We then proceeded to solve the Schrödinger equation with this potential to determine the wave-functions of bound $c\bar{c}$ and $b\bar{b}$ states in the plasma. The radial Schrödinger equation is no longer sufficient as the potential carries angular dependence. We employ a finite difference time domain method (in Euclidean time) on a three-dimensional lattice to obtain the wave-functions and the binding energies. Some medium effects are neglected in this approach. However, solving for the full non-relativistic Green function including

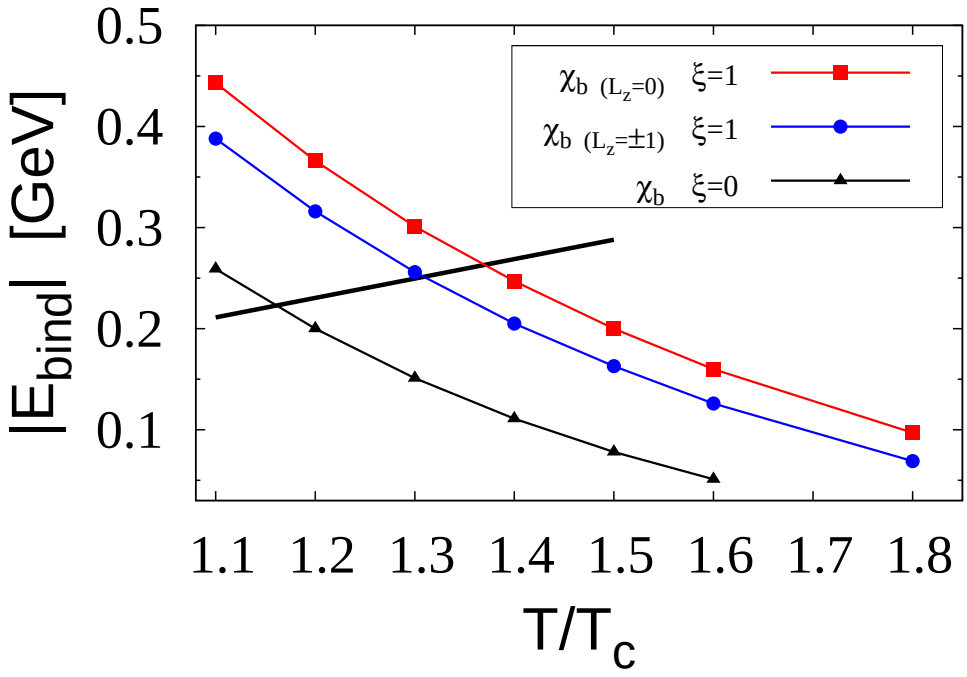

Figure 6.8: Temperature-dependence of the binding energy for the $1P$ state of bottomonium for two values of the plasma anisotropy parameter ξ. The straight line corresponds to a binding energy equal to the temperature.

threshold effects in three dimensions is beyond the scope of this work.

We found that just above the critical temperature $T_c \simeq 192$ MeV for deconfinement (in QCD with $N_c = 3$ colors) in an anisotropic medium both the $1S$ state of charmonium as well as the $1S$ and $1P$ states of bottomonium have binding energies larger than T; the temperature may serve as a rough estimate for the width of the states. The binding energies decrease with temperature and cease to exceed the estimated width $\Gamma \sim T$ at some higher temperatures. We note, also, that the BOLTZMANN enhancement factor $\exp(-E_{\rm bind}/T)$ for bound states is negligible anyways when $|E_{\rm bind}| \leq T$.

The decrease of $|E_{\rm bind}|$ with T is due to two effects: First, the continuum threshold $V_\infty(T)$ decreases approximately like $\sim 1/T$. The energy gap between the bound state and the continuum, which is the binding energy, therefore decreases, too. In fact, for the model adopted here, we find this to be the dominant effect on the $1S$ ground state of bottomonium whose wave-function is rather insensitive to the presence of the medium. The state is too small to be affected strongly by screening. Hence, the Υ peak in the dilepton invariant mass distribution may not experience a large shift although one should expect substantial broadening near the dissociation temperature.

Larger states such as the $1S$ ground state of charmonium and the $1P$ excited state of bottomonium, however, may also experience some modifications due to screening. The root-mean-square radii of these states increase rather rapidly with T around the dissociation point $|E_{\rm bind}| \sim T$.

The two main results of this chapter are as follows. At fixed T, the screening mass

decreases with increasing ξ. In the KMS model, the asymptotic value of the potential is intrinsically related to the screening mass via $V_\infty(\theta) \sim 1/\mu(\theta;\xi,T)$. Hence, less screening translates into an increase of the potential at infinite separation. This implies that the binding energies of bound states increase, too. The effect is quite substantial even for moderate anisotropies $\xi \simeq 1$ considered here: we find that just above T_c the binding energy of the bottomonium ground state increases by about 30%, that of $1S$ charmonium and of $1P$ bottomonium by 50%. Thus, such quarkonium states may exist up to somewhat higher temperatures than in case of an isotropic, perfectly equilibrated medium (for $\xi = 0$ the J/ψ and the Υ are expected to dissociate by $1.2\,T_c$ and $1.8\,T_c$, respectively, in agreement with previous potential model calculations).

The other important new effect identified here is that the angular dependence of the inter-quark potential in an anisotropic medium induces a polarization of states with non-zero angular momentum. According to our estimates, the splitting of the χ_b with $L_z = 0$ and $L_z = \pm 1$, respectively, is on the order of 50 MeV. At $T \simeq 200$ MeV, the population of the state with $L_z = 0$ is BOLTZMANN-enhanced by about 30% as compared to the states with angular momentum along the direction of anisotropy, respectively. The experimental confirmation of such a polarization at RHIC or LHC may provide first evidence for a non-zero viscosity of QCD near T_c.

The next step of our investigation is the determination of the imaginary part of the potential, which will provide insight into how the anisotropy of the medium affects the widths of the states. In Chapter 7, we will discuss the decay width which appears at leading order in the perturbative expansion.

7 Quarkonium decay width in an anisotropic QCD plasma

So far we have considered the real part of the perturbative heavy-quark potential which arises due to one-gluon exchange. Such a potential enables us to determine the effective screening mass $\mu(\theta;\xi,T)$ at short distances in an anisotropic plasma which can be used to generalize the KMS potential model to the anisotropic case. In this model, both the perturbative and non-perturbative effects are included. Furthermore, we solved the three-dimensional SCHRÖDINGER equation with the generalized KMS potential and determined the binding energy of quarkonium states.

Experimentally, the properties of thermally produced heavy quarkonium can be observed through its decay into a virtual photon, which then produces a dilepton pair. Measuring their energy spectrum yields the information on the properties of heavy quarkonium in the QCD medium. For example, The dissociation of quarkonium states corresponds to the disappearance of the quarkonium resonance peak from the dilepton production rate.

However, merely estimating the energy levels from a potential model does not allow us to reconstruct the spectral function which determines the production rate. In fact, stationary levels would correspond to infinitely narrow peaks in the spectral function. An intuitive picture is that a resonance peak should dissolve through becoming gradually wider. Indeed, it has been pointed out in Ref. [48] that by defining a static potential through the SCHRÖDINGER equation satisfied by a certain heavy quarkonium GREEN function, and computing it systematically in the weak-coupling expansion, the static potential obtains both a standard DEBYE-screened real part, as well as an imaginary part, originating from the LANDAU damping of almost static color fields. The imaginary part of the static potential then leads to a finite width for the quarkonium resonance peak in the spectral function.

In fact, as the computation is formulated within finite-temperature field theory, the information about the decay width should be contained in the heavy-quark potential. Such a potential will generate an imaginary part which we discuss more systematically in this chapter [1].

7.1 The Dyson-Schwinger equation in real time formalism

As discussed in Sec. 3.1, when the *real time formalism* is employed, both the propagators and self-energies are 2×2 matrices which are equivalently described by retarded, advanced and symmetric propagators in KELDYSH representation. However, up to now, only the retarded solution is considered and its FOURIER transform in the static limit determines the real part of the heavy-quark potential. In this chapter, we are going to generalize our consideration to all three kinds of propagators in the KELDYSH representation and it turns

[1] This chapter is based on the work published in [142].

out the information about the decay width of heavy quarkonia in medium which corresponds to the imaginary part of the potential can be obtained and such a decay width is related to the symmetric propagator.

In general, the calculation of the propagators is complicated when the distribution function becomes anisotropic. The corresponding calculation in an equilibrated, weakly-coupled high-temperature plasma can be found in Refs. [65, 80, 66]. As we have already seen in Sec. 5.3, the real part of the heavy-quark potential in an anisotropic QCD plasma can only be determined numerically. Here, we would like to study the analytical behavior of the potential including both real and imaginary parts by considering the small anisotropy limit. For simplicity, we shall restrict ourselves to a plasma close to equilibrium. As a result, the phase-space distribution of particles in a hot QCD plasma is given by

$$\begin{aligned} f(\mathbf{k}) &= f_{\rm iso}\left(\sqrt{k^2+\xi(\mathbf{k}\cdot\mathbf{n})^2}\right) \\ &\approx f_{\rm iso}(k)\left[1-\xi\frac{(\mathbf{k}\cdot\mathbf{n})^2}{2kT}\left(1\pm f_{\rm iso}(k)\right)\right] \\ &= f_{\rm iso}(k)-\xi\frac{(\mathbf{k}\cdot\mathbf{n})^2}{2kT}\left[1\pm f_{\rm iso}(k)\right]f_{\rm iso}(k) \\ &\equiv f_{(0)}(k)+f_{(1)}(k)\,. \end{aligned} \tag{7.1}$$

The second line in Eq. (7.1) follows from an expansion in the anisotropy parameter ξ. We use $f_{(0)}$ to denote the distribution at order of $\mathcal{O}(\xi^0)$, i.e. the isotropic Bose-Einstein or Fermi-Dirac distribution. The correction due to the presence of anisotropy at order of $\mathcal{O}(\xi^1)$ is denoted by $f_{(1)}$. Such a correction to the equilibrium distribution exhibits precisely the structure expected from viscous hydrodynamics for a fluid element expanding one-dimensionally along the direction $\mathbf{n}$, provided the relationship between the anisotropy parameter and shear viscosity is given by Eq. (4.3). As usual in viscous hydrodynamics, the temperature T as well as the entropy density s appearing in Eqs. (7.1) and (4.3) are defined at equilibrium. All viscous corrections are accounted for explicitly by $f_{(1)}$ in Eq. (7.1).

As defined in Eq. (5.10), when we consider the heavy-quark potential that arises due to one-gluon exchange, our basic task is to determine the resummed propagator of which we should perform the Fourier transform. In Sec. 5.2, we determined the (retarded) resummed gluon propagator from the Dyson-Schwinger equation

$$D^*{}_R = D_R + D_R\Pi_R D^*{}_R\,. \tag{7.2}$$

Note that we use the subscripts "R", "A" and "F" to denote the retarded, advanced and symmetric propagators or self-energies, respectively. As before, D^* indicates a resummed propagator and D is the bare propagator.

In fact, we can write the Dyson-Schwinger *equation* explicitly as

$$\begin{bmatrix} D^*_{11} & D^*_{12} \\ D^*_{21} & D^*_{22} \end{bmatrix} = \begin{bmatrix} D_{11} & D_{12} \\ D_{21} & D_{22} \end{bmatrix} + \begin{bmatrix} D_{11} & D_{12} \\ D_{21} & D_{22} \end{bmatrix} \begin{bmatrix} \Pi_{11} & \Pi_{12} \\ \Pi_{21} & \Pi_{22} \end{bmatrix} \begin{bmatrix} D^*_{11} & D^*_{12} \\ D^*_{21} & D^*_{22} \end{bmatrix}. \tag{7.3}$$

Using the identities (3.8) for the bare and resummed propagators and (3.15) for the self-energies, it is easy to show that the Dyson-Schwinger equation for retarded propagator is given by Eq. (7.2) and a similar expression holds for advanced propagator.

In addition, the resummed symmetric propagator satisfies

$$D^*{}_F = D_F + D_R\Pi_R D^*{}_F + D_F\Pi_A D^*{}_A + D_R\Pi_F D^*{}_A\,. \tag{7.4}$$

The bare propagators satisfy the following relation [2]

$$D_F(P) = (1+2N(\mathbf{p}))\,\mathrm{sgn}(p_0)\,[D_R(P) - D_A(P)]\,, \tag{7.5}$$

then we find the explicit solution for $D^*{}_F$ can be expressed in the form

$$\begin{aligned} D^*{}_F(P) &= (1+2N(\mathbf{p}))\,\mathrm{sgn}(p_0)\,[D^*{}_R(P) - D^*{}_A(P)] \\ &+ D^*{}_R(P)\,\{\Pi_F(P) - (1+2N(\mathbf{p}))\,\mathrm{sgn}(p_0)\,[\Pi_R(P) - \Pi_A(P)]\}\,D^*{}_A(P)\,. \end{aligned} \tag{7.6}$$

In equilibrium, we have

$$\Pi_F(P) = [1+2N_{\mathrm{eq}}(p_0)]\,\mathrm{sgn}(p_0)\,[\Pi_R(P) - \Pi_A(P)]\,. \tag{7.7}$$

As a result, the second term in Eq. (7.6) vanishes. However, this is no longer true out of equilibrium.

Actually, in order to determine the static potential at leading order, we only require the temporal component of the gluon propagator. On the other hand, small anisotropies are more relevant for quarkonium studies, thus more interesting for our consideration here. Therefore, we will calculate the temporal component of the gluon propagator in small ξ limit. At leading order in ξ (or in the shear viscosity) the calculation of D^{*00} is easiest in Coulomb *gauge*. The temporal component decouples from the other components which simplifies the calculation significantly. Recall that in this gauge (with the gauge parameter $\eta = 0$) the bare or resummed propagators satisfy

$$p^i \cdot D^{0\,i} = 0 \;\;, i = 1,2,3\,. \tag{7.8}$$

In the isotropic case this reduces to $D^{0\,i} = 0$. As a result, for an isotropic system we can write Eq. (7.2) as

$$D^{*L}_{R(0)} = D^L_R + D^L_R\Pi^L_{R(0)}D^{*L}_{R(0)}\,. \tag{7.9}$$

Here, L denotes the temporal component, $D^L \equiv D^{00}$. A similar relation holds for the advanced propagator.

Eq. (7.9) no longer holds for the anisotropic system due to breaking of isotropy in momentum space. However, for small anisotropy, we can expand the resummed propagators and self-energies in ξ:

$$D^* = D^*_{(0)} + \xi D^*_{(1)} + \mathcal{O}(\xi^2)\,, \quad \Pi = \Pi_{(0)} + \xi\Pi_{(1)} + \mathcal{O}(\xi^2)\,. \tag{7.10}$$

The propagators to order $\mathcal{O}(\xi^0)$, namely $D^*_{(0)}$ satisfy the equilibrium relations, i.e. for retarded or advanced propagator, we have Eq. (7.9) and for symmetric propagator,

$$D^{*L}_{F(0)}(P) = (1+2N_{(0)}(p_0))\,\mathrm{sgn}(p_0)\,[D^{*L}_{R(0)} - D^{*L}_{A(0)}]\,. \tag{7.11}$$

[2] In equilibrium, $N(\mathbf{p})$ is given by Bose-Einstein distribution $N_{\mathrm{eq}}(p_0) \equiv N_{(0)}(p_0)$. This equation is true even in the non-equilibrium case [143].

For the linear term of order ξ, we have the following expression

$$D^*{}_{R(1)} = D_R\,\Pi_{R(1)} D^*{}_{R(0)} + D_R\,\Pi_{R(0)} D^*{}_{R(1)}\,. \tag{7.12}$$

The explicit expression for the temporal component is

$$D^{*L}_{R(1)} = (D_R)^{0\,\mu}\,(\Pi_{R(1)})_{\mu\,\nu}(D^*{}_{R(0)})^{\nu\,0} + (D_R)^{0\,\mu}\,(\Pi_{R(0)})_{\mu\,\nu}(D^*{}_{R(1)})^{\nu\,0}\,. \tag{7.13}$$

Since $(D_R)^{0\,i} = 0$, $(D^*{}_{R(0)})^{0\,i} = 0$ and $(\Pi_{R(0)})^{0\,i} \sim p^i$ [3], according to Eq. (7.8), it follows that [4]

$$D^{*L}_{R(1)} = D^L_R\,\Pi^L_{R(1)} D^{*L}_{R(0)} + D^L_R\,\Pi^L_{R(0)} D^{*L}_{R(1)}\,. \tag{7.14}$$

Again, a similar relation holds for the advanced propagator. For the symmetric propagator, finally,

$$\begin{aligned} D^{*L}_{F(1)}(P) &= (1+2N_{(0)}(p_0))\,\mathrm{sgn}(p_0)\,[D^{*L}_{R(1)}(P) - D^{*L}_{A(1)}(P)] \\ &+ 2N_{(1)}(\mathbf{p})\,\mathrm{sgn}(p_0)\,[D^{*L}_{R(0)}(P) - D^{*L}_{A(0)}(P)] \\ &+ D^{*L}_{R(0)}(P)\,\{\Pi^L_{F(1)}(P) - (1+2N_{(0)}(p_0))\,\mathrm{sgn}(p_0)\,[\Pi^L_{R(1)}(P) - \Pi^L_{A(1)}(P)] \\ &- 2N_{(1)}(\mathbf{p})\,\mathrm{sgn}(p_0)\,[\Pi^L_{R(0)}(P) - \Pi^L_{A(0)}A(P)]\}\,D^{*L}_{A(0)}(P)\,. \end{aligned} \tag{7.15}$$

7.2 Calculation of propagators in Keldysh representation

We now proceed to calculate explicitly the gluon self-energies from which we obtain the propagators via the relations above. Here, we employ the diagrammatic *hard-loop* approach. The same results can be derived from Vlasov transport theory [75] as we already proved before. Actually, we derived the retarded self-energy for general ξ in Sec. 5.2 and the advanced solution has a similar expression with $+i\,\epsilon$ prescription replaced by $-i\,\epsilon$. However, this is not sufficient to get the symmetric propagator in an anisotropic system according to Eq. (7.15) and the calculation of symmetric self-energy becomes necessary. This calculation is more convenient to do in the diagrammatic approach. In order to show the equivalence of the two approaches explicitly, namely to compare the results from the diagrammatic approach to those obtained in Eq. (4.22), we calculate all three kinds of self-energies in the Keldysh representation.

We start with the contribution from the quark-loop to the gluon self-energy

$$\Pi^{\mu\nu}(P) = -\frac{i}{2} N_f g^2 \int \frac{\mathrm{d}^4K}{(2\pi)^4} \mathrm{Tr}\,[\gamma^\mu S(Q)\gamma^\nu S(K)]\,, \tag{7.16}$$

The calculation is similar to what we did in Sec. 3.3 where the spatial components are considered. Summing the "11" and "12" components of the Keldysh representation leads

[3] This can be seen directly from the bases introduced in Eq. (5.12).

[4] The temporal component of the retarded propagator to order ξ^2, $D^{*L}_{R(2)}$, fails to satisfy such a relation. In fact, it includes a product of $(D_R)^{0\,\mu}\,(\Pi_{R(1)})_{\mu\,\nu}(D^*{}_{R(1)})^{\nu\,0}$, but $(\Pi_{R(1)})^{0\,i}$ is not proportional to p^i. As a result, $\sum \Pi^{0\,i}_{R(1)} D^{*\,i\,0}_{R(1)}$ doesn't give zero automatically. This term will therefore depend on the spatial components of the self-energy and propagator which makes the calculation more complicated.

to

$$\Pi_R^L(P) = -iN_f g^2 \int \frac{\mathrm{d}^4K}{(2\pi)^4}(q_0k_0 + \mathbf{q}\cdot\mathbf{k})\Big[\tilde{\Delta}_F(Q)\tilde{\Delta}_R(K) + \tilde{\Delta}_A(Q)\tilde{\Delta}_F(K) + \tilde{\Delta}_A(Q)\tilde{\Delta}_A(K) + \tilde{\Delta}_R(Q)\tilde{\Delta}_R(K)\Big]. \tag{7.17}$$

The distribution function which appears in the symmetric propagator has the form

$$n(\mathbf{k}) = n_{\mathrm{eq}}(k) - \xi n_{\mathrm{eq}}^2(k)\frac{e^{k/T}}{2k\,T}(\mathbf{k}\cdot\mathbf{n})^2 + \mathcal{O}(\xi^2)\,, \tag{7.18}$$

with $n_{\mathrm{eq}}(k)$ a FERMI-DIRAC function. Again, the last two terms of the integrand vanish after integration over k_0 and the first two terms give the same contributions to the final result. Then,

$$\Pi_R^L(P) = 4\pi N_f g^2 \int \frac{k\mathrm{d}k\mathrm{d}\Omega}{(2\pi)^4} n(\mathbf{k})\Big[(2k^2 - p_0k - \mathbf{k}\cdot\mathbf{p})\frac{1}{P^2 - 2kp_0 + 2\mathbf{k}\cdot\mathbf{p} - i\,\mathrm{sgn}(k-p_0)\epsilon} + (2k^2 + p_0k - \mathbf{k}\cdot\mathbf{p})\frac{1}{P^2 + 2kp_0 + 2\mathbf{k}\cdot\mathbf{p} - i\,\mathrm{sgn}(-k-p_0)\epsilon}\Big]. \tag{7.19}$$

Adopting the HL approximation, we can expand the integrand in the square bracket in powers of the coupling and the leading term

$$\frac{2k^2}{-2kp_0 + 2\mathbf{k}\cdot\mathbf{p} - i\,\epsilon} + \frac{2k^2}{2kp_0 + 2\mathbf{k}\cdot\mathbf{p} + i\,\epsilon}\,, \tag{7.20}$$

vanishes after integrating over $\mathrm{d}\Omega$. The next to leading term comes from the following four terms in the expansion of the integrand in the square bracket

$$\frac{-p_0k - \mathbf{k}\cdot\mathbf{p}}{-2kp_0 + 2\mathbf{k}\cdot\mathbf{p} - i\,\epsilon} + \frac{p_0k - \mathbf{k}\cdot\mathbf{p}}{2kp_0 + 2\mathbf{k}\cdot\mathbf{p} + i\,\epsilon} - \frac{2k^2P^2}{(-2kp_0 + 2\mathbf{k}\cdot\mathbf{p} - i\,\epsilon)^2} - \frac{2k^2P^2}{(2kp_0 + 2\mathbf{k}\cdot\mathbf{p} + i\,\epsilon)^2}\,. \tag{7.21}$$

This is very similar as the calculation of the spatial components. As a result, the *retarded self-energy* can be expressed as

$$\Pi_R^L(P) = \frac{4\pi N_f g^2}{(2\pi)^4}\int k\mathrm{d}k\mathrm{d}\Omega\, n(\mathbf{k})\frac{1 - (\hat{\mathbf{k}}\cdot\hat{\mathbf{p}})^2}{(\hat{\mathbf{k}}\cdot\hat{\mathbf{p}} + \frac{p_0 + i\,\epsilon}{p})^2}\,. \tag{7.22}$$

Note that three-momenta with a hat denote unit vectors.

Using the distribution function (7.18) it is now straightforward to calculate the retarded self-energy:

$$\Pi_R^L(P) = \frac{g^2}{2\pi^2}N_f \sum_{i=0,1}\int_0^\infty k\,\Phi_{(i)}(k)\mathrm{d}k\int_{-1}^1 \Psi_{(i)}(s')\mathrm{d}s'\,, \tag{7.23}$$

with

$$\begin{aligned}
\Phi_{(0)}(k) &= n_{\rm eq}(k)\,, \\
\Phi_{(1)}(k) &= -\xi n_{\rm eq}^2(k)\,\frac{e^{k/T}k}{2T}\,, \\
\Psi_{(0)}(s') &= \frac{1-s'^2}{(s'+\frac{p_0+i\epsilon}{p})^2}\,, \\
\Psi_{(1)}(s') &= \cos^2\theta_n\,\frac{s'^2(1-s'^2)}{(s'+\frac{p_0+i\epsilon}{p})^2} + \frac{\sin^2\theta_n}{2}\,\frac{(1-s'^2)^2}{(s'+\frac{p_0+i\epsilon}{p})^2}\,.
\end{aligned} \tag{7.24}$$

Here, θ_n is the angle between $\mathbf{n}$ and $\mathbf{p}$ and $s' \equiv \hat{\mathbf{k}}\cdot\hat{\mathbf{p}}$. This integral can be performed analytically and the leading contribution for the isotropic term is

$$\begin{aligned}
\Pi^L_{R(0)}(P) &= \frac{g^2}{2\pi^2}N_f\int_0^\infty k\,\Phi_{(0)}(k)\mathrm{d}k\int_{-1}^1\Psi_{(0)}(s')\mathrm{d}'s \\
&= N_f\frac{g^2T^2}{6}\left(\frac{p_0}{2p}\ln\frac{p_0+p+i\epsilon}{p_0-p+i\epsilon}-1\right)\,.
\end{aligned} \tag{7.25}$$

To linear order in ξ, the result is

$$\begin{aligned}
&\Pi^L_{R(1)}(P) = \frac{g^2}{2\pi^2}N_f\int_0^\infty k\,\Phi_{(1)}(k)\mathrm{d}k\int_{-1}^1\Psi_{(1)}(s')\mathrm{d}s' \\
&= N_f\frac{g^2T^2}{6}\left(\frac{1}{6}+\frac{\cos(2\theta_n)}{2}\right)+\Pi^L_{R(0)}(P)\left[\cos(2\theta_n)-\frac{p_0^2}{2p^2}(1+3\cos(2\theta_n))\right]\,.
\end{aligned} \tag{7.26}$$

In the hard-loop limit the gluon-loop contributions to the gluon self-energy have the same structure as the one due to a quark-loop. For the same reason, the gluon self-energy in the hard-loop approximation is gauge invariant. We can simply replace $N_f\frac{g^2T^2}{6}$ by m_D^2 to generalize the QED result to QCD. In the following, the DEBYE mass m_D^2 is to be understood as what we defined in Eq. (4.8), namely

$$m_D^2 = -\frac{g^2}{2\pi^2}\int_0^\infty \mathrm{d}k\,k^2\,\frac{\mathrm{d}f_{\rm iso}(k)}{\mathrm{d}k}\,. \tag{7.27}$$

This is independent of ξ as all viscous corrections shall be written explicitly. The isotropic distribution function $f_{\rm iso}$ in our case is just a sum of the FERMI-DIRAC and BOSE-EINSTEIN distributions (with appropriate pre-factors counting the number of degrees of freedom [60]). For N_f massless quark flavors and N_c colors,

$$m_D^2 = \frac{g^2T^2}{6}(N_f+2N_c)\,. \tag{7.28}$$

Analogously, the *advanced self-energy* is given by

$$\Pi^L_{A(0)}(P) = m_D^2\left(\frac{p_0}{2p}\ln\frac{p_0+p-i\epsilon}{p_0-p-i\epsilon}-1\right)\,, \tag{7.29}$$

and

$$\Pi^L_{A(1)}(P) = m_D^2 \left(\frac{1}{6} + \frac{\cos(2\theta_n)}{2}\right) + \Pi^L_{A(0)}(P) \left[\cos(2\theta_n) - \frac{p_0^2}{2p^2}\left(1 + 3\cos(2\theta_n)\right)\right] . \quad (7.30)$$

Note that the above results coincide with those obtained in Eq. (4.22).

Using Eqs. (7.9) and (7.14), it is straightforward to obtain the temporal component of the *retarded propagator* in COULOMB gauge

$$D^{*L}_{R(0)} = \left(p^2 - m_D^2(\frac{p_0}{2p}\ln\frac{p_0+p+i\epsilon}{p_0-p+i\epsilon} - 1)\right)^{-1} , \quad (7.31)$$

$$D^{*L}_{R(1)} = \frac{m_D^2(\frac{1}{6} + \frac{\cos(2\theta_n)}{2}) + \Pi^L_{R(0)}[\cos(2\theta_n) - \frac{p_0^2}{2p^2}(1 + 3\cos(2\theta_n))]}{(p^2 - m_D^2(\frac{p_0}{2p}\ln\frac{p_0+p+i\epsilon}{p_0-p+i\epsilon} - 1))^2} . \quad (7.32)$$

Similar results can be obtained for the *advanced propagator*. Again, these results are identical to the ones obtained within the transport theory approach.

Next we calculate the *symmetric self-energy*, Π^L_F within the HL approximation. Eq. (7.6) shows that this quantity is necessary to obtain the resummed symmetric propagator out of equilibrium. Summing the "11" and "22" components of the KELDYSH representation, we obtain

$$\begin{aligned}\Pi^L_F(P) &= -iN_f g^2 \int \frac{\mathrm{d}^4K}{(2\pi)^4}(q_0k_0 + \mathbf{q}\cdot\mathbf{k})\Big[\tilde\Delta_F(Q)\tilde\Delta_F(K) - (\tilde\Delta_R(Q) - \tilde\Delta_A(Q)) \\ &\quad \times(\tilde\Delta_R(K) - \tilde\Delta_A(K))\Big] . \end{aligned} \quad (7.33)$$

Using $\tilde\Delta_R(Q) - \tilde\Delta_A(Q) = -2\pi i\,\mathrm{sgn}(q_0)\delta(Q^2)$ and the HL approximation, we find that the symmetric self-energy can be expressed as

$$\Pi^L_F(P) = 4iN_f g^2\pi^2 \int \frac{k^2\mathrm{d}k\mathrm{d}\Omega}{(2\pi)^4} n(\mathbf{k})(n(\mathbf{k}) - 1)\frac{2}{p}\Big[\delta(s + \frac{p_0}{p}) + \delta(s - \frac{p_0}{p})\Big] . \quad (7.34)$$

Again, we can expand the anisotropic distribution function to order ξ and finally arrive at

$$\begin{aligned}\Pi^L_{F(0)}(P) &= -2\pi i\, m_D^2 \frac{T}{p}\Theta(p^2 - p_0^2) , \\ \Pi^L_{F(1)}(P) &= \frac{3}{2}\pi i\, m_D^2 \frac{T}{p}\left(\sin^2\theta_n + (3\cos^2\theta_n - 1)\frac{p_0^2}{p^2}\right)\Theta(p^2 - p_0^2) . \end{aligned} \quad (7.35)$$

Next, we can calculate the *symmetric propagator*. We first consider the isotropic case with $\xi = 0$ and perform a TAYLOR expansion assuming $p_0 \to 0$:

$$D^{*L}_{R(0)}(P) - D^{*L}_{A(0)}(P) = \frac{m_D^2}{2p}\frac{-2\pi i}{(p^2 + m_D^2)^2}\, p_0 , \quad (7.36)$$

which follows from

$$\lim_{p_0\to 0}(\ln\frac{p_0 + p + i\,\epsilon}{p_0 - p + i\,\epsilon} - \ln\frac{p_0 + p - i\,\epsilon}{p_0 - p - i\,\epsilon}) = -2\pi i . \quad (7.37)$$

Similarly, when p_0 is small, the distribution function of thermal gluons is

$$(1+2N_{\rm eq}(p))\,{\rm sgn}(p_0) = \frac{2T}{p_0}\,, \tag{7.38}$$

where the on-shell condition was used.

In the above equation, terms that do not contribute to the symmetric propagator in the static limit have been neglected. Finally, we can determine the temporal component of the symmetric propagator explicitly in the isotropic limit:

$$D^{*L}_{F(0)}(p_0=0) = -\frac{2\pi i T m_D^2}{p\,(p^2+m_D^2)^2}\,. \tag{7.39}$$

We now consider the contribution to order ξ. From Eq. (7.15), the gluon distribution function can be expanded as

$$N(\mathbf{p}) = N_{(0)} + \xi N_{(1)} = \frac{T}{|p_0|} - \frac{T\cos^2\theta_n}{2|p_0|}\xi\,. \tag{7.40}$$

The calculation is similar to the isotropic case. In addition, we need the following TAYLOR expansion to linear order in p_0:

$$\begin{aligned} D^{*L}_{R(1)}(P) - D^{*L}_{A(1)}(P) &= -2\pi i\left[\frac{m_D^4(1-3\cos(2\theta_n))}{6p(p^2+m_D^2)^3} + \frac{m_D^2\cos(2\theta_n)}{2p(p^2+m_D^2)^2}\right] p_0\,, \\ \Pi^{*L}_{R(1)}(P) - \Pi^{*L}_{A(1)}(P) &= \frac{-\pi i m_D^2\cos(2\theta_n)}{p}\,p_0\,. \end{aligned} \tag{7.41}$$

Now the $\mathcal{O}(\xi)$ term of the symmetric propagator in the static limit can be derived from the above equations

$$D^{*L}_{F(1)}(p_0=0) = \frac{3\pi i T m_D^2}{2p\,(p^2+m_D^2)^2}\sin^2\theta_n - \frac{4\pi i T m_D^4}{p\,(p^2+m_D^2)^3}(\sin^2\theta_n - \frac{1}{3})\,. \tag{7.42}$$

7.3 Quarkonium decay width in a QCD plasma with small anisotropy

In the real time formalism, the static heavy-quark potential due to one-gluon exchange can be determined through the FOURIER transform of the physical "11" component of the gluon propagator in the static limit [5]:

$$\begin{aligned} V(\mathbf{r},\xi) &= -g^2C_F\int\frac{{\rm d}^3\mathbf{p}}{(2\pi)^3}\,(e^{i\mathbf{p}\cdot\mathbf{r}}-1)\left(D^{*L}(p_0=0,\mathbf{p},\xi)\right)_{11} \\ &= -g^2C_F\int\frac{{\rm d}^3\mathbf{p}}{(2\pi)^3}\,(e^{i\mathbf{p}\cdot\mathbf{r}}-1)\frac{1}{2}\left(D^{*L}_R + D^{*L}_A + D^{*L}_F\right) \\ &= -g^2C_F\int\frac{{\rm d}^3\mathbf{p}}{(2\pi)^3}\,(e^{i\mathbf{p}\cdot\mathbf{r}}-1)\frac{1}{2}\left(D^{*L}_R + D^{*L}_A\right) \\ &- g^2C_F\int\frac{{\rm d}^3\mathbf{p}}{(2\pi)^3}\,(e^{i\mathbf{p}\cdot\mathbf{r}}-1)\frac{1}{2}D^{*L}_F\,. \end{aligned} \tag{7.43}$$

[5] This is a general definition in real time formalism. Before, we used the retarded propagator to define the potential which only gives the real part.

In the above equation, we have also introduced an $\mathbf{r}$ independent term which can be considered as the perturbative free energy of quarkonium at infinite separation (twice the free energy of a single heavy quark). In the static limit, $\frac{1}{2}\left(D^{*L}_R + D^{*L}_A\right) = D^{*L}_R = D^{*L}_A$. The FOURIER transform of this quantity gives the real part of the potential which determines the quarkonium binding energies [6]. Using Eqs. (5.45) and (6.14), the *real part of the potential* can be expressed as

$$\mathbf{Re}V_{(0)}(\mathbf{r},\xi=0) = -g^2 C_F \int \frac{\mathrm{d}^3\mathbf{p}}{(2\pi)^3}\frac{e^{i\mathbf{p}\cdot\mathbf{r}}-1}{p^2+m_D^2} = -\frac{g^2 C_F}{4\pi}\left[m_D + \frac{e^{-\hat{r}}}{r}\right], \tag{7.44}$$

and

$$\begin{aligned}\mathbf{Re}\,\xi V_{(1)}(\mathbf{r},\xi) &= -g^2 C_F\,\xi m_D^2 \int \frac{\mathrm{d}^3\mathbf{p}}{(2\pi)^3}\,(e^{i\mathbf{p}\cdot\mathbf{r}}-1)\,\frac{\frac{2}{3}-(\mathbf{p}\cdot\mathbf{n})^2/p^2}{(p^2+m_D^2)^2} \\ &= \xi\frac{g^2 C_F}{4\pi}\left[\frac{m_D}{6}+\frac{e^{-\hat{r}}}{r}\mathcal{F}(\hat{r},\theta)\right].\end{aligned} \tag{7.45}$$

In the above equation, the function $\mathcal{F}$ is defined in Eq. (5.46).

Here, we instead consider the *imaginary part of the potential* which comes from the FOURIER transform of the symmetric propagator. From Eqs. (7.39) and (7.42), the isotropic contribution is given by

$$\mathbf{Im}\ V_{(0)}(r) = -g^2 C_F \int \frac{\mathrm{d}^3\mathbf{p}}{(2\pi)^3}(e^{i\mathbf{p}\cdot\mathbf{r}}-1)\frac{-\pi T m_D^2}{p\,(p^2+m_D^2)^2} = -\frac{g^2 C_F T}{4\pi}\,\phi(\hat{r}), \tag{7.46}$$

with

$$\phi(\hat{r}) = 2\int_0^\infty dz \frac{z}{(z^2+1)^2}\left[1-\frac{\sin(z\,\hat{r})}{z\,\hat{r}}\right], \tag{7.47}$$

and $\hat{r}\equiv r\,m_D$. This result has been derived before in Refs. [48, 126]. The term of order ξ can be expressed as

$$\begin{aligned}\mathbf{Im}\ \xi V_{(1)}(\mathbf{r}) &= -g^2 C_F\,\xi \int \frac{\mathrm{d}^3\mathbf{p}}{(2\pi)^3}\,(e^{i\mathbf{p}\cdot\mathbf{r}}-1) \\ &\times \left[\frac{3\pi T m_D^2}{4p\,(p^2+m_D^2)^2}\sin^2\theta_n - \frac{2\pi T m_D^4}{p\,(p^2+m_D^2)^3}(\sin^2\theta_n - \frac{1}{3})\right] \\ &= \frac{g^2 C_F \xi T}{4\pi}\left[\psi_1(\hat{r},\theta)+\psi_2(\hat{r},\theta)\right],\end{aligned} \tag{7.48}$$

where θ is the angle between $\mathbf{r}$ and $\mathbf{n}$ and

$$\psi_1(\hat{r},\theta) = \int_0^\infty \mathrm{d}z \frac{z}{(z^2+1)^2}\left(1-\frac{3}{2}\left[\sin^2\theta\frac{\sin(z\,\hat{r})}{z\,\hat{r}}+(1-3\cos^2\theta)G(\hat{r},z)\right]\right), \tag{7.49}$$

[6] In fact, the real part of Eq. (7.43) should be identified with the free energy of the $Q\bar{Q}$ pair rather than the potential. This contains an entropy contribution at $r\to\infty$ which should be removed. Lattice measurements indicate that the remainder behaves approximately like $V_\infty \simeq a/T$, with $a>0$ a constant of dimension two (see Ref. [123] and references therein) but this contribution can not be obtained from perturbation theory since T is the only scale. In the relevant range of quark masses and temperature, $M_Q < 5$ GeV, $T < 500$ MeV, the temperature (and viscosity) dependence of the binding energies is dominantly due to $V_\infty(T)$ [129].

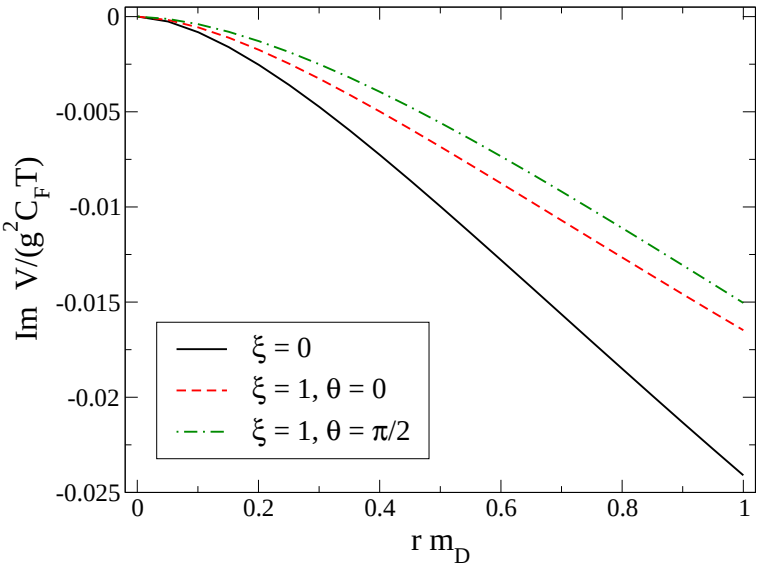

Figure 7.1: Imaginary part of the static potential as a function of distance ($\hat{r} \equiv r\, m_D$). The vertical axis is Im $V/(g^2 C_F T)$. The curves, from bottom to top, correspond to an anisotropy of $\xi = 0$ and $\xi = 1$, $\theta = 0$, $\theta = \pi/2$.

$$\begin{aligned} \psi_2(\hat{r},\theta) &= -\int_0^\infty \mathrm{d}z \frac{\frac{4}{3}z}{(z^2+1)^3} \\ &\times \left(1 - 3\left[\left(\frac{2}{3} - \cos^2\theta\right)\frac{\sin(z\,\hat{r})}{z\,\hat{r}} + (1-3\cos^2\theta)G(\hat{r},z)\right]\right), \end{aligned} \tag{7.50}$$

with

$$G(\hat{r},z) = \frac{\hat{r}z\cos(\hat{r}z) - \sin(\hat{r}z)}{(\hat{r}z)^3}\,. \tag{7.51}$$

The result is shown in Fig. 7.1. The imaginary part decreases with ξ (or with the viscosity, respectively). When $\hat{r}$ is small, we can expand the potential. This is relevant for bound states of very heavy quarks whose Bohr radii $\sim 1/(g^2 M_Q)$ are smaller than the Debye length $1/m_D$. For the imaginary part, at leading order, the corresponding functions take the following forms:

$$\begin{aligned} \phi(\hat{r}) &= -\frac{1}{9}\,\hat{r}^2(-4 + 3\gamma_E + 3\ln\hat{r})\,, \\ \psi_1(\hat{r},\theta) &= \frac{1}{600}\,\hat{r}^2[123 - 90\gamma_E - 90\ln\hat{r} + \cos(2\theta)(-31 + 30\gamma_E + 30\ln\hat{r})]\,, \\ \psi_2(\hat{r},\theta) &= \frac{1}{90}\,\hat{r}^2(-4 + 3\cos(2\theta))\,, \end{aligned} \tag{7.52}$$

where γ_E is the Euler-Gamma constant. At leading logarithmic order then

$$\mathbf{Im}\; V(\mathbf{r},\xi) = -\frac{g^2 C_F T}{4\pi}\,\hat{r}^2\,\ln\frac{1}{\hat{r}}\left(\frac{1}{3} - \xi\frac{3-\cos(2\theta)}{20}\right). \tag{7.53}$$

Treating the imaginary part of the potential as a perturbation of the vacuum COULOMB potential provides an estimate for the *decay width*,

$$\begin{aligned}\Gamma &= \frac{g^2 C_F T}{4\pi} \int \mathrm{d}^3\mathbf{r}\ |\Psi(r)|^2\ \hat{r}^2 \ln\frac{1}{\hat{r}} \left(\frac{1}{3} - \xi\frac{3-\cos(2\theta)}{20}\right) \\ &= \frac{16\pi T}{g^2 C_F}\frac{m_D^2}{M_Q^2}\left(1-\frac{\xi}{2}\right)\ln\frac{g^2 C_F M_Q}{8\pi m_D}\,. \end{aligned} \tag{7.54}$$

Here, M_Q is the quark mass and $\Psi(r)$ is the ground state COULOMB wave-function. Thus, at leading order in the deviation from equilibrium (i.e., viscosity) the quarkonium decay width is smaller. For a moderate anisotropy $\xi \simeq 1$, Γ decreases by about 50% as compared to an ideal, fully equilibrated plasma.

Finally, we should mention that the imaginary part of the heavy-quark potential at non-zero plasma anisotropy is also considered in Ref. [144]. The authors point out that the $\mathcal{O}(\xi)$ correction contributes already at leading non-trivial order to the quarkonium decay width, which agrees with our finding. Their result differs from ours numerically but can be reproduced if the second contribution on the right-hand side of Eq. (7.6) is omitted. From private communication with M. LAINE, this appears to be due to a different setup of the non-equilibrium system: Ref. [144] considers a situation where the soft gluons are in equilibrium at a temperature T while the hard gluons are out of equilibrium and are characterized by a different hard scale T'. In contrast, we assume that the deviation from equilibrium follows viscous hydrodynamics, Eq. (7.1).

8 Conclusions and outlook

In this work, we have investigated the properties of quarkonium states in an anisotropic quark-gluon plasma. The anisotropy was considered as an important feature of the quark-gluon plasma as created in heavy-ion collisions. The different expansion rate in the longitudinal and transverse directions causes a local anisotropy of the plasma in momentum space. We concentrated particularly on the comparison between our results and those in an isotropic thermal medium which is the only case addressed before.

Due to the large mass of the heavy quark, the non-relativistic limit was considered and a quantum mechanical description of the quarkonium bound states becomes feasible. One can determine the binding energies of these bound states by solving the three-dimensional SCHRÖDINGER equation with some specified potential model which describes the force between a quark and anti-quark. Employing a specific anisotropic distribution function, we studied the perturbative heavy-quark potential in an anisotropic quark-gluon plasma. The leading-order potential arises due to one-gluon exchange which can be defined through the FOURIER transform of the gluon propagator in the static limit.

We found that in an anisotropic plasma the screening effect is reduced; the potential between the quark and anti-quark is deeper as compared to that in an isotropic plasma. As the anisotropy parameter ξ is increasing, the potential becomes closer to the vacuum COULOMB potential which indicates the quarkonium states are bound more strongly in an anisotropic plasma. This is caused partly by the lower density of the anisotropic plasma. When the distance between the quark and anti-quark is very small, the potential approaches to the vacuum COULOMB potential; while when $\hat{r} \equiv r m_D \sim 1$, the medium effect becomes important.

Another important feature of the potential in an anisotropic plasma is the appearance of the angular dependence. The potential depends on the angle θ between the quark pair separation $\mathbf{r}$ and the direction of anisotropy $\mathbf{n}$. Such an angular dependence disappears more rapidly at small $\hat{r}$, while at relatively large $\hat{r}$, we found that the effect of anisotropy becomes most important when $\mathbf{r}$ is parallel to $\mathbf{n}$. This implies that there is stronger attraction on distance scales on the order of the inverse DEBYE mass for quark pairs aligned along the direction of anisotropy than for transverse alignment. For other θ between 0 and $\pi/2$, the anisotropic effect is expected to be smaller than the special case where $\mathbf{r} \parallel \mathbf{n}$ but larger than the other one where $\mathbf{r} \perp \mathbf{n}$.

We extended our investigation to the properties of charmonium and bottomonium which are of particular interest for us. However, in this case, it is insufficient to consider only the (screened) COULOMB part of the potential which arises from one-gluon exchange. Rather, one should then sum the medium-dependent contributions due to one-gluon exchange and due to the string. We generalized the phenomenological potential model introduced by KARSCH, MEHR and SATZ to the anisotropic case. The original KMS potential model assumes that the very same screening scale m_D which emerges in the DEBYE-COULOMB potential also appears in the non-perturbative, long-distance contribution due to the string.

We took over this assumption to anisotropic plasmas and replaced the general isotropic DEBYE mass by the anisotropic one which is determined effectively from the one-gluon exchange potential.

Solving the three-dimensional SCHRÖDINGER equation, we found that the binding energy decreases as the screening mass $m_D(T)$ increases with temperature T. Our results also indicate that $|E_{\mathrm{bind}}|$ increases with the anisotropy ξ. For moderate anisotropies $\xi \simeq 1$, the binding energy of the bottomonium ground state increases by about 30% near the critical temperature $T_c \simeq 192$ MeV as compared to the isotropic case, that of $1S$ charmonium and of $1P$ bottomonium by 50%. Thus, such quarkonium states may exist up to somewhat higher temperatures than in case of an isotropic, perfectly equilibrated medium.

The decrease of $|E_{\mathrm{bind}}|$ with T is due to two effects: First, the continuum threshold $V_\infty(T)$ decreases approximately like $\sim 1/T$. The energy gap between the bound state and the continuum, which is the binding energy, therefore decreases, too. Actually, this is the dominant effect on the $1S$ ground state of bottomonium whose wave-function is rather insensitive to the presence of the medium. The state is too small to be affected strongly by screening. Hence, the Υ peak in the dilepton invariant mass distribution may not experience a large shift although one should expect substantial broadening near the dissociation temperature. Larger states such as the $1S$ ground state of charmonium and the $1P$ excited state of bottomonium, however, may also experience some modifications due to screening. The root-mean-square radii of these states increase rather rapidly with T around the dissociation point $|E_{\mathrm{bind}}| \sim T$.

The other important new effect identified here is that the angular dependence of the inter-quark potential in an anisotropic medium induces a polarization of states with non-zero angular momentum. According to our estimates, the splitting of the χ_b with $L_z = 0$ and $L_z = \pm 1$, respectively, is on the order of 50 MeV. At $T \simeq 200$ MeV, the population of the state with $L_z = 0$ is BOLTZMANN-enhanced by about 30% as compared to the states with angular momentum along the direction of anisotropy, respectively. The experimental confirmation of such a polarization at RHIC or LHC may provide first evidence for a non-zero viscosity of QCD near T_c.

Furthermore, we studied the decay width of the bound states in an anisotropic QCD plasma. Using hard-loop approximation in the weak-coupling limit, we found that the imaginary part of the heavy-quark potential is smaller (in magnitude) than at vanishing viscosity. This implies a smaller decay width of quarkonium bound states in an anisotropic plasma.

In order to get a better understanding of the properties of quarkonium states in the medium, further work is needed. Potential models utilize a set of potentials between the lower and upper limit constrained by lattice free energy and internal energy. A quantitative difference appears in different models. Due to the uncertainty in the potential model, the effective field theories from QCD at finite temperature are expected to give the exact determination of quarkonium properties.

Based on the generalized KMS potential model, our work presented here is only a very rough estimate of the properties of quarkonium states in an anisotropic plasma. Theoretically, we can use the perturbative QCD to determine the potential or free energy at short distances. However, the long-distance behavior of the potential is not accessible by this approach. Both perturbative QCD (at leading order) as well as exactly conformal gauge theories obtained using AdS/CFT, can only generate a pure entropy contribution to the

free energy of the $Q\bar{Q}$ pair at infinite separation, and so $V_\infty = 0$ in both cases. The non-perturbative contribution at infinite separation, especially in the anisotropic case is still not clear which also needs to be investigated in the future.

Furthermore, we estimated the dissociation of a bound state by comparing the binding energy with the temperature. Actually, this is only for a qualitative purpose. We studied perturbatively the decay width of the quarkonium bound states. However, for quarkonium sizes realized in nature the validity of the perturbative calculations is not reliable. There are also additional contributions to the width, for example, from collisional broadening. It is rather difficult to get a quantitatively precise decay width.

All of the above discussions refer to quarkonium at rest. Finite momentum calculations are necessary for the quantitative results. It is expected that a moving quarkonium dissociates faster [33].

To study the physical phenomena in an anisotropic quark-gluon plasma is actually a very interesting topic. Besides the instabilities and quarkonium bound states mentioned here, the calculation of the dilepton production in an anisotropic QCD plasma was performed recently [145, 146]. It was shown that high-energy dilepton production is sensitive to the plasma isotropization time, and can therefore be used to experimentally determine the time of onset for hydrodynamic expansion of a quark-gluon plasma and the magnitude of expected early-time momentum-space anisotropies. Other phenomena, for example, the jet energy loss in an hot QCD plasma with local momentum anisotropy, are also worthwhile to investigate in the future.

Appendices

A Notation and conventions

We summarize in this appendix the notation and conventions which we use in this dissertation.

- Natural units:

  $\hbar = c = 1\,.$

  In this system, $[\text{length}] = [\text{time}] = [\text{energy}]^{-1} = [\text{mass}]^{-1}\,.$

- Metrics:

  In Minkowski space:

  $g^{\mu\nu} = g_{\mu\nu} = \text{diag}(1,-1,-1,-1)\ ,$ with $\mu,\nu = 0,1,2,3.$

  In Euclidean space:

  $\delta^{\mu\nu} = \text{diag}(1,1,1,1)\ ,$ with $\mu,\nu = 1,2,3,4.$

- Four-vectors: Indicated by Greek indices.

  In Minkowski space:

  $$\begin{aligned} X^\mu &= (x^0,x^1,x^2,x^3) = (t,\mathbf{x})\,, & X_\mu &= (t,-\mathbf{x})\,,\\ K^\mu &= (k^0,k^1,k^2,k^3) = (E_k,\mathbf{k})\,, & K_\mu &= (E_k,-\mathbf{k})\,. \end{aligned}$$

  In Euclidean space:

  $$\begin{aligned} \tilde{X}^\mu &= (x^4,x^1,x^2,x^3) = (\tau,\mathbf{x})\,, & \tilde{X}^\mu &= \tilde{X}_\mu\,,\\ \tilde{K}^\mu &= (k^4,k^1,k^2,k^3) = (-\tilde{E}_k,\mathbf{k})\,, & \tilde{K}^\mu &= \tilde{K}_\mu\,. \end{aligned}$$

- Scalar product:

  In Minkowski space:

  $$\begin{aligned} K\cdot X &= g_{\mu\nu}K^\mu X^\nu = E_k t - \mathbf{k}\cdot\mathbf{x}\,,\\ K^2 &= K^\mu K_\mu = E_k^2 - k^2\,, & &\text{with}\ \ k\equiv|\mathbf{k}|\,. \end{aligned}$$

  In Euclidean space:

  $$\begin{aligned} \tilde{K}\cdot\tilde{X} &= -\tilde{E}_k\tau + \mathbf{k}\cdot\mathbf{x}\,,\\ \tilde{K}^2 &= \tilde{E}_k^2 + k^2\,, & &\text{with}\ \ k\equiv|\mathbf{k}|\,. \end{aligned}$$

- From Euclidean to Minkowski space:

  Metric tensor: $\delta^{\mu\nu} \to -g^{\mu\nu}$.

  Fourth components: $x_4 \to ix_0$, $\quad k_4 = -\tilde{E}_k \to ik_0$.

  Scalar product: $\tilde{K}^2 = -K^2$.

- Three-vectors: Indicated by lowercase Latin characters.

  Upper Latin indices like i, j, k use a Euclidean three-metric, e.g.

$$\mathbf{k} = k^i \,, \qquad k^i k^i = \mathbf{k}^2 \,.$$

- FOURIER transform in Minkowski space:

$$\begin{aligned} j^\mu(K) &= \int \mathrm{d}^4 X e^{iK\cdot X} j^\mu(X) \,, \\ j^\mu(X) &= \int \frac{\mathrm{d}^4 K}{(2\pi)^4} e^{-iK\cdot X} j^\mu(K) \,, \\ K_\mu &= i\partial_\mu \,. \end{aligned}$$

B Perturbative heavy-quark free energy in small anisotropy expansion

We define the dimensionless free energy as $\hat{F}_Q \equiv 8\pi F_Q/(g^2 C_F m_D)$, which is given by

$$\hat{F}_Q = \frac{1}{2\pi^2}\int \mathrm{d}\hat{k}\,\mathrm{d}y\mathrm{d}\phi\;(G_1+G_2)\;, \tag{B.1}$$

where

$$G_1 = \frac{m_\alpha^2+m_\gamma^2-m_+^2}{m_+^2-m_-^2}\frac{m_+^2}{\hat{k}^2+m_+^2} \quad , \quad G_2 = \frac{m_-^2-m_\alpha^2-m_\gamma^2}{m_+^2-m_-^2}\frac{m_-^2}{\hat{k}^2+m_-^2}\;, \tag{B.2}$$

and the dimensionless momentum $\hat{k}$ is defined as $\hat{k} \equiv |\mathbf{k}|/m_D$.

The dimensionless "masses" can be expressed in the form [1]

$$\begin{aligned}
m_\alpha^2 &= -\frac{1}{2(1-y^2)\sqrt{\xi}}\left(y^2\mathrm{arctan}\sqrt{\xi}-\frac{y}{\sqrt{1+\xi-\xi y^2}}\mathrm{arctan}\frac{\sqrt{\xi}y}{\sqrt{1+\xi-\xi y^2}}\right)\;,\\
m_\beta^2 &= \frac{(\sqrt{\xi}+(1+\xi)\mathrm{arctan}\sqrt{\xi})(1+\xi-\xi y^2)+\xi\left(y^2\sqrt{\xi}+\frac{y(1+\xi)}{\sqrt{1+\xi-\xi y^2}}\mathrm{arctan}\frac{\sqrt{\xi}y}{\sqrt{1+\xi-\xi y^2}}\right)}{2\sqrt{\xi}(1+\xi)(1+\xi-\xi y^2)}\;,\\
m_\gamma^2 &= \frac{(1+y^2)\mathrm{arctan}\sqrt{\xi}}{2(1-y^2)\sqrt{\xi}}-\frac{1}{2(\xi-\xi y^2+1)}-\frac{y(\frac{2}{1-y^2}+3\xi)}{2\sqrt{\xi}(1+\xi-\xi y^2)^{\frac{3}{2}}}\mathrm{arctan}\frac{\sqrt{\xi}y}{\sqrt{1+\xi-\xi y^2}}\;,\\
m_\delta^4 &= \frac{\pi^2\xi^2y^2(1-y^2)}{16(1+\xi-\xi y^2)^3}\;,
\end{aligned} \tag{B.3}$$

where y denotes the cosine of the angle between $\mathbf{k}$ and $\mathbf{n}$. m_+^2 and m_-^2 are given by

$$\begin{aligned}
2m_\pm^2 &= M^2 \pm \sqrt{M^4-4(m_\beta^2(m_\alpha^2+m_\gamma^2)-m_\delta^4)}\;,\\
M^2 &= m_\alpha^2+m_\beta^2+m_\gamma^2\;.
\end{aligned} \tag{B.4}$$

Note that m_+^2 is positive and the contribution to $\hat{F}_Q$ from G_1 is therefore given by

$$\hat{F}_{Q1} = \frac{1}{2}\int_0^1 \mathrm{d}y\, m_+\frac{m_\alpha^2+m_\gamma^2-m_+^2}{m_+^2-m_-^2}\;. \tag{B.5}$$

This integrand can now be expanded in powers of ξ, only integer powers appear.

[1] They can be easily obtained from Eq. (4.20). They differ from those defined in Eq. (4.20) by a factor of m_D^2. However, we still use the same notations to denote them.

On the other hand, m_-^2 is not positive definite which signals the presence of unstable modes of the gauge field [60]. To proceed, we divide the area of the y-ϕ plane into two parts: $\mathcal{A}_+$ denotes the region where m_-^2 is positive and $\mathcal{A}_-$ is the complement. The latter does not contribute [2] to $\hat{F}_Q$ while the former gives

$$\hat{F}_{Q2+} = \frac{1}{2}\int_{\mathcal{A}_+(\xi)} \mathrm{d}y\, m_- \frac{m_-^2 - m_\alpha^2 - m_\gamma^2}{m_+^2 - m_-^2} = \mathbf{Re}\int_0^1 \mathrm{d}y \sqrt{m_-^2}\, \frac{m_-^2 - m_\alpha^2 - m_\gamma^2}{m_+^2 - m_-^2}\,. \tag{B.6}$$

This integrand is not analytic in ξ; the leading "anomalous" contribution appears at order $\xi^{5/2}$, given by

$$\hat{F}_{Q\mathrm{anom}} = -\frac{\pi^2}{16\sqrt{3}}\,\xi^{5/2}\,\mathbf{Re}\int_0^1 \mathrm{d}y\, \left[y^2\sqrt{1-2y^2}(y^2-1)\right] + \ldots \approx 0.0185\,\xi^{5/2} + \ldots\,. \tag{B.7}$$

Such a contribution of order $\xi^{5/2}$ also appears in the FOURIER transform of the static propagator, i.e. in the potential.

[2] The same is not true for the potential.

C A model of the heavy-quark potential for general anisotropy

Considering small anisotropies, up to leading order in ξ [1], an analytical expression of the heavy-quark potential can be obtained. In general, we can only evaluate the potential numerically. For the convenience of further studies, in this appendix, we will introduce a toy model which can describe the potential even for large anisotropies. We assume that the heavy-quark potential in an anisotropic QCD plasma retains the form as the DEBYE screened potential in an isotropic medium, namely,

$$V(\mathbf{r},\xi) = -\frac{g^2 C_F}{4\pi r}\, e^{-r\mu}\,, \tag{C.1}$$

where the screening mass $\mu(\theta;\xi,T)$ in an anisotropic medium now depends not only on the temperature T but also on the anisotropy parameter ξ and the angle between $\mathbf{r}$ and $\mathbf{n}$. With this assumption, the anisotropy effects appear only in the screening mass. For convenience, we introduce a dimensionless screening mass $\bar{\mu}$ which is defined as

$$\mu = m_D \bar{\mu}\,. \tag{C.2}$$

We use the following model to describe the behavior of the potential in two special cases. Firstly, when the separation of $Q\bar{Q}$ is parallel to direction of anisotropy, we assume

$$\bar{\mu} = \frac{1}{(1+1.85\,\xi^{1.27})^{0.20}}\,, \tag{C.3}$$

while for the other case, where $\mathbf{r}$ is perpendicular to $\mathbf{n}$, we assume

$$\bar{\mu} = \frac{1}{(1+0.74\,\xi^{1.20})^{0.23}}\,. \tag{C.4}$$

With the above assumptions, we can easily check that when $\xi = 0$, we have $\bar{\mu} = 1$ which coincides with the DEBYE screened potential. The vacuum COULOMB potential appears at infinitely large anisotropy since $\bar{\mu} \to 0$ as $\xi \to \infty$. For a finite $\xi > 0$, the anisotropic screening mass is always less than the isotropic DEBYE mass m_D which means the screening is reduced in an anisotropic plasma.

Actually, the above assumptions give a very accurate description of the potential. We compare the model with our numerical results for different anisotropies. The comparison for the case where $\mathbf{r}$ is parallel to $\mathbf{n}$ is shown in Fig. C.1. Similarly, for $\mathbf{r}$ being perpendicular to $\mathbf{n}$, the results are given in Fig. C.2. In both cases, our model works very well as one can see from the figures.

[1] In fact, we can still calculate the potential at the order of ξ^2. However, beyond this order, a fractional power of ξ appears and the general TAYLOR expansion doesn't work.

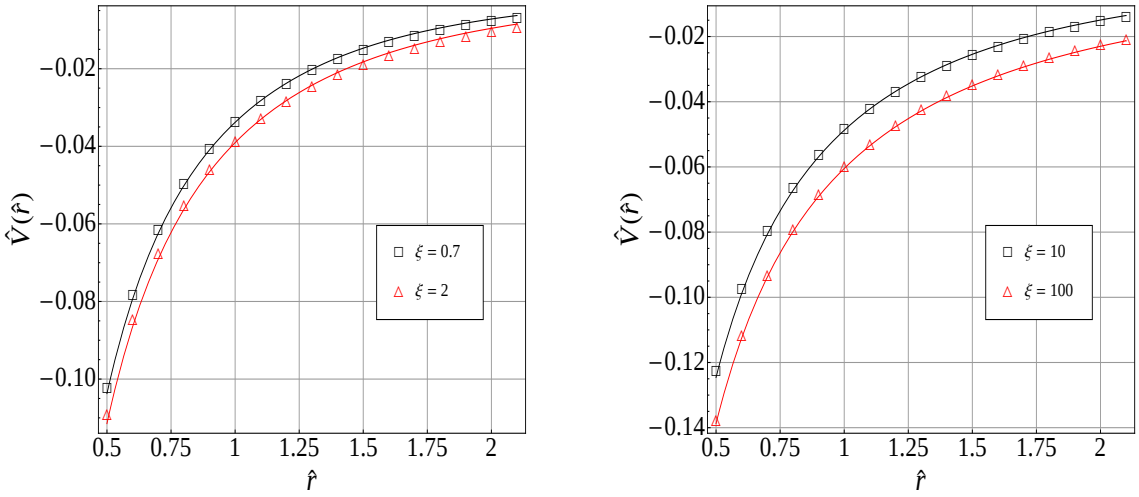

Figure C.1: Comparison of $\hat{V}$ as a function of $\hat{r}$ between numerical results and our model for different values of ξ. In the plots, we show the case where $\mathbf{r}$ is parallel to $\mathbf{n}$. The symbols indicate the data obtained from numerical calculations and the solid lines indicate the results from our model.

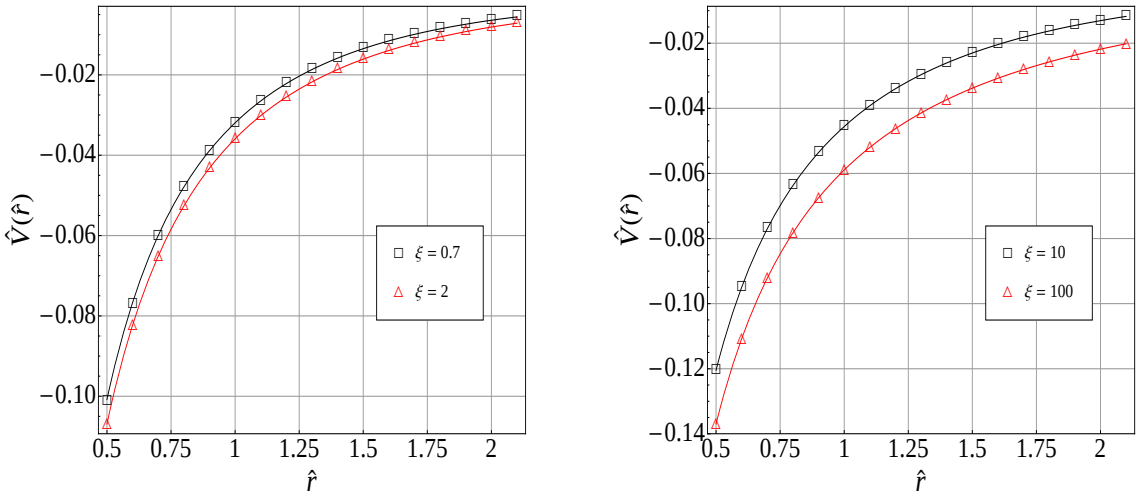

Figure C.2: Comparison of $\hat{V}$ as a function of $\hat{r}$ between the numerical results and our model when $\mathbf{r}$ is perpendicular to $\mathbf{n}$.

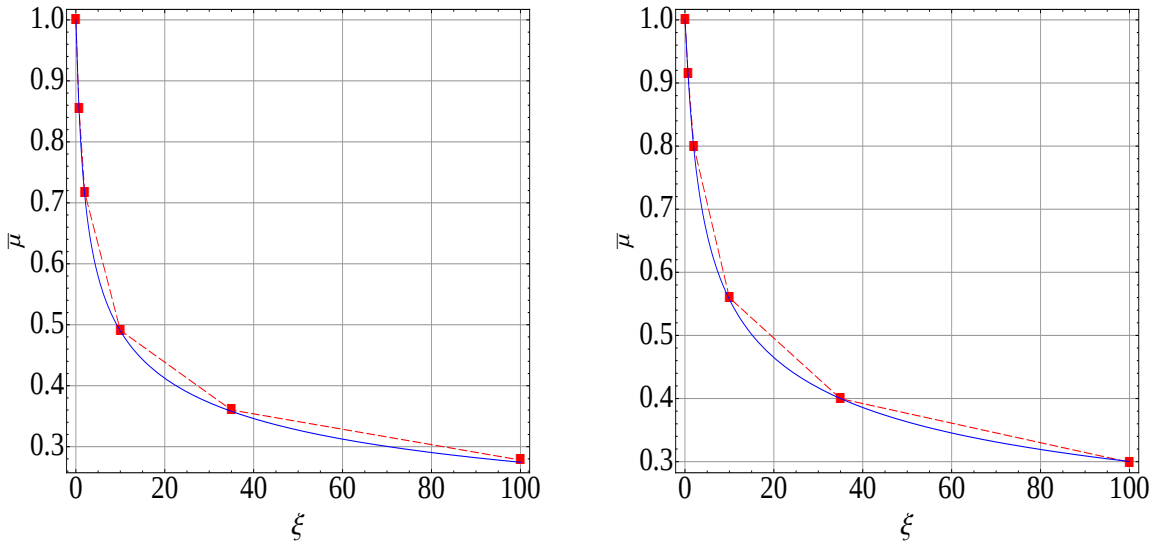

Figure C.3: Comparison of $\bar{\mu}$ as a function of ξ between numerical results and our model. The square symbols are obtained from numerical data and the smooth line corresponds to our model.
Left: $\mathbf{r}$ is parallel to $\mathbf{n}$. Right: $\mathbf{r}$ is perpendicular to $\mathbf{n}$.

We can rewrite Eq. (C.1) as

$$g^2 C_F \hat{r} \hat{V}(\hat{r}, \xi) = -\frac{g^2 C_F}{4\pi} e^{-\hat{r}\bar{\mu}}, \tag{C.5}$$

where all the quantities are dimensionless. From this equation, we can expect that the dimensionless screening mass $\bar{\mu}$ may have a $\hat{r}$ dependence. However, our numerical results show this dependence is very weak and our assumption $\mu(\theta; \xi, T)$ is still reasonable. So we can determine the dimensionless screening mass $\bar{\mu}$ from the numerical results through the equation

$$\bar{\mu} = -\log(-4\pi \hat{V}), \tag{C.6}$$

where we choose $\hat{r} = 1$.

Comparing the dimensionless screening mass $\bar{\mu}$ determined from the numerical calculations with those from our model, we find that this model actually works very well as shown in Fig. C.3. Furthermore, we model the angular dependence of the potential by the following assumption

$$V(\mathbf{r}, \xi) = -\frac{g^2 C_F}{4\pi r} e^{-r m_D \bar{\mu}(\xi, \theta)}, \tag{C.7}$$

with

$$\bar{\mu}(\xi, \theta) = \frac{1}{(1 + 1.85\,\xi^{1.27})^{0.20}} + \sin^2\theta \Big[\frac{1}{(1 + 0.74\,\xi^{1.20})^{0.23}} - \frac{1}{(1 + 1.85\,\xi^{1.27})^{0.20}}\Big]. \tag{C.8}$$

Here, the $\sin^2\theta$ is only a very rough estimate for the angular dependence. However, numerically we found such a dependence is very weak and quantitatively, we do not expect a big error with this assumption. So the above model given in Eqs. (C.7) and (C.8) can be expected to give a quantitative description of the anisotropic potential for a general ξ.

Bibliography

[1] S. Weinberg, *The first three minutes: a modern view of the origin of the universe*. Harper-Collins Publishers, New York, 1993.

[2] T. Padmanabhan, *After the first three minutes: the story of our universe*. Cambridge University Press, Cambridge, 1998.

[3] J. W. Harris, *Relativistic heavy ion physics and the relativistic heavy ion collider*, . Prepared for Lake Louise Winter Institute: Quantum Chromodynamics, Lake Louise, Alberta, Canada, 15-21 Feb 1998.

[4] J. Letessier and J. Refelski, *Hadrons and quark-gluon plasma*. World Scientific, Singapore, 2001.

[5] C. E. Detar, *Quark - gluon plasma in numerical simulations of lattice QCD*, `hep-ph/9504325`.

[6] e. . Hwa, R. C., *Quark - gluon plasma*, . Singapore, Singapore: World Scientific (1990) 712 p. (Advanced series on directions in high energy physics, 6).

[7] Z. Fodor and S. D. Katz, *Lattice determination of the critical point of QCD at finite T and mu*, *JHEP* **03** (2002) 014, [`hep-lat/0106002`].

[8] F. Karsch, E. Laermann, and A. Peikert, *The pressure in 2, 2+1 and 3 flavour QCD*, *Phys. Lett.* **B478** (2000) 447–455, [`hep-lat/0002003`].

[9] F. Karsch, *Lattice QCD at high temperature and density*, *Lect. Notes Phys.* **583** (2002) 209–249, [`hep-lat/0106019`].

[10] M. Cheng *et al.*, *The transition temperature in QCD*, *Phys. Rev.* **D74** (2006) 054507, [`hep-lat/0608013`].

[11] **CP-PACS** Collaboration, A. Ali Khan *et al.*, *Phase structure and critical temperature of two flavor QCD with renormalization group improved gauge action and clover improved Wilson quark action*, *Phys. Rev.* **D63** (2001) 034502, [`hep-lat/0008011`].

[12] M. Gyulassy and L. McLerran, *New forms of QCD matter discovered at RHIC*, *Nucl. Phys.* **A750** (2005) 30–63, [`nucl-th/0405013`].

[13] K. Rajagopal and F. Wilczek, *The condensed matter physics of QCD*, `hep-ph/0011333`.

[14] T. D. Lee and G. C. Wick, *Vacuum Stability and Vacuum Excitation in a Spin 0 Field Theory*, *Phys. Rev.* **D9** (1974) 2291.

[15] M. A. Stephanov, *QCD phase diagram: An overview*, *PoS* **LAT2006** (2006) 024, [hep-lat/0701002].

[16] H. Fritzsch, M. Gell-Mann, and H. Leutwyler, *Advantages of the Color Octet Gluon Picture*, *Phys. Lett.* **B47** (1973) 365–368.

[17] D. J. Gross and F. Wilczek, *ULTRAVIOLET BEHAVIOR OF NON-ABELIAN GAUGE THEORIES*, *Phys. Rev. Lett.* **30** (1973) 1343–1346.

[18] H. D. Politzer, *RELIABLE PERTURBATIVE RESULTS FOR STRONG INTERACTIONS?*, *Phys. Rev. Lett.* **30** (1973) 1346–1349.

[19] S. Bethke, *Experimental tests of asymptotic freedom*, *Prog. Part. Nucl. Phys.* **58** (2007) 351–386, [hep-ex/0606035].

[20] J. M. Maldacena, *The large N limit of superconformal field theories and supergravity*, *Adv. Theor. Math. Phys.* **2** (1998) 231–252, [hep-th/9711200].

[21] E. Witten, *Anti-de Sitter space and holography*, *Adv. Theor. Math. Phys.* **2** (1998) 253–291, [hep-th/9802150].

[22] O. Aharony, S. S. Gubser, J. M. Maldacena, H. Ooguri, and Y. Oz, *Large N field theories, string theory and gravity*, *Phys. Rept.* **323** (2000) 183–386, [hep-th/9905111].

[23] F. Karsch, *SIMULATING THE QUARK - GLUON PLASMA ON THE LATTICE*, *Adv. Ser. Direct. High Energy Phys.* **6** (1990) 61–115.

[24] H. Leutwyler, *On the foundations of chiral perturbation theory*, *Ann. Phys.* **235** (1994) 165–203, [hep-ph/9311274].

[25] A. Pineda and J. Soto, *Effective field theory for ultrasoft momenta in NRQCD and NRQED*, *Nucl. Phys. Proc. Suppl.* **64** (1998) 428–432, [hep-ph/9707481].

[26] C. W. Bauer, S. Fleming, D. Pirjol, and I. W. Stewart, *An effective field theory for collinear and soft gluons: Heavy to light decays*, *Phys. Rev.* **D63** (2001) 114020, [hep-ph/0011336].

[27] C. W. Bauer, D. Pirjol, and I. W. Stewart, *Soft-Collinear Factorization in Effective Field Theory*, *Phys. Rev.* **D65** (2002) 054022, [hep-ph/0109045].

[28] M. Gyulassy, I. Vitev, X.-N. Wang, and B.-W. Zhang, *Jet quenching and radiative energy loss in dense nuclear matter*, nucl-th/0302077.

[29] R. Rapp, D. Blaschke, and P. Crochet, *Charmonium and bottomonium production in heavy-ion collisions*, 0807.2470.

[30] P. Braun-Munzinger and J. Stachel, *Charmonium from Statistical Hadronization of Heavy Quarks – a Probe for Deconfinement in the Quark-Gluon Plasma*, 0901.2500.

[31] L. Kluberg and H. Satz, *Color Deconfinement and Charmonium Production*, 0901.3831.

[32] T. Matsui and H. Satz, *J/psi Suppression by Quark-Gluon Plasma Formation*, *Phys. Lett.* **B178** (1986) 416.

[33] A. Mocsy, *Potential Models for Quarkonia*, 0811.0337.

[34] W. E. Caswell and G. P. Lepage, *Effective Lagrangians for Bound State Problems in QED, QCD, and Other Field Theories*, *Phys. Lett.* **B167** (1986) 437.

[35] B. A. Thacker and G. P. Lepage, *Heavy quark bound states in lattice QCD*, *Phys. Rev.* **D43** (1991) 196–208.

[36] G. T. Bodwin, E. Braaten, and G. P. Lepage, *Rigorous QCD analysis of inclusive annihilation and production of heavy quarkonium*, *Phys. Rev.* **D51** (1995) 1125–1171, [hep-ph/9407339].

[37] N. Brambilla, A. Pineda, J. Soto, and A. Vairo, *Potential NRQCD: An effective theory for heavy quarkonium*, *Nucl. Phys.* **B566** (2000) 275, [hep-ph/9907240].

[38] E. Eichten, K. Gottfried, T. Kinoshita, K. D. Lane, and T.-M. Yan, *Charmonium: Comparison with Experiment*, *Phys. Rev.* **D21** (1980) 203.

[39] S. Necco and R. Sommer, *The N(f) = 0 heavy quark potential from short to intermediate distances*, *Nucl. Phys.* **B622** (2002) 328–346, [hep-lat/0108008].

[40] F. Karsch, M. T. Mehr, and H. Satz, *Color Screening and Deconfinement for Bound States of Heavy Quarks*, *Z. Phys.* **C37** (1988) 617.

[41] N. Brambilla, J. Ghiglieri, A. Vairo, and P. Petreczky, *Static quark-antiquark pairs at finite temperature*, *Phys. Rev.* **D78** (2008) 014017, [0804.0993].

[42] T. Umeda, K. Nomura, and H. Matsufuru, *Charmonium at finite temperature in quenched lattice QCD*, *Eur. Phys. J.* **C39S1** (2005) 9–26, [hep-lat/0211003].

[43] M. Asakawa and T. Hatsuda, *J/psi and eta/c in the deconfined plasma from lattice QCD*, *Phys. Rev. Lett.* **92** (2004) 012001, [hep-lat/0308034].

[44] S. Datta, F. Karsch, P. Petreczky, and I. Wetzorke, *Behavior of charmonium systems after deconfinement*, *Phys. Rev.* **D69** (2004) 094507, [hep-lat/0312037].

[45] H. Iida, T. Doi, N. Ishii, H. Suganuma, and K. Tsumura, *Charmonium properties in deconfinement phase in anisotropic lattice QCD*, *Phys. Rev.* **D74** (2006) 074502, [hep-lat/0602008].

[46] G. Aarts *et al.*, *Charmonium spectral functions in N_f = 2 QCD at high temperature*, *PoS* **LAT2006** (2006) 126, [hep-lat/0610065].

[47] A. Mocsy and P. Petreczky, *Can quarkonia survive deconfinement ?*, *Phys. Rev.* **D77** (2008) 014501, [0705.2559].

[48] M. Laine, O. Philipsen, P. Romatschke, and M. Tassler, *Real-time static potential in hot QCD*, *JHEP* **03** (2007) 054, [hep-ph/0611300].

[49] S. Mrowczynski, *Plasma instability at the initial stage of ultrarelativistic heavy ion collisions*, *Phys. Lett.* **B314** (1993) 118–121.

[50] S. Mrowczynski, *Color collective effects at the early stage of ultrarelativistic heavy ion collisions*, *Phys. Rev.* **C49** (1994) 2191–2197.

[51] S. Mrowczynski, *Color filamentation in ultrarelativistic heavy-ion collisions*, *Phys. Lett.* **B393** (1997) 26–30, [hep-ph/9606442].

[52] E. S. Weibel, *Spontaneously Growing Transverse Waves in a Plasma Due to an Anisotropic Veloc ity Distribution*, *Phys. Rev. Lett.* **2** (1959) 83–84.

[53] M. Tatarakis *et al.*, *Propagation Instabilities of High-Intensity Laser-Produced Electron Beams*, *Phys. Rev. Lett.* **90** (2003) 175001.

[54] A. Bret, M. C. Firpo, and C. Deutsch, *Characterization of the Initial Filamentation of a Relativistic Electron Beam Passing through a Plasma*, *Phys. Rev. Lett.* **94** (2005) 115002.

[55] P. Arnold, J. Lenaghan, and G. D. Moore, *QCD plasma instabilities and bottom-up thermalization*, *JHEP* **08** (2003) 002, [hep-ph/0307325].

[56] R. Baier, A. H. Mueller, D. Schiff, and D. T. Son, *'Bottom-up' thermalization in heavy ion collisions*, *Phys. Lett.* **B502** (2001) 51–58, [hep-ph/0009237].

[57] B. Muller, *Quark matter 2005: Theoretical summary*, nucl-th/0508062.

[58] A. Dumitru, Y. Nara, B. Schenke, and M. Strickland, *Jet broadening in unstable non-Abelian plasmas*, *Phys. Rev.* **C78** (2008) 024909, [0710.1223].

[59] J. Randrup and S. Mrowczynski, *Chromodynamic Weibel instabilities in relativistic nuclear collisions*, *Phys. Rev.* **C68** (2003) 034909, [nucl-th/0303021].

[60] P. Romatschke and M. Strickland, *Collective Modes of an Anisotropic Quark-Gluon Plasma*, *Phys. Rev.* **D68** (2003) 036004, [hep-ph/0304092].

[61] R. D. Pisarski, *Nonabelian Debye screening, tsunami waves, and worldline fermions*, hep-ph/9710370.

[62] J. Kapusta, *Finite-temperature field theory.* Cambridge University Press, Cambridge, 1989.

[63] M. L. Bellac, *Thermal field theory.* Cambridge University Press, Cambridge, 1996.

[64] J.-P. Blaizot and E. Iancu, *Kinetic theory and quantum electrodynamics at high temperature*, *Nucl. Phys.* **B390** (1993) 589–620.

[65] E. Braaten and R. D. Pisarski, *Soft Amplitudes in Hot Gauge Theories: A General Analysis*, *Nucl. Phys.* **B337** (1990) 569.

[66] J. Frenkel and J. C. Taylor, *High Temperature Limit of Thermal QCD*, *Nucl. Phys.* **B334** (1990) 199.

[67] J. P. Blaizot, J.-Y. Ollitrault, and E. Iancu, *Collective phenomena in the quark - gluon plasma*, . In *Hwa, R.C. (ed.): Quark-gluon plasma, vol.2* 135-210.

[68] J. C. Taylor and S. M. H. Wong, *THE EFFECTIVE ACTION OF HARD THERMAL LOOPS IN QCD*, *Nucl. Phys.* **B346** (1990) 115–128.

[69] J.-P. Blaizot and E. Iancu, *The quark-gluon plasma: Collective dynamics and hard thermal loops*, *Phys. Rept.* **359** (2002) 355–528, [hep-ph/0101103].

[70] H.-T. Elze and U. W. Heinz, *Quark - Gluon Transport Theory*, *Phys. Rept.* **183** (1989) 81–135.

[71] P. Arnold, G. D. Moore, and L. G. Yaffe, *Photon emission from ultrarelativistic plasmas*, *JHEP* **11** (2001) 057, [hep-ph/0109064].

[72] A. Hosoya and K. Kajantie, *Transport Coefficients of QCD Matter*, *Nucl. Phys.* **B250** (1985) 666.

[73] P. Arnold, G. D. Moore, and L. G. Yaffe, *Transport coefficients in high temperature gauge theories: (I) Leading-log results*, *JHEP* **11** (2000) 001, [hep-ph/0010177].

[74] A. D. Linde, *Infrared Problem in Thermodynamics of the Yang-Mills Gas*, *Phys. Lett.* **B96** (1980) 289.

[75] S. Mrowczynski and M. H. Thoma, *Hard loop approach to anisotropic systems*, *Phys. Rev.* **D62** (2000) 036011, [hep-ph/0001164].

[76] J. P. Blaizot and E. Iancu, *Kinetic equations for long wavelength excitations of the quark - gluon plasma*, *Phys. Rev. Lett.* **70** (1993) 3376–3379, [hep-ph/9301236].

[77] J. P. Blaizot and E. Iancu, *Soft collective excitations in hot gauge theories*, *Nucl. Phys.* **B417** (1994) 608–673, [hep-ph/9306294].

[78] B. Schenke, *Collective Phenomena in the Non-Equilibrium Quark-Gluon Plasma*, 0810.4306.

[79] O. K. Kalashnikov and V. V. Klimov, *Polarization Tensor in QCD for Finite Temperature and Density*, *Sov. J. Nucl. Phys.* **31** (1980) 699.

[80] H. A. Weldon, *Covariant Calculations at Finite Temperature: The Relativistic Plasma*, *Phys. Rev.* **D26** (1982) 1394.

[81] H. A. Weldon, *Effective Fermion Masses of Order gT in High Temperature Gauge Theories with Exact Chiral Invariance*, *Phys. Rev.* **D26** (1982) 2789.

[82] P. F. Kelly, Q. Liu, C. Lucchesi, and C. Manuel, *Classical transport theory and hard thermal loops in the quark - gluon plasma*, *Phys. Rev.* **D50** (1994) 4209–4218, [hep-ph/9406285].

[83] N. P. Landsman and C. G. van Weert, *Real and Imaginary Time Field Theory at Finite Temperature and Density*, *Phys. Rept.* **145** (1987) 141.

[84] K.-c. Chou, Z.-b. Su, B.-l. Hao, and L. Yu, *Equilibrium and Nonequilibrium Formalisms Made Unified*, *Phys. Rept.* **118** (1985) 1.

[85] L. V. Keldysh, *Diagram technique for nonequilibrium processes*, *Zh. Eksp. Teor. Fiz.* **47** (1964) 1515–1527.

[86] A. Peshier, K. Schertler, and M. H. Thoma, *One-loop self energies at finite temperature*, *Annals Phys.* **266** (1998) 162–177, [hep-ph/9708434].

[87] M. E. Carrington, D.-f. Hou, and M. H. Thoma, *Equilibrium and non-equilibrium hard thermal loop resummation in the real time formalism*, *Eur. Phys. J.* **C7** (1999) 347–354, [hep-ph/9708363].

[88] T. S. Biro, E. van Doorn, B. Muller, M. H. Thoma, and X. N. Wang, *Parton equilibration in relativistic heavy ion collisions*, *Phys. Rev.* **C48** (1993) 1275–1284, [nucl-th/9303004].

[89] R. Baier, M. Dirks, K. Redlich, and D. Schiff, *Thermal photon production rate from non-equilibrium quantum field theory*, *Phys. Rev.* **D56** (1997) 2548–2554, [hep-ph/9704262].

[90] M. Le Bellac and H. Mabilat, *Infrared and pinching singularities in out of equilibrium QCD plasmas*, *Z. Phys.* **C75** (1997) 137–146.

[91] K. Geiger, *Space-time description of ultrarelativistic nuclear collisions in the QCD parton picture*, *Phys. Rept.* **258** (1995) 237–376.

[92] U. W. Heinz, *QUARK - GLUON TRANSPORT THEORY*, *Nucl. Phys.* **A418** (1984) 603c–612c.

[93] S. Mrowczynski, *STREAM INSTABILITIES OF THE QUARK - GLUON PLASMA*, *Phys. Lett.* **B214** (1988) 587.

[94] Y. E. Pokrovsky and A. V. Selikhov, *FILAMENTATION IN A QUARK - GLUON PLASMA*, *JETP Lett.* **47** (1988) 12–14.

[95] Y. E. Pokrovsky and A. V. Selikhov, *Filamentation in the quark-gluon plasma at finite temperatures*, *Sov. J. Nucl. Phys.* **52** (1990) 385–387.

[96] P. Romatschke and M. Strickland, *Collective modes of an anisotropic quark-gluon plasma. II*, *Phys. Rev.* **D70** (2004) 116006, [hep-ph/0406188].

[97] A. Dumitru and Y. Nara, *QCD plasma instabilities and isotropization*, *Phys. Lett.* **B621** (2005) 89–95, [hep-ph/0503121].

[98] L. V. Gribov, E. M. Levin, and M. G. Ryskin, *Semihard Processes in QCD*, *Phys. Rept.* **100** (1983) 1–150.

[99] A. H. Mueller and J.-w. Qiu, *Gluon Recombination and Shadowing at Small Values of x*, *Nucl. Phys.* **B268** (1986) 427.

[100] J. P. Blaizot and A. H. Mueller, *The Early Stage of Ultrarelativistic Heavy Ion Collisions*, *Nucl. Phys.* **B289** (1987) 847.

[101] M. Asakawa, S. A. Bass, and B. Muller, *Anomalous transport processes in anisotropically expanding quark-gluon plasmas*, *Prog. Theor. Phys.* **116** (2007) 725–755, [hep-ph/0608270].

[102] M. Martinez and M. Strickland, *Constraining relativistic viscous hydrodynamical evolution*, 0902.3834.

[103] T. N. Kato, *Saturation mechanism of the Weibel instability in weakly magnetized plasmas*, *Phys. Plasmas* **12** (2005) 080705, [physics/0501110].

[104] P. Arnold and J. Lenaghan, *The abelianization of QCD plasma instabilities*, *Phys. Rev.* **D70** (2004) 114007, [hep-ph/0408052].

[105] A. Jakovac, P. Petreczky, K. Petrov, and A. Velytsky, *Quarkonium correlators and spectral functions at zero and finite temperature*, *Phys. Rev.* **D75** (2007) 014506, [hep-lat/0611017].

[106] G. Aarts, C. Allton, M. B. Oktay, M. Peardon, and J.-I. Skullerud, *Charmonium at high temperature in two-flavor QCD*, *Phys. Rev.* **D76** (2007) 094513, [0705.2198].

[107] A. Mocsy and P. Petreczky, *Quarkonia correlators above deconfinement*, *Phys. Rev.* **D73** (2006) 074007, [hep-ph/0512156].

[108] A. Dumitru, Y. Guo, and M. Strickland, *The heavy-quark potential in an anisotropic (viscous) plasma*, *Phys. Lett.* **B662** (2008) 37–42, [0711.4722].

[109] M. E. Peskin and D. V. Schroeder, *An introduction to quantum field theory*. Harper-Collins Publishers, New York, 1995.

[110] Y. Guo, *Gluon Propagator and Heavy Quark Potential in an Anisotropic QCD Plasma*, *Nucl. Phys.* **A820** (2009) 275c–278c, [0809.3873].

[111] J. Noronha and A. Dumitru, *The Heavy Quark Potential as a Function of Shear Viscosity at Strong Coupling*, 0903.2804.

[112] O. Kaczmarek, F. Karsch, F. Zantow, and P. Petreczky, *Static quark anti-quark free energy and the running coupling at finite temperature*, *Phys. Rev.* **D70** (2004) 074505, [hep-lat/0406036].

[113] Y. Guo, *Small Quarkonium states in an anisotropic QCD plasma*, 0805.2551.

[114] W. Lucha, F. F. Schoberl, and D. Gromes, *Bound states of quarks*, *Phys. Rept.* **200** (1991) 127–240.

[115] N. Brambilla, A. Pineda, J. Soto, and A. Vairo, *Effective field theories for heavy quarkonium*, *Rev. Mod. Phys.* **77** (2005) 1423, [hep-ph/0410047].

[116] E. V. Shuryak, *Quantum Chromodynamics and the Theory of Superdense Matter*, *Phys. Rept.* **61** (1980) 71–158.

[117] D. J. Gross, R. D. Pisarski, and L. G. Yaffe, *QCD and Instantons at Finite Temperature*, *Rev. Mod. Phys.* **53** (1981) 43.

[118] A. Mocsy and P. Petreczky, *Heavy quarkonia survival in potential model*, *Eur. Phys. J.* **C43** (2005) 77–80, [hep-ph/0411262].

[119] C.-Y. Wong, *Heavy quarkonia in quark gluon plasma*, *Phys. Rev.* **C72** (2005) 034906, [hep-ph/0408020].

[120] W. M. Alberico, A. Beraudo, A. De Pace, and A. Molinari, *Quarkonia in the deconfined phase: Effective potentials and lattice correlators*, *Phys. Rev.* **D75** (2007) 074009, [hep-ph/0612062].

[121] W. M. Alberico, A. Beraudo, A. De Pace, and A. Molinari, *Potential models and lattice correlators for quarkonia at finite temperature*, *Phys. Rev.* **D77** (2008) 017502, [0706.2846].

[122] D. Cabrera and R. Rapp, *T-matrix approach to quarkonium correlation functions in the QGP*, *Phys. Rev.* **D76** (2007) 114506, [hep-ph/0611134].

[123] A. Mocsy and P. Petreczky, *Color Screening Melts Quarkonium*, *Phys. Rev. Lett.* **99** (2007) 211602, [0706.2183].

[124] T. Umeda, *A constant contribution in meson correlators at finite temperature*, *Phys. Rev.* **D75** (2007) 094502, [hep-lat/0701005].

[125] e. . Armesto, N. *et al.*, *Heavy Ion Collisions at the LHC - Last Call for Predictions*, *J. Phys.* **G35** (2008) 054001, [0711.0974].

[126] M. Laine, O. Philipsen, and M. Tassler, *Thermal imaginary part of a real-time static potential from classical lattice gauge theory simulations*, *JHEP* **09** (2007) 066, [0707.2458].

[127] M. Laine, *A resummed perturbative estimate for the quarkonium spectral function in hot QCD*, *JHEP* **05** (2007) 028, [0704.1720].

[128] A. Beraudo, J. P. Blaizot, and C. Ratti, *Real and imaginary-time $Q\bar{Q}$ correlators in a thermal medium*, *Nucl. Phys.* **A806** (2008) 312–338, [0712.4394].

[129] A. Dumitru, Y. Guo, A. Mocsy, and M. Strickland, *Quarkonium states in an anisotropic QCD plasma*, *Phys. Rev.* **D79** (2009) 054019, [0901.1998].

[130] P. Petreczky, *Heavy quark potentials and quarkonia binding*, *Eur. Phys. J.* **C43** (2005) 51–57, [hep-lat/0502008].

[131] E. V. Shuryak and I. Zahed, *Towards a theory of binary bound states in the quark gluon plasma*, *Phys. Rev.* **D70** (2004) 054507, [hep-ph/0403127].

[132] O. Kaczmarek, *Screening at finite temperature and density*, *PoS* **CPOD07** (2007) 043, [0710.0498].

[133] E. Megias, E. Ruiz Arriola, and L. L. Salcedo, *Dimension two condensates and the Polyakov loop above the deconfinement phase transition*, *JHEP* **01** (2006) 073, [hep-ph/0505215].

[134] E. Megias, E. Ruiz Arriola, and L. L. Salcedo, *The quark-antiquark potential at finite temperature and the dimension two gluon condensate*, *Phys. Rev.* **D75** (2007) 105019, [hep-ph/0702055].

[135] E. Megias, E. Ruiz Arriola, and L. L. Salcedo, *Trace Anomaly, Thermal Power Corrections and Dimension Two condensates in the deconfined phase*, 0903.1060.

[136] G. S. Bali, K. Schilling, and A. Wachter, *Complete O(v**2) corrections to the static interquark potential from SU(3) gauge theory*, *Phys. Rev.* **D56** (1997) 2566–2589, [hep-lat/9703019].

[137] I. Sudiarta and D. Geldart, *Solving the Schrödinger equation using the finite difference time domain method*, *Journal of Physics* **A40** (2007) 1885.

[138] M. Strickland and D. Yager-Elorriaga, *A Parallel Algorithm for Solving the 3d Schrodinger Equation*, 0904.0939.

[139] O. Kaczmarek and F. Zantow, *Static quark anti-quark interactions in zero and finite temperature QCD. I: Heavy quark free energies, running coupling and quarkonium binding*, *Phys. Rev.* **D71** (2005) 114510, [hep-lat/0503017].

[140] D. Kharzeev, L. D. McLerran, and H. Satz, *Nonperturbative quarkonium dissociation in hadronic matter*, *Phys. Lett.* **B356** (1995) 349–353, [hep-ph/9504338].

[141] B. L. Ioffe and D. E. Kharzeev, *Quarkonium polarization in heavy ion collisions as a possible signature of the quark gluon plasma*, *Phys. Rev.* **C68** (2003) 061902, [hep-ph/0306176].

[142] A. Dumitru, Y. Guo, and M. Strickland, *The imaginary part of the static gluon propagator in an anisotropic (viscous) QCD plasma*, *Phys. Rev.* **D79** (2009) 114003, [0903.4703].

[143] M. E. Carrington, D.-f. Hou, and M. H. Thoma, *Ward identities in non-equilibrium QED*, *Phys. Rev.* **D58** (1998) 085025, [hep-th/9801103].

[144] Y. Burnier, M. Laine, and M. Vepsalainen, *Quarkonium dissociation in the presence of a small momentum space anisotropy*, 0903.3467.

[145] M. Martinez and M. Strickland, *Measuring QGP thermalization time with dileptons*, *Phys. Rev. Lett.* **100** (2008) 102301, [0709.3576].

[146] M. Martinez and M. Strickland, *Pre-equilibrium dilepton production from an anisotropic quark-gluon plasma*, *Phys. Rev.* **C78** (2008) 034917, [0805.4552].

Acknowledgments

First I would like to express my gratitude to my parents for their support, which made my studies and this dissertation possible.

I am indebted to my supervisors Prof. Dr. Carsten Greiner and Assoc. Prof. Dr. Adrian Dumitru for their advice and help. I feel fortunate to work under their kind guidance and support.

I thank Asst. Prof. Dr. Michael Strickland for great collaboration. The inspiring discussions with him always give me a great help during this work.

I thank Asst. Prof. Dr. Ágnes Mócsy for her collaboration in some parts of this work and many helpful discussions.

I thank Mauricio Martinez, Dr. Jorge Noronha and Dr. Björn Schenke for some helpful discussions.

In addition I thank my office-mates Mauricio Martinez, Volodymyr Konchakovski and Michael Hauer for many additional discussions beyond physics and a great time at the university.

I thank Dr. Henner Büsching for his interest in my work and his great help in many issues.

Last but not least, I would like to thank all members of Helmholtz Research School for their efforts to make the school warm and enjoyable. I appreciate their kindnesses which make my stay in Frankfurt memorable.

Thanks also to the Helmholtz foundation and the Otto Stern School at Frankfurt university for their support and the center for scientific computing (CSC) for computational resources.

Curriculum vitae

Personal Particulars:

Name:	Yun Guo
Sex:	Male
Date of Birth:	03. Oct. 1981
Place of Birth:	Sichuan, P.R. China
Nationality:	Chinese
Address:	Ruth-Moufang-Str. 1, 60438, Frankfurt am Main
Email:	yun@fias.uni-frankfurt.de

Educational Background:

- 2000-2004, Physics (National Base of Basic Science and Education), College of Physical Science and Technology, Central China Normal University, Bachelor of Science.
- 2004-2006, Theoretical Physics, Institute of Particle Physics, College of Physical Science and Technology , Central China Normal University, Master of Science.
- Since Oct. 2006, Theoretical Physics, Helmholtz Research School for Quark Matter Studies, Goethe University Frankfurt am Main.

Publications:

- Adrian Dumitru, Yun Guo and Michael Strickland, *The imaginary part of the static gluon propagator in an anisotropic (viscous) QCD plasma*, Phys. Rev. D 79, 114003 (2009) [arXiv:0903.4703 [hep-ph]].
- Adrian Dumitru, Yun Guo, Agnes Mocsy and Michael Strickland, *Quarkonium states in an anisotropic QCD plasma*, Phys. Rev. D 79, 054019 (2009) [arXiv:0901.1998 [hep-ph]].
- Yun Guo, *Gluon propagator and heavy-quark potential in an anisotropic QCD plasma*, contributed to Strong and ElectroWeak Matter 2008, Nucl. Phys. A 820, 275C (2009) [arXiv:0809.3873 [hep-ph]].
- Yun Guo, *Small quarkonium states in an anisotropic QCD plasma*, contributed to Quark Matter 2008, to be published in Indian Journal of Physics [arXiv:0805.2551 [hep-ph]].

- Adrian Dumitru, Yun Guo and Michael Strickland, *The heavy-quark potential in an anisotropic plasma*, Phys. Lett. B 662, 37 (2008) [arXiv:0711.4722 [hep-ph]].
- Yun Guo, Ben-Wei Zhang and Enke Wang, *Parton energy loss at twist-six in deeply inelastic e-A scattering*, Phys. Lett. B 641, 38 (2006) [arXiv: hep-ph/0606312].
- Yun Guo and Enke Wang, *A new calculational approach to the amplitude of gluon radiation in e-A DIS*, High Energy Phys. Nucl. Phys. 30, 417 (2006).

Academic Tutors:

- Helmholtz Lecture Week

  Marcus Bleicher, Hans Rudolf Schmidt, Ralf Averbeck, Volker Koch, Piotr Salabura, Carlos Salgado, Marco van Leeuwen

- Helmholtz Basic Lecture

  Christoph Blume, Harald Appelshäuser, Miklos Gyulassy, Horst Stöcker, Peter Braun-Munzinger, Bengt Friman, Stefan Leupold, Henner Büsching

- ITP Lecture

  Adrian Dumitru, Igor Mishustin, Elena Bratkovskaya

Index